Diss. ETH No. 18441

Modelling of thermoelectric devices for electric power generation

Dissertation submitted to the
SWISS FEDERAL INSTITUTE OF TECHNOLOGY ZURICH
(ETH ZURICH)

for the degree of
Doctor of Sciences

presented by
ANDREAS BITSCHI
Dipl.Ing., Technical University of Vienna
born January 27, 1973
citizen of Austria

accepted on the recommendation of
Prof. Dr. K. Fröhlich, examiner
Prof. Dr. A. Weidenkaff, co-examiner

2009

gewidmet meinen lieben Eltern

Danksagung

Die vorliegende Arbeit entstand während meiner Zeit als wissenschaftlicher Mitarbeiter am Institut für elektrische Energieübertragung und Hochspannungstechnik (HVL) der ETH Zürich.

Besonderer Dank gilt meinem Doktorvater Prof. Dr. Klaus Fröhlich für die grundsätzliche Möglichkeit diese Arbeit durchzuführen, seine kompetente Unterstützung in allen Belangen, seine grosse Menschlichkeit und die sehr angenehme Zusammenarbeit.

Prof. Dr. Anke Weidenkaff danke ich für Ihre Bereitschaft zur Kooperation mit ihrer Forschungsgruppe Festkörperchemie und Katalyse der EMPA Dübendorf, für die Übernahme des Korreferats, ihre gewinnbringenden Hinweise und ihre insgesamt so positive und motivierende Art. Besonderer Dank geht an dieser Stelle auch an Dr. Rosa Robert, Dr. Laura Bocher , Matthias Trottmann, Sven Toggweiler und Petr Tomes für die konstruktive Zusammenarbeit.

Meine Arbeit wurde während der gesamten Zeit vom Bundesamt für Energie (BfE) finanziell unterstützt. Hier gilt mein besonderer Dank Herrn Roland Brüniger, der als Projektbegleiter äusserst souverän und unkompliziert agierte.

Ebenfalls sehr bedanken möchte ich mich bei Herrn Dr. Timm Teich, welcher meine Ausführungen in verständliches Englisch umsetzte und gleichzeitig durch Hinweise und kritisches Hinterfragen noch aufwertete. Weiterer Dank gilt meinen Bürokollegen, Bernd, Christian, Dominique, Patrick und Thomas für die vielen tollen Momente.

Ein ganz spezieller Dank geht an meine lieben Eltern, die mich in meinem Bestreben stets unterstützt und motiviert haben. Ihre Zuversicht und ihr unerschütterlicher Glaube an mich haben meinen bisherigen Lebensweg stets begleitet und mich immer wieder neu ermutigt. Ohne diesen Rückhalt wäre vieles nicht möglich gewesen.

Zürich, im Juli 2009 Andreas Bitschi

Abstract

The efficient usage of energy at all stages along the energy supply chain and the utilization of renewable energies are very important elements of a sustainable energy supply system. Especially at the conversion from thermal to electrical power a large amount of unused energy ("waste heat") remains. This energy, because of its relatively low temperature und low energy density can generally not be used for the generation of electrical power by the conventional thermodynamic cycles (Clausius Rankine, ORC, Kalina). Direct thermal to electrical energy conversion, without the intermediate step of kinetic energy, that is with no moving parts, therefore gives an alternative of high potential. The improvements in material sciences and the progress of nanotechnology bring thermoelectric materials and therefore thermoelectric converters to renewed significance. The efficiency of thermoelectric converters in general depends on material parameters summarized in the figure of merit ZT. Furthermore design aspects, especially the leg length, and heat transfer conditions have a significant influence on power output and efficiency. The main goal of the project "The thermoelectric power plant", a cooperation of EMPA Dübendorf and ETH Zurich, Power systems and High voltage laboratories, is to show the feasibility of a thermoelectric power generation unit. Therefore theoretical calculations and selected experiments have been carried out. The goal of this work was the development of tools for the evaluation of thermoelectric power generation units and devices. The modelling has been done on two size levels. On the large scale level a high number of thermoelectric modules have been integrated in a heat transfer unit, respectively a cross-flow heat exchanger. On the lower size level the modules were modelled in 3D including all non-linearities and irreversibilities and simulated with the method of the finite elements (FE). For the validation of the FE-simulation prototypes of thermoelectric oxide modules (TOM) were created at EMPA Dübendorf, the power output characteristics measured and compared with the results of the simulation. The conformity of the results was quite satisfying and could be multiple reproduced. The simulation gives new access to the interior of thermoelectric modules, which will be very important for future development steps. Different optimization strategies can be operated with little expenditure of time

and resources. As an example electric power generation based on a thermoelectric generator utilizing geothermal energy is presented and discussed. The next step would be the integration into several energy systems and the simulation of their dynamic behaviour.

Kurzfassung

Eine effiziente Nutzung der Energie entlang der gesamten Umwandlungskette und die Nutzung erneuerbarer Energien sind wichtige Bestandteile eines zukünftigen, nachhaltigen Energieversorgungssystems. Speziell bei der Wandlung von thermischer Energie in elektrische Energie fallen meist grosse Mengen an ungenützter Energie („Abfallwärme“) an. Diese Energie kann aufgrund ihrer niedrigen Temperatur und geringen Energiedichte nur selten mit den bekannten thermodynamischen Prozessen (Clausius-Rankine, ORC, Kalina) für die elektrische Energieerzeugung genutzt werden. Die direkte Wandlung von thermischer Energie in elektrische Energie ohne den Zwischenschritt der kinetischen Energie, sprich ohne bewegte Teile, bietet dafür eine Alternative mit grossem Potential. Durch die Entwicklungen der Materialwissenschaft in Kombination mit den Errungenschaften der Nanotechnologie erleben speziell die thermoelektrischen Materialien bzw. die thermoelektrischen Wandler eine Renaissance. Die Effizienz von thermoelektrischen Wandlern wird grundsätzlich durch Materialgrössen bestimmt, die in der Gütezahl ZT zusammengefasst sind. Aber auch Design-Aspekte des Moduls, speziell die Länge der Schenkel, und die Bedingungen für die Wärmeübertragung haben einen grossen Einfluss auf Ausgangsleistung und Wirkungsgrad. Das Ziel des Projektes „Das thermoelektrische Kraftwerk“, eine Kooperation der EMPA Dübendorf und der ETH Zürich, Institut für Elektrische Energieübertragung und Hochspannungstechnik, ist es, die Machbarkeit eines solchen thermoelektrischen Kraftwerkes zu zeigen. Dazu wurden theoretische Berechnungen sowie ausgewählte Experimente durchgeführt. Das Ziel dieser Arbeit war die Entwicklung von Werkzeugen für die Beurteilung von thermoelektrischen Energieerzeugungseinheiten. Die Modellierung erfolgte auf zwei Dimensionsebenen. Einmal wurde eine Vielzahl von thermoelektrischen Modulen in eine Energieübertragungseinheit sprich einen Gegenstromwärmetauscher integriert. In kleineren Dimensionen wurden einzelne Module in 3D modelliert, alle Nichtlineritäten und Irreversibilitäten berücksichtigend, und mit der Methode der finiten Elemente (FE) simuliert. Für die Validierung der FE-Simulation wurden erste Prototypen von Thermoelektrischen Oxid Modulen (TOM)

aufgebaut, deren Leistungscharakteristiken messtechnisch bestimmt und mit den simulierten Daten verglichen. Die Übereinstimmung der Ergebnisse war gut und konnte auch mehrfach reproduziert werden. Mit der Simulation können neue Einblicke in das Innenleben eines thermoelektrischen Moduls gewonnen werden, welche für den Aufbau der nächsten Entwicklungsstufen sehr hilfreich sein werden. Verschiedene Optimierungsstrategien können sehr Zeit - und Ressourcen - schonend durchgeführt werden. Als Beispiel wird die elektrische Energieerzeugung aus geothermischen Quellen mit einem thermoelektrischen Generator dargestellt und diskutiert. Der nächste Schritt wäre die Integration der Simulation in verschiedene Energiesysteme und die Simulation des dynamischen Verhaltens in jenen.

Content

Chapter 1

Problem statement

The use of thermoelectric power generators for electrical power generation out of low temperature heat sources is the general topic of this work. This chapter describes the actual situation, future trends and required actions. Thermoelectric power generation seems to be an interesting possibility for the direct heat to power conversion.

1.1 Low temperature heat sources

Two of the main issues with respect to a sustainable energy supply system are the more efficient usage of energy at all stages along the energy supply chain and the intended use of renewable resources (e.g. geothermal energy). Despite this, we have been wasting enormous amounts of heat from various sources, such as factories, transportation systems and even private houses or public buildings. The waste heat is difficult to use due to its nature of low temperature and low energy density, although the total energy amount is very large. Especially the utilisation of heat which is at too low temperature to drive a turbo generator should be a major task for future energy conversion research and development.

1.2 Actual thermal to electrical energy conversion

So far today's electrical energy production is mostly affected by generators based on electromagnetic induction. Reciprocating steam engines, internal combustion engines, and steam and gas turbines have been coupled with such generators in utilizing chemical heat sources such as oil, coal and natural gas and nuclear heat for the production of electrical energy. Renewable energy sources like geothermal energy,

solar energy and biomass energy are also being added to the list of heat sources used in modern electric power plants. Furthermore, solar energy provides hydropower indirectly.

The steam-Rankine cycle is the principle exploited for producing electric power from high temperature fluid streams. Gas and steam cogeneration and combined heat and power technologies (CHP) help to improve the electrical and total efficiencies of modern power plants from 35% to about 60%. For the conversion of low temperature heat (below 150°C) e.g. out of geothermal sources, into power, modifications of the steam-Rankine cycle like the Organic–Rankine cycle (ORC) [40] or the Kalina - process [40] are well known possibilities although also with quite limited potential and high costs. For making efficient use of the low temperature waste heat (< 80°C) generated by prime movers such as micro-turbines, internal combustion engines, fuel cells and other electricity and/or heat producing technologies, the energy content of the waste heat must be sufficient to operate equipment found in cogeneration and trigeneration power and energy systems such as absorption chillers, refrigeration applications, heat amplifiers, dehumidifiers, heat pumps for hot water, turbine inlet air cooling and other similar devices.

All these power plants have, however, a common disadvantage; the conversion of thermal energy into electric energy is accomplished by the utilization of moving and wear-subjected machine equipment. The massive bulk of equipment, the irreversibilities and complexities of the operation involved in these conversion methods accentuate the desirability of some more direct method for conversion of thermal energy into electrical energy with no moving parts. The degree of directness of a particular conversion process may depend on whether the original form of the energy is chemical, solar or heat. There are several methods known for direct conversion of thermal energy into electricity, such as:

- the thermoelectric conversion,
- the thermionic conversion,
- magnetohydrodynamic (MHD) conversion and
- electrogasdynamic conversion (EGD).

1.3 Direct Heat to Electricity Conversion

Efficient Direct Heat to Electricity Conversion (DHEC) has been sought for decades. To date work has focused on two primary directions as mentioned above. There are the thermionic converters, which are only capable of high power densities and efficiency only at temperature in excess of 1000°C, and thermoelectric converters, which operate at low temperature but suffer from low efficiency. The challenge for the future is to create a direct heat to electricity converter of high power and acceptable efficiency, but which is also capable of generating power over a relatively wide range of temperatures. The performance of heat engines and direct conversion devices is limited by the same laws of thermodynamics, and the real application environment therefore plays an important role in determining actual and acceptable performance.

Thermoelectric devices, on which this work is focused, allow the direct conversion of heat from sources like geothermal energy, solar energy or waste heat into electrical power. The main advantages are the low maintenance requirement, the high modularity and the possibility of utilising heat sources over a wide temperature range. Efficient solid state energy conversion based on the Seebeck effect calls for materials with high electrical conductivity σ, high Seebeck coefficient α and low thermal conductivity λ. These properties can be summarized in the thermoelectric figure of merit $ZT = \frac{\alpha^2 \cdot \sigma}{\lambda} \cdot T$. Today's materials have maximum ZTs of about at most unity. This gives efficiencies of about 10 to 15 % of the particular Carnot efficiency $\eta_{Carnot} = \frac{T_H - T_C}{T_H}$ containing the temperatures T_H of the heat source and T_C of the sink.

For commercial electricity generation it is necessary to seriously consider generation costs. Thermoelectrics suffer from low efficiency, however, when the heat source is nearly free of charge the low generating cost will offset the capital cost of the thermoelectric generator over its lifetime. To minimise the investment cost one would choose to keep the number of thermoelectric modules per kWe low and limit the amount of expensive material used by reducing the thermoelement leg length, which leads in general to higher power output, however, to lower efficiency.

To avoid any lacks of clarity and misinterpretation here a definition of the terms concerning thermoelectric "devices" used in this work is given (figure 1.1).

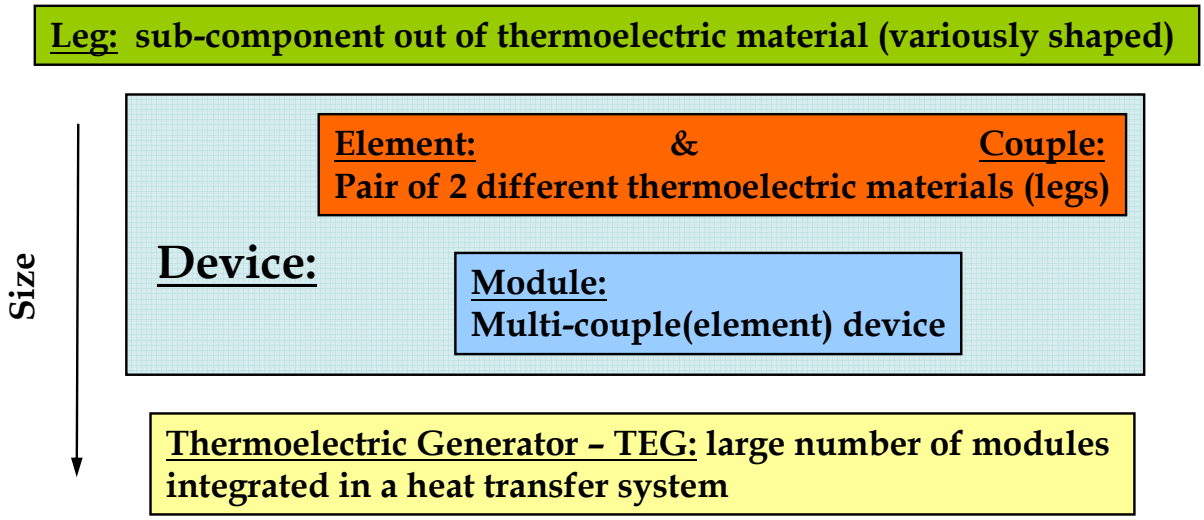

Figure 1.1: *Definition of the terms concerning thermoelectrics used in this work*

1.4 Basic considerations for thermoelectric power generation technologies

Even in the proposed 2000 W society (www.novatlantis.ch) the demand on electrical power of a single household with 4 persons is 5 to 6 kW. If we provide a low temperature heat source of around 100 °C to a thermoelectric module consisting of several tens of thermocouples, it can produce 1 to 2 watt of electric power. Consequently a 5 to 6 kW low temperature generator would require several thousands of thermoelectric modules. A large number of parallel channels are also required to provide the warm input and cold output flows. For bulk power generation utilizing e.g. geothermal heat sources the number of modules and the size of the total system would increase considerably more.

In these dimensions, optimisation for the specific applications and requirements and adaption to the given conditions is very important. Therefore models, which allow the optimisation corresponding to various objectives, should be available for the total system as also for

sub-systems like the heat transfer system or single modules. Several modern modelling and simulation techniques from analytical descriptions and numerical methods as well as detail analysis with finite element simulations should be considered and verified by way of existing modules.

Therefore the main goals of this work are formulated and given in the following

- Clarifying the general feasibility of thermoelectric bulk power generation
- General performance studies with today's and future materials
- Evaluation of power generation and symbiotic generation from renewable energy sources especially geothermal energy and waste heat recovery based on thermoelectrics.

The development of useful tools to deal with these tasks is the focus of this work. Detailed explanation and the modus operandi are given in chapter 3.

Chapter 2

State of the art and previous models

"The usefulness of comparing real processes with the corresponding reversible ones appears questionable in classical thermodynamics. Reversible limits are not close enough to real performances to be useful in guiding the improvements of processes." (freely adapted from the preface of [1]). These remarks have led many authors to the examination of whether it is possible to give more relevant limits of the performance of actual processes. An attempt to clarify these concepts with respect on thermoelectric energy production will be made in the following.

Thus, a general introduction to thermoelectrics and an overview of the most relevant modelling approaches is given in this chapter which opens with a short survey of the subsequently covered topics.

These are:

- a general explanation of thermoelectric devices and their main applications,
- recent trends in thermoelectric materials development,
- a simple thermodynamic analysis incorporating the basic magnitudes and performance criteria of a reversible thermoelectric generator
- thermoelectric modelling and simulation also considering established models

2.1 Thermoelectric devices

A thermocouple consists – as the name implies – usually two junctions incorporating different metals or alloys. When the two junctioms are at different temperatures, a low voltage – of the order of tens of µV/K – is generated. This is called the Seebeck effect [1, 9 20] and can be utilized in temperature measurement and control.

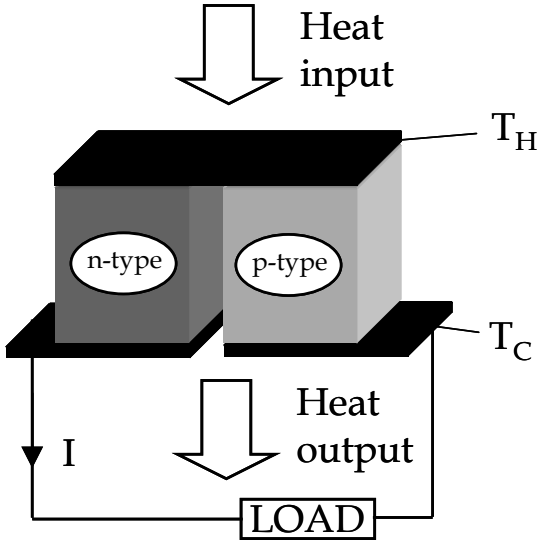

Figure 2.1: *Bulk semiconductor thermocouple in generating mode*

The reverse effect – where a junction is cooled by the passage of current – is known as the Peltier effect. This can be utilized for the vibration-free cooling of electronic devices and detectors such as photomultipliers.

In thermocouples for power generation or more potent cooling the metals/alloys have partly been replaced by contemporary semiconductors in pellet form, contacted with highly conducting metal strips as shown in Fig. 2.1 . With such materials, one order of magnitude greater Seebeck- coefficients are achieved; these can also be utilized in thin-film devices for temperature measurement. Therefore the thermocouple layers of micrometer thickness are deposited by a variety of techniques onto a supporting electrically insulating thin film substrate.

2.2 Thermoelectric materials

Three parameters are considered in the classification of thermoelectric materials: electrical conductivity σ, thermal conductivity λ, end the Seebeck coefficient α. Electrical conductivity is given as the product of the concentration and the mobility of charge carriers. It is high with metals, very low with insulators, with an intermediate position taken by semiconductors. As a measure of the potential usefulness of a thermoelectric material a figure of merit (def. see section 1.3) has been introduced; the three parameters mentioned above depending on carrier concentration (see Fig. 2.2) form the essential part of it. To facilitate optimization, a quantity $\alpha^2\sigma$ has been introduced and called "electrical power factor" The Seebeck-coefficient falls with increasing carrier concentration while the electrical conductivity increases; as a consequence the electrical power factor has a maximum which is typically found around a carrier concentration of around $10^{19}/cm^3$. There are two components of the thermal conductivity: lattice vibration and the electronic part. The latter also increases with carrier concentration and typically contributes about one third to the thermal conductivity. The maximum of the quantity $\alpha^2\sigma$ (the numerator of the equation for the figure of merit) falls into the realm of semiconductors (see Fig. 2.2). Consequently, semiconductors have been the materials of choice for further development of thermoelectric devices. Thermoelectric devices have been further classified with respect to the temperature ranges over which they can be usefully employed.

	Low temperature (300-450 K)	Intermediate temperature (-850 K)	High temperature (-1300 K)
Material composition(s)	Bi	PbTe	SiGe
Further components	Sb, Te, Se		

Tab. 1 *Temperature classification of thermoelectric materials*

The materials in the table and further detailed in Fig. 2.3 have so far been principal contenders for commercial applications in generation and

cooling, however, new materials of improved thermoelectric properties have been successfully synthesized.

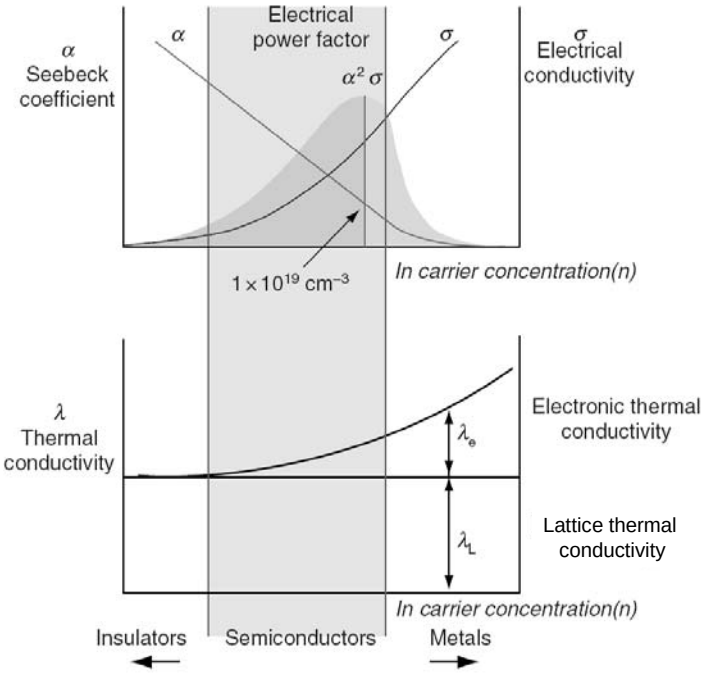

Figure 2.2: *Dependence of electrical conductivity, Seebeck coefficient, power factor and thermal conductivity on concentration of free carriers [19]*

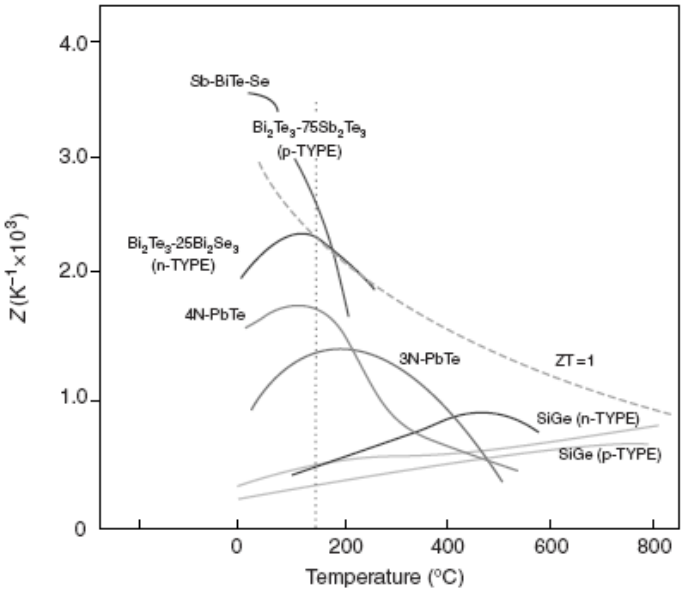

Figure 2.3: *Figure of Merit Z over temperature for various, established thermoelectric materials [19]*

One successful direction of development has been the reduction of lattice thermal conductivity, another the search for so-called "phonon glass electronic crystals" [17, 22], in which it is assumed that crystal structures containing weakly bound atoms or molecules that "rattle" within an atomic cage should conduct heat like a glass, but conduct electricity like a crystal. Candidate materials receiving considerable attention are the filled skutterudites, the clathrates and the thermoelectric oxides. During the past decade material scientists have been optimistic in their belief that low-dimensional structures such as quantum wells, (materials which are so thin as to be essentially of two dimensions (2D), quantum wires (extremely small cross-section and considered to be of one dimension (1D), and referred to as nanowires) quantum dots which are quantum confined in all directions and superlattices (a multiple-layered structure of quantum wells) will provide a route for achieving significantly improved thermoelectric figures-of-merit. The expectation is that the reduced dimensions of these structures will result in an increase in phonon interface scattering and a consequent reduction in lattice thermal conductivity [22].

There are also ongoing attempts to improve the competitiveness of thermoelectric materials in directions other than the figure-of-merit, such as decreasing costs, and developing more environmentally friendly materials.

Energy conversion using diode-like structures

A thermal diode [12, 22] is essentially a diode, implemented in a thermoelectric semiconductor, and designed either for energy conversion or for refrigeration. In an *np*-diode structure, electrons from a hot *n*-type emitter region are injected into the base (the solid gap region), and diffuse to a cold collector. Devices were studied in which the gap region is very wide (0.2–5 mm), and where the gap doping is intrinsic or weakly *n* type. A schematic picture is shown in Fig. 2.4. Two mechanisms which enhance the open-circuit voltage in thermal diodes have been observed. Injection of electrons into the hot side of the solid gap region and the transport of electrons from the emitter to the solid gap is ballistic across the potential barrier. Under zero-current conditions, the forward thermoelectric current and injected current must be balanced by an ohmic return current (which can be obstructed). In the presence of current injection, more ohmic return current is required than in the

thermoelectric case, which requires more thermally induced voltage. An increase in the open-circuit voltage translates into an increase in the integral figure of merit by the square of the voltage enhancement. A multi-junction approach is based on the fact that after five to ten scatterings after the first barrier, a carrier returns to non-perturbed Fermi distribution and the next barrier formed has the same effect as the first one. For a given temperature difference thermoelectric performance is a function of material properties. Barrier effects are additive and large gain in efficiency can be expected.

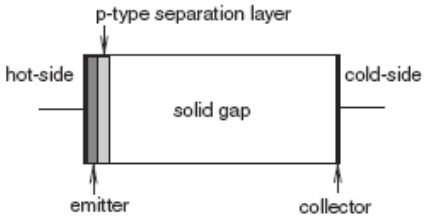

Figure 2.4: *Scheme of a basic thermal diode [19]*

After a general introduction of thermoelectric devices and the requirements on thermoelectric materials a basic thermodynamic description with the definition of relevant quantities and the results of the literature study concerning existing analytical and numerical models are given.

2.3 Modelling thermoelectric devices

A large number of analyses of the performance of thermoelectric generators have been carried out over the last decades. In the following the results and formulas for the description of thermoelectric generator performance as presented in literature are summarized and discussed.

2.3.1 Basic arrangement and characterizing quantities

For a better understanding a simple thermodynamic analysis, as it can be found in a number of books and helps to step into the topic, is reviewed. Here we follow exemplary Decher [9] who described the thermoelectric converter as a heat engine and like all heat engines it responds to the laws of thermodynamics (equ. 2.1-2.22). A representative configuration for a thermoelectric generator where a number of n series units (here n = 2) are cascaded to generate useful output voltages to the load resistance R is shown in Fig. 2.5. The hot and cold junctions are connected by *p* and *n* doped semiconductor legs.

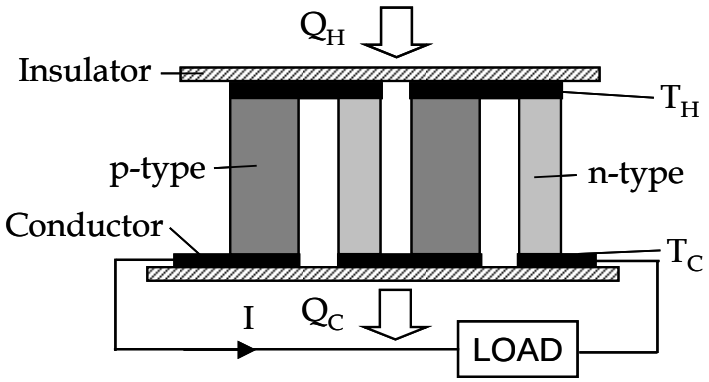

Figure 2.5: *Two series-connected thermoelectric generator units*

σ_p, σ_n and λ_p, λ_n are the electrical and thermal conductivities of the *p* and *n* legs .

A block of length L and cross-sectional area A owns a thermal conductance K given by

$$K_i = \lambda_i \frac{A_i}{L_i} \qquad \text{(Equ. 2.1)}$$

where the index i refers to either *p* or *n*.

From the thermal point of view [1, 9, 20] the two conductor types are in parallel, so that the total thermal conductance K for n elements is given by

$$K = K_P + K_N = n \cdot \left(\lambda_P \cdot \frac{A_P}{L_P} + \lambda_N \cdot \frac{A_N}{L_N} \right) \qquad \text{(Equ. 2.2)}$$

The electrical resistance is calculated in a similar way except that the n elements are in series. The resistance R [1, 9, 20] of the power-generating portion (semiconductor legs without the connecting metal stripes) of the circuit, as viewed by the load, is

$$R = R_P + R_N = n \cdot \left[\left(\sigma_P \cdot \frac{A_P}{L_P} \right)^{-1} + \left(\sigma_N \cdot \frac{A_N}{L_N} \right)^{-1} \right] \qquad \text{(Equ. 2.3)}$$

These quantities are used to draw an energy balance over the thermoelectric device and in a further step to determine the magnitudes for the performance description.

The energy conservation statement applied to the hot and cold junctions involves four quantities associated with the various energy transport mechanisms [9].
These are, for the hot junction:

- Thermal input (Q_H) from an outside heat source;
- Internal input from resistive heating (Q_{Joule});
- Electrical energy output from thermoelectric effect (P_{TE}); and
- Thermal output by conduction (Q_{Cond}) away from the hot junction toward the cold one.

For the cold junction, the contributions are:

- Thermal output (Q_C) to the cold source;
- Internal input from resistive heating (Q_{Joule});
- Electrical energy input of thermoelectric power (P_{TE}), and
- Thermal input from conduction (Q_{Cond}) from the hot junction.

These terms are summarized in Fig. 2.6, which shows the directions of the single terms. Note that there should no significance be given to the magnitude of the vectors in the drawing. Since the Seebeck coefficient is a function of temperature, the coefficient for the two junctions must be calculated from

$$\overline{\alpha} = \frac{1}{T_H - T_C} \int_{T_C}^{T_H} (\alpha_P - \alpha_N)\, dT \qquad \text{(Equ. 2.4)}$$

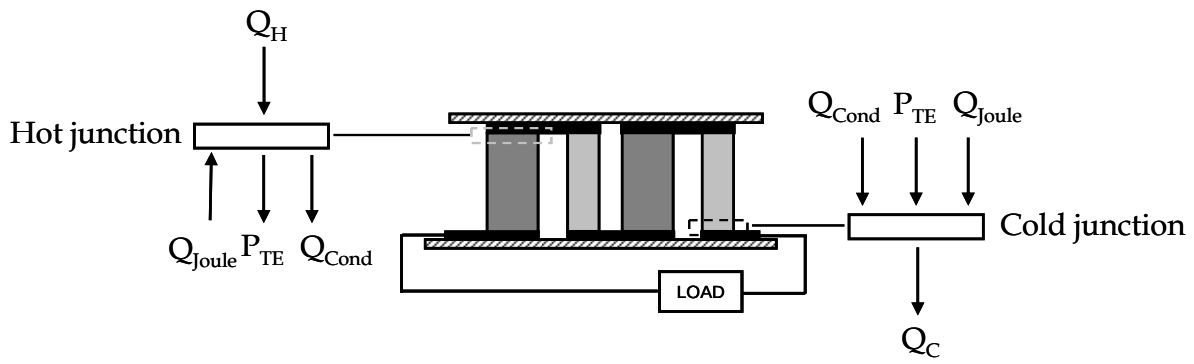

Figure 2.6: *Energy balances on thermoelectric junctions*

in order for the reversibility argument to be valid [9, 20]. This allows the writing of the hot and cold junction thermoelectric power terms as $n \cdot \overline{\alpha} \cdot T_H \cdot I$ and $n \cdot \overline{\alpha} \cdot T_C \cdot I$, respectively.

The magnitudes of the heat input and output are:

$$Q_H = n \cdot \overline{\alpha} \cdot T_H \cdot I + K \cdot \Delta T - \frac{1}{2} \cdot I^2 R \qquad \text{(Equ. 2.5)}$$

$$Q_C = n \cdot \overline{\alpha} \cdot T_C \cdot I + K \cdot \Delta T + \frac{1}{2} \cdot I^2 R \qquad \text{(Equ. 2.6)}$$

Note that for the materials of interest, it may be assumed that the temperature profiles are nearly linear and therefore the joule heating is equal from both cold and hot junctions [9, 20]. The conversion efficiency is the ratio of electrical power delivered to the load of resistance R_L relative to thermal power input:

$$\eta = \frac{I^2 \cdot R_L}{Q_H} = \frac{I^2 \cdot R_L}{n \cdot \overline{\alpha} \cdot T_H \cdot I + K \cdot \Delta T - \frac{1}{2} \cdot I^2 R} \qquad \text{(Equ. 2.7)}$$

This expression may be simplified by eliminating the current:

$$I = \frac{n \cdot \overline{\alpha} \cdot \Delta T}{R + R_L} = \frac{n \cdot \overline{\alpha} \cdot \Delta T}{R \cdot (1 + \mu)}; \quad \mu = \frac{R_L}{R} \qquad \text{(Equ. 2.8)}$$

where μ is a parametric measure of the load resistance relative to the generator resistance (equ. 2.8). The efficiency expression then becomes

$$\eta = \frac{\mu \cdot \Delta T}{(1+\mu) \cdot T_H + (1+\mu)^2 / Z - \Delta T/2} \qquad \text{(Equ. 2.9)}$$

Here Z is a figure of merit for the thermoelectric generator materials defined by

$$Z = \frac{n^2 \cdot \overline{\alpha}^2}{K \cdot R} \qquad \text{(Equ. 2.10)}$$

which is equivalent to the reciprocal of a characteristic temperature for the materials [9]. That this quantity represents a temperature may be deduced from the units or from the equation for η. Note that both *K* and *R* are proportional to *n*, so that Z is independent of it. This product may be written as

$$K \cdot R = n^2 \left(\frac{\kappa_p}{\sigma_p} \right) \cdot \left(1 + \frac{1}{x \, k_{pm}} + x \cdot \sigma_{pn} + \frac{\sigma_{pn}}{k_{pm}} \right) \qquad \text{(Equ. 2.11)}$$

where

$$\sigma_{pn} = \frac{\sigma_p}{\sigma_n}, \; k_{pn} = \frac{k_p}{k_n}, \text{ and } \; x = \frac{A_p}{A_n} \frac{L_n}{L_p} \qquad \text{(Equ. 2.12-2.14)}$$

The parameter x is a geometric factor, which can be chosen to maximize Z. [9] From Equation 2.11, the value of x for minimum KR is

$$x_{\min KR} = \frac{1}{\sqrt{k_{pn}\,\sigma_{pn}}} \text{ and} \qquad \text{(Equ. 2.15)}$$

$$(KR)_{\min} = n^2 \frac{k_p}{\sigma_p}\left(1+\sqrt{\frac{\sigma_{pn}}{k_{pn}}}\right)^2 \qquad \text{(Equ. 2.16)}$$

From this the maximum value of Z follows:

$$Z_{\max} = \left[\frac{\frac{1}{T_H - T_C}\int_{T_C}^{T_H}\alpha_{pn}\,dT}{\left(\sqrt{\frac{k_p}{\sigma_p}}+\sqrt{\frac{k_n}{\sigma_n}}\right)}\right]^2 \equiv \frac{1}{T^*} \qquad \text{(Equ. 2.17)}$$

Here $Z_{\max}$ is written in terms of a characteristic temperature because of its units. In order to see the variation of η with load resistance (μ), $Z_{\max}$ is treated parametrically, noting that its inverse varies between 200 and 1000 °K for the materials considered here. Fig. 2.7 shows this variation of η for the temperatures noted. The plot is for "nominal values", T_H = 900 K, T_C = 300 K, and T^* = 400 K. Individual changes from these values are given indicated. The Carnot efficiency of a heat engine operating between the temperatures of the nominal case is 0.67. For a fixed set of temperatures and choice of p and n materials, the efficiency depends only on the normalized load resistance $\mu = R_L/R$. The optimum load resistance is given by

$$\frac{\partial\eta}{\partial\mu} = 0 \text{ or}$$

$$\mu_{\max\eta} = \left(\frac{R_L}{R}\right)_{\max\eta} = \sqrt{1+Z_{\max}\cdot\frac{(T_C+T_H)}{2}} \qquad \text{(Equ. 2.18)}$$

from which the maximum efficiency may be determined using Equ. 2.9. It is not so appropriate to plot η as a function of reservoir temperatures (T_H and/or T_C) because the Seebeck coefficient is strongly temperature dependent, as is Z_{max} . The product ZT is of order unity or less and

strongly peaked between 400 and 1000 °K for a variety of materials. Since the current is determined by a fixed maximum voltage and resistances the voltage-current characteristic is linear with an open circuit voltage (V_{OC}) and short-circuit current (I_{SC}) given by:

$$V_{OC} = n \cdot \overline{\alpha_{pn}} \cdot \Delta T \qquad \text{(Equ. 2.19)}$$

$$I_{SC} = \frac{n \cdot \overline{\alpha_{pn}} \cdot \Delta T}{R} \qquad \text{(Equ. 2.20)}$$

where R is the generator internal resistance (Equ. 2.3). The linear voltage-current characteristic and resulting power output are sketched in Fig. 2.8 The ratio I/I_{SC} is related to the resistance parameter μ by

$$\frac{I}{I_{SC}} = \frac{1}{1+\mu} \qquad \text{(Equ. 2.21)}$$

The maximum power output is at half-open-circuit voltage and half-short-circuit current (as with all matched loads). The maximum power output is

$$P_{\max} = \frac{\left(m \cdot \overline{\alpha_{pn}} \cdot \Delta T\right)^2}{4 \cdot R} \qquad \text{(Equ. 2.22)}$$

and from Equ. 2.21 the load resistance at this point is R so that $\mu_{P\max} = 1$. One may conclude that the advantage of simple and potentially very reliable thermoelectric systems must be balanced with relatively low thermal efficiency. The load resistances for maximum power and maximum efficiency are not far from another (see Fig. 2.7).

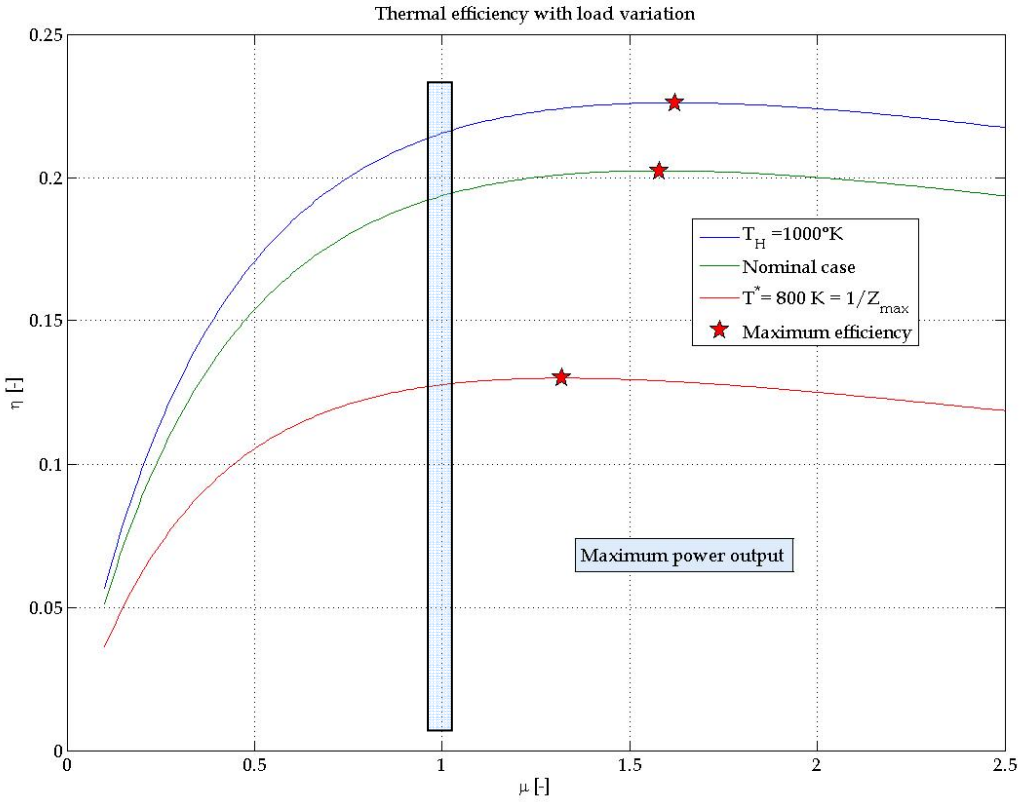

Figure 2.7: *Thermal efficiency variation with load resistance. Nominal case is T_H= 900 K, T_C= 300 K, and T* = 1/Zmax = 400 K. Other cases with changes are indicated. [9]*

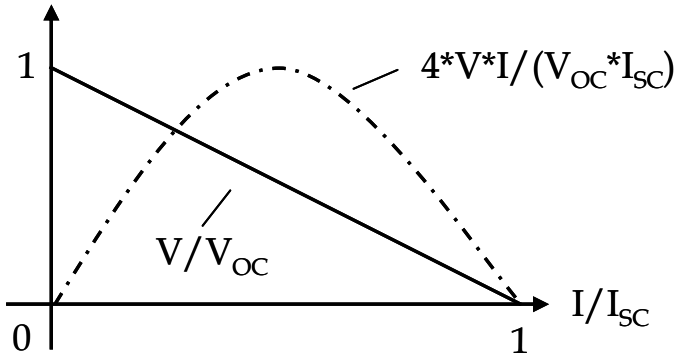

Figure 2.8: *Voltage – current and power characteristics of the thermoelectric generator [9]*

The efficiency at maximum power output is not much less than its absolutely possible maximum. The power output is scaled directly by the magnitude of the Seebeck effect voltage, which can be established for chosen materials. A small electrical resistance of the semiconductor helps to increase the power output, although this is not a property that can be readily manipulated. The above explanations all base on reversibility

and so do not include any terms of irreversibilities. This makes it impossible to optimize/evaluate loss sources for improving the performance of thermoelectric devices and generators.

2.3.2 Existing analytical models for thermoelectric devices and generators

The performance of a thermoelectric generator is influenced by both internal and external irreversibility [39]. The internal irreversibility is caused by the ohmic losses and conduction heat transfer, and the external irreversibility is caused by the temperature differences between the hot and cold junctions and the heat source and sink in the real thermoelectric generator. Wu [37] accounted for this in his theoretical analysis on waste-heat thermoelectric power generators. He developed an analytical model, which gave a much more realistic generator specific power and efficiency prediction than does the ideal thermoelectric generator. Rowe and Min [24-28] found a useful approximation for the performance values power output and conversion efficiency considering both thermal and electrical contact effects in the case of isothermal conditions at the hot and cold side of the module. The method was used to evaluate and optimize several commercially available modules and the results showed that a thermoelectric module is a promising device for low-temperature waste-heat recovery. Matsuura et al. and Rowe [15-18] found good expressions for the generator voltage, current and power output. An effective internal resistance of a single thermocouple, which is affected by fluid interaction conditions, was used to examine the maximum power output. Chen et al. [3, 5] analyzed the performance of a multi-couple thermoelectric generator with external and internal irreversibility applying an irreversible model. As a result the optimal range of the "parameter for device-design" was determined and the problems concerning maximum power output and maximum efficiency were discussed. Esarte et al. [10] used a NTU (Number of Transfer Units) – ε methodology to investigate the influence of fluid flow rate, heat exchanger geometry, fluid properties and inlet temperatures on the electrical power supplied by the thermoelectric generator. In this work strategies and procedures for the determination of the optimum operating parameters of a thermoelectric generator can be found.

Stevens [30] developed a procedure for the design of a thermoelectric generator utilizing small temperature differences. For a fixed thermal resistance in the heat exchangers, the optimal configuration splits the total temperature drop equally between the thermoelectric modules and the heat exchangers. For time-varying heat exchanger thermal resistances optimal configurations were also derived for linear, sawtooth function and sinusoidal variations [39]. Chen et al. [4] studied the performance of a multi-element thermoelectric generator with the irreversibility of finite-rate heat transfer. The influence of heat transfer and the number of elements on the performance were analyzed. As a conclusion it was stated that the optimal structure parameters must be chosen from the points of view of the compromise optimization between power output and efficiency in order to obtain the best performance [39]. Pramanick and Das [23] performed a study on "constructal design" of a thermoelectric device. Employing finite time thermodynamics a model for a cascaded module thermoelectric generator, which incorporated all the essential features of a real heat engine, was developed. In the model, control volume formulation of cascaded thermocouples was carried out over a small but finite temperature gap to comply with the principles of irreversible thermodynamics. Also various design considerations were discussed to optimize the device performance.

In the literature quoted above, those publications have mainly been focused on the analytical analysis of single or multiple thermoelectric elements for thermoelectric power generation. These analytical methods provided some significant guidelines for the design of thermoelectric devices in terms of the principles of thermodynamics.

2.3.3 Existing numerical models of thermoelectric generators

In practical situations a real thermoelectric generator always combines thermoelectric modules with the specific heat exchangers in very large scale installations to produce useful amounts of electricity from low-grade heat sources [39]. Therefore, research on the constructive design of the thermoelectric conversion systems and operating performance also has attracted researchers' wide attention in this area. Suzuki and Tanaka [34] studied thermoelectric power generation with large-scale flat thermoelectric panels exposed to two thermal fluids. Electric power was estimated in case of the large-scale flat thermoelectric panels exposed to two thermal fluids. The output powers of the proposed 15 systems were analytically deduced from heat transfer theory, and written by non-dimensional functions to reflect the characteristics of system design. The multiplication of thermoelectric panels can shorten significantly the device area, although the output from the multi-panels decreases a few percent. The worse heat conductivity, λ of thermoelectric materials and the better heat transfer at the surfaces are desired for these fluid systems, in addition to the better figure of merit, Z. Further studies on the thermoelectric power generation with cylindrical multi-tubes and roll-cake type tubes were carried out in a similar way by Suzuki and Tanaka [32, 33, 35]. Crane and Jackson [8] investigated thermoelectric generators with advanced heat exchangers for waste-heat recovery. Numerical heat exchanger models integrated with models for Bi_2Te_3 thermoelectric modules were created and validated. The results showed that heat exchangers with Bi_2Te_3 thermoelectrics could achieve net power densities over 40 W/m^2.

Generally, in the case of thermoelectric generator which involves different types of heat exchangers, the problem of the heat transfer through heat exchanger and the thermal energy conversion becomes very complex [39]. More precise analysis of large scale thermoelectric generators with the concrete type of heat exchanger should be taken into consideration in order to estimate the device performance. The numerical analysis provides therefore an effective approach for evaluating the performance of thermoelectric generators. In particular, the numerical approaches are able to offer much more detailed information as analytical methods [39].

Although, some work has been done in previous literature, more information such as the temperature changes at heat exchanger and the temperature difference through thermoelectric elements in the thermoelectric generator with the concrete type of heat exchanger is required to identify aspects of further improvement on thermoelectric generators for power generation [39], what will be main part of this work.

Chapter 3

Scope of the work - Assignment of tasks

The development of useful tools for the evaluation of power generating systems based on thermoelectric generators is the general topic of this work. The focus will be on general studies utilizing low temperature heat sources such as renewable energy sources and waste heat. This chapter describes the questions to be addressed and shows a modus operandi to reach the defined goals (chapter 1.4).

Many analytical and numerical models for thermoelectric generators as well as design rules can be found in the literature, as summarized in chapter 2. Unfortunately, some of them are very limited in usefulness due to restrictive boundary conditions or due to not considering Peltier heat or effective internal resistance. The aim is to link together the best known models of thermoelectric generators and to combine it with a model of a heat transfer system. Both power output and efficiency of a real large scale thermoelectric generator supplied by convective heat sources will be evaluated varying several parameters. The model should enable to define the optimal generator assembly, running conditions and system integration.

3.1 Modelling of thermoelectric devices and generators

Considering the possibility of power generation from low temperature heat sources using thermoelectric devices, necessary tools for the evaluation and optimization of thermoelectric generators and devices shall be prepared. The adaptability of the design of thermoelectric generators permits optimisation to suit the source of thermal energy. For example, if the heat is costly the conversion efficiency will be a main consideration. In applications where space is at a premium, minimising the volume is a priority, while in applications where the heat is almost for free (waste heat recovery), reducing capital costs becomes a main objective. To fulfil these and above named requirements the following modelling procedure has been developed and is presented in figure 3.1.

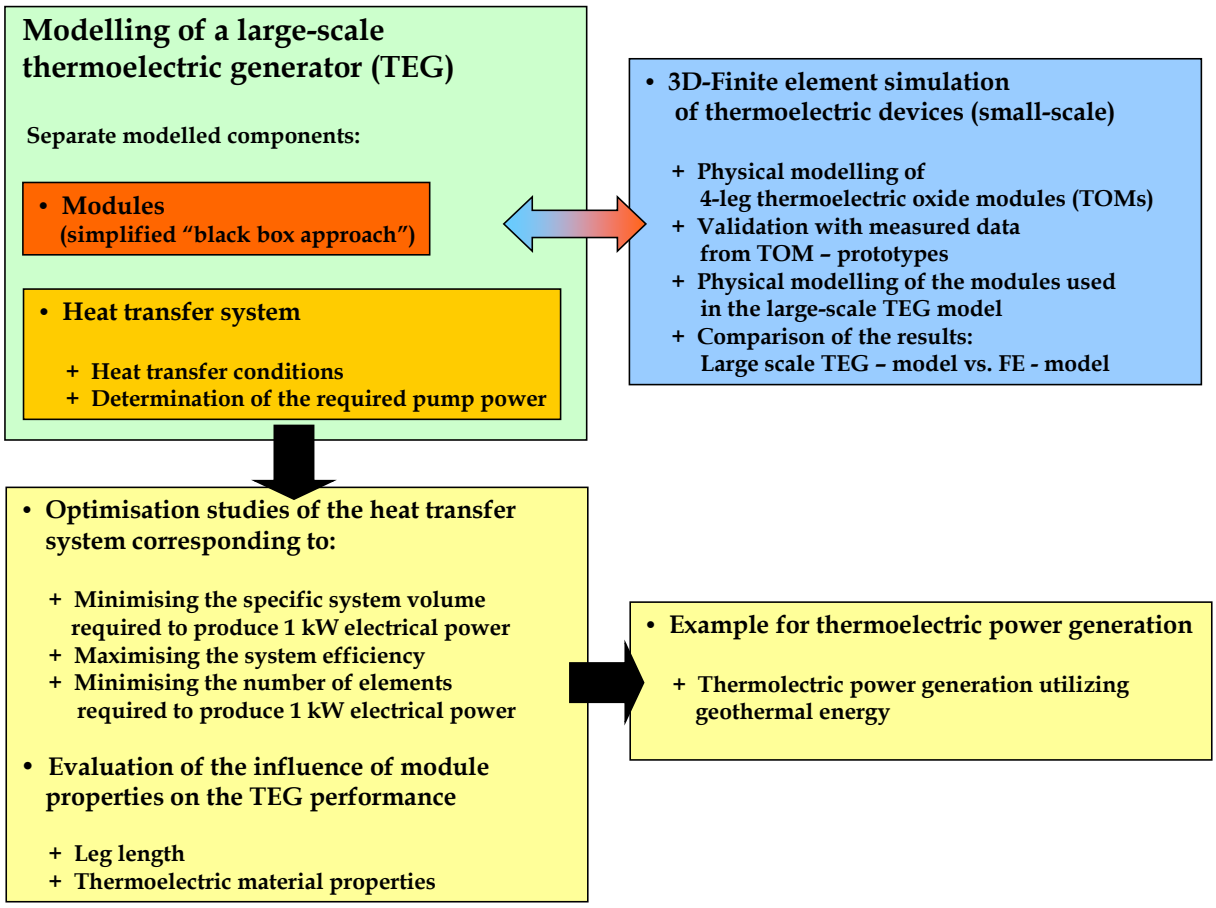

Figure 3.1: *Flowchart of the procedure executed in this work*

In a first step a realistic theoretical model of a large scale thermoelectric power generator will be developed. The model describes the essential elements of a thermoelectric generator: these are the heat transfer system and the thermoelectric devices itself. Here the thermoelectric devices are simplified described as a kind of a "black box" consisting of a large number of thermoelectric couples characterized by its dimensions and average material properties. Linearity and one-dimensionality of temperature and electrical potential distributions are also assumed for above mentioned examinations. To evaluate if these simplifications are acceptable a physical 3D model of small scale thermoelectric devices, including all nonlinearities and irreversibilities will be developed and simulated with the method of finite elements. The results of this simulation will be validated with the experimental data of thermoelectric prototype modules created at EMPA Dübendorf.

If the validation of the 3D model leads to a good fit with the experimental data a possible usage of the simulation as development tool will be given.

Furthermore, the blackbox assumptions will be compared with the simulation results, checked on compatibility and adapted if required.

Using the proofed large-scale model, procedures to optimise the heat transfer system will be developed. The optimum dimensions of the heat transport system to convey the thermal energy to and off the thermoelectric generator should be explored corresponding to the following objectives:

- Minimising the *size* of the system (system volume) required to produce one kilowatt electric power
- Maximising the system *efficiency* or maximizing the electrical *power output*
- Minimising the *number* of thermoelectric modules (costs) to produce one kilowatt of electrical power.

Also the influence of module properties on the performance of the TEG will be investigated. Therefore the leg length of the modules and the thermoelectric material properties will be the varied parameters. Last, a representative example for thermoelectric power generation utilizing geothermal heat will be given.

Summarizing a list of the main tasks of this work is given.

Approach and list of tasks for this work:

- Evaluation of existing analytical and numerical models from single couples to total thermoelectric generators integrated in heat exchanger units,
- Synergetic combination or integration of models or parts of models to increase the consideration of relevant effects (contact effects, thermal interfaces,…),
- Development of a 3D–finite element model to verify the simplifying assumptions still existing in the analytical/numerical model,
- Validation of the 3-D model with prototype modules,
- Optimization and evaluation studies on large-scale thermoelectric generators with representative example

3.2 Relation to other research activities

In cooperation with EMPA Dübendorf the project "Das thermoelektrische Kraftwerk" has been initiated, sponsored by the Swiss Federal Office of Energy.

The main goal of this project is to show the feasibility of a thermoelectric power plant by theoretical considerations and selective experiments. Therefore highly efficient novel thermoelectric materials exhibiting low heat conductivity, small resistivity and large Seebeck coefficients are under development at the Solid State Chemistry and Analyses Group at EMPA Dübendorf. First prototypes created with these materials will be used for the validation of the 3D model mentioned in the previous chapter (3.1).

Chapter 4

Modelling a large-scale thermoelectric generator

Modelling approach:

A large scale thermoelectric generator consists in essence of a large number of thermoelectric modules sandwiched between heat transfer tubes, which carry the warm input and cold output flows of the working fluid (figure 4.1a).

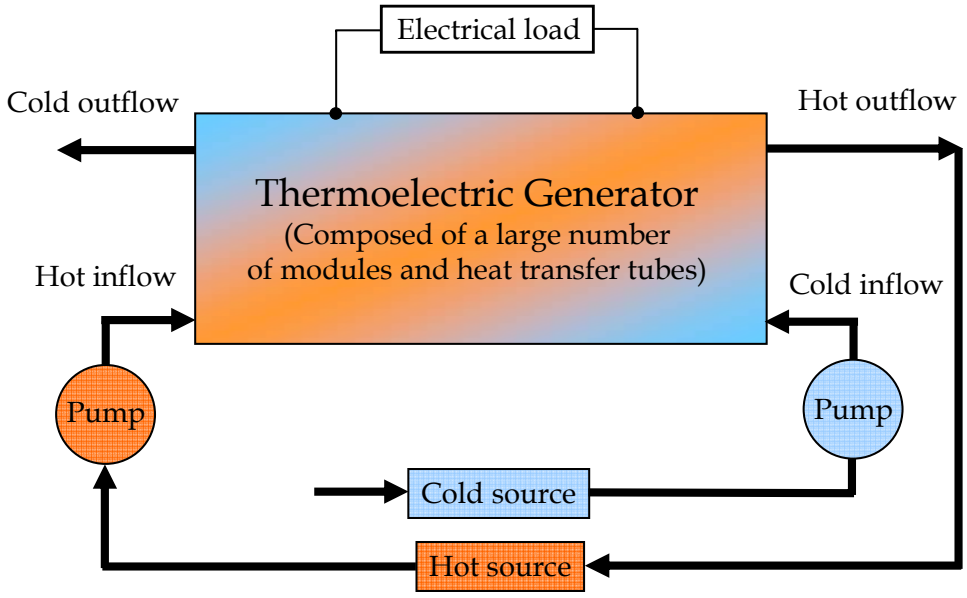

Figure 4.1a: *Basic arrangement of a complete thermoelectric generator system*

The design of the generator is therefore considered from the point of view of optimising both the modules and the heat transfer system. A realistic model of a thermoelectric generator has been developed by combining established model approaches with new features. The numerical model in general is a one-dimensional description with using a control volume approach along with the method of average

parameters. For the heat transfer unit a parallel-plate heat exchanger with of counter flow type was selected. The following assumptions to simplify the modelling have been made.

- The axial heat conduction within the thermocouples is ignored, as transverse conduction along the thermocouples will be dominant.
- The surfaces of the TEG exposed to the ambient are thermally ideal insulated.
- The thermal contact resistance between the heat exchanger plates and the modules are ignored
- The gap between the thermoelectric legs are ignored

Following the above assumptions a more detailed description of the modelling of the several components is given in the next chapters.

4.1 Thermoelectric generator modelling

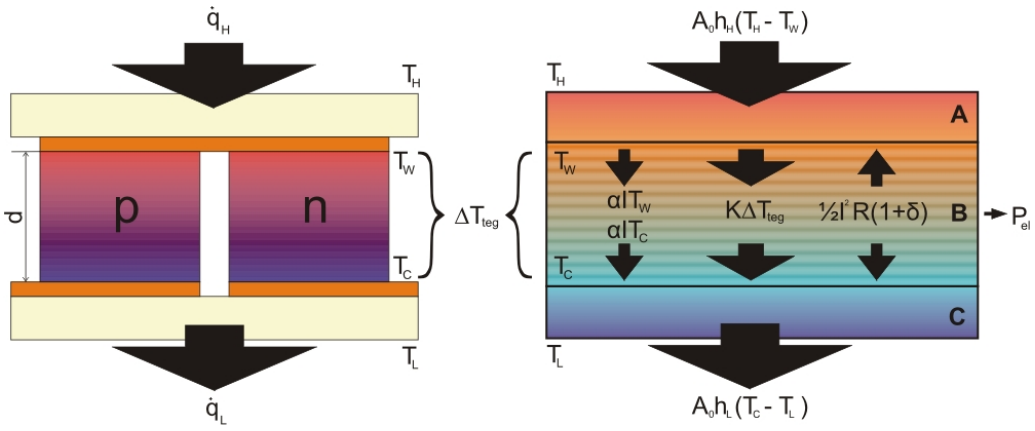

Figure 4.1b: *Scheme of thermocouple (left), segmentation of theTEG for modelling (right)*

For modelling, the TEG was divided into three main parts as shown in figure 4.1b.

Part A (hot side) in figure 4.1b includes the bottom plate of the heat exchanger, the electrical insulating plate (ceramic) and the conducting

copper strips. The overall heat transfer coefficient h_H, which links the heat transfer from the (hot) fluid to the hot side of the legs is given by

$$h_H = \frac{1}{\frac{1}{h_{Wf}} + \frac{l_{ceramic}}{\lambda_{ceramic}} + \frac{l_{copper}}{\lambda_{copper}}} \qquad \text{(equ. 4.1a)}$$

Similar for the part C (cold side) the heat transfer coefficient is given by

$$h_C = \frac{1}{\frac{1}{h_{Cf}} + \frac{l_{ceramic}}{\lambda_{ceramic}} + \frac{l_{copper}}{\lambda_{copper}}} \qquad \text{(equ. 4.1b)}$$

$l_{ceramic}$ and $\lambda_{ceramic}$ are the thickness and the thermal conductivity of the ceramic layer, respectively, l_{copper} and λ_{copper} are the thickness and the thermal conductivity of the copper layer. h_{Hf} and h_{Cf} are the convective heat transfer coefficients from the fluid to the inside surface of the flow channel at the hot and cold sides.

From the modelling view part B is a layer of two different thermoelectric materials (p-, n- doped semiconductors), segmented in blocks with the thickness d and average values of the material properties.

Therfore two important quantities used in the following are defined.

The internal resistance R describes the electrical resistance and K is the heat conductance of the thermocouple legs:

$$R = \frac{\rho_n \cdot d}{A_n} + \frac{\rho_p \cdot d}{A_p} \qquad \text{(equ. 4.2a)}$$

$$K = \frac{\lambda_n \cdot A_n}{d} + \frac{\lambda_p \cdot A_p}{d} \qquad \text{(equ. 4.2b)}$$

The energy balance equations along the heat transfer tube of a single thermocouple are given as follows:

$$\dot{q}_{H_i} = A_0 \cdot h_H \cdot \left(T_{H_i} - T_{W_i}\right) \qquad \text{(equ. 4.3)}$$

$$\dot{q}_{H_i} = K \cdot \Delta T_{teg_i} + \alpha I T_{W_i} - \frac{1}{2} I^2 R(1+\delta) \qquad \text{(equ. 4.4)}$$

$$\dot{q}_{L_i} = A_0 \cdot h_C \cdot \left(T_{C_i} - T_{L_i}\right) \qquad \text{(equ. 4.5)}$$

$$\dot{q}_{L_i} = K \cdot \Delta T_{teg_i} + \alpha I T_{C_i} + \frac{1}{2} I^2 R(1+\delta) \qquad \text{(equ. 4.6)}$$

$A_0 \cdot h_H \cdot \left(T_{H_i} - T_{W_i}\right)$ is the heat flux from the convective heat source through part A with the surface area A_0, which is the heat exchanger area corresponding to one single thermocouple. This heat flux has to be in equilibrium with the thermal energy going into part B. At this interface the expression for the energy comprises out of the terms for heat conduction $K \cdot \Delta T_{teg_i}$, the term for the Peltier heat $\alpha I T_{W_i}$ and the term for Joule losses $0.5 \cdot I^2 R(1+\delta)$. It is assumed here that one half of the Joule losses goes to the hot side and one half to the cold side and that all the surfaces exposed to the ambient are insulated (no losses due to radiation or natural convection). In the numerical calculation of a large scale thermoelectric generator the single thermocouples are connected electrically in series and thermally in parallel. The index i therefore identifies the ith thermocouple of a series connection of N thermocouples. At the cold side the heat flux emerges in a similar way, as described by equation 4.5. The generated electrical power is evaluated by equations 4.12 and 4.13.

$$\Delta T_{teg_i} = T_{W_i} - T_{C_i} \qquad \text{(equ. 4.7)}$$

$$T_{H_{i+1}} = T_{H_i} - \frac{\dot{q}_{H_i}}{C_p \dot{m}_H} \qquad \text{(equ. 4.8)}$$

$$T_{L_i} = T_{L_{i+1}} + \frac{\dot{q}_{L_{i+1}}}{C_p \dot{m}_L} \qquad \text{(equ. 4.9)}$$

$$I = \frac{\sum_{i=1}^{N} \alpha \cdot \Delta T_{teg_i}}{NR(1+\delta) + R_L} \qquad \text{(equ. 4.10)}$$

$$V = I \cdot R_L \qquad \text{(equ. 4.11)}$$

$$P_{el} = I^2 R_L = \sum_{i=1}^{N} \left(\dot{q}_{H_i} - \dot{q}_{L_i}\right) \qquad \text{(equ. 4.12)}$$

$$= \sum_{i=1}^{N} \left(\alpha I T_{W_i} - \alpha I T_{C_i}\right) = I \sum_{i=1}^{N} \alpha \Delta T_{teg_i} \qquad \text{(equ. 4.13)}$$

$$\eta = \frac{P_{el}}{\sum_{i=1}^{N} \dot{q}_{H_i}} \qquad \text{(equ. 4.14)}$$

Electrical contact resistances are also included as thermal contact resistances of the contact layers as well as the contact resistance between

the fluid and solid part of the generator are combined in the overall heat transfer coefficients $h_{H,C}$, as explained above.

$\dot{m}_H$ and $\dot{m}_L$ are the mass flow rates through the hot and cold side heat transfer tubes. The mass flow rates can be varied independently to adjust to various applications respectively to adjust them for considered heat transfer coefficients depending on the various fluid conditions.

In steady – state the resulting current I depends on the sum of the generated voltage of all thermocouples the internal resistance, the load resistance and the relation $\delta = R_C/R$ between the electrical contact resistance and the internal resistance as described in equation 4.10.

Up to here the heat transfer from the working fluid to the TEG was described by the overall heat transfer coefficients h_H and h_C. Considering a realistic configuration of a TEG with heat transfer tubes of defined dimensions, the correlations and conditions to get the desired heat transfer coefficients need more detailed description, what is the task of the following explanations.

4.2 Modelling of the heat transfer system

A configuration for a thermoelectric generator in form of a stack structure is shown in figure 4.2. The heat transfer system, a parallel-plate cross-flow heat exchanger, is described by its main geometric dimensions, such as:

- L the length of the heat transfer tubes,
- D the depth of the heat transfer tubes and
- W the width of the heat transfer tubes

A TEG unit comprises one layer of thermoelectric modules sandwiched between half a hot fluid flow heat transfer tube and half a cold fluid flow heat transfer tube.

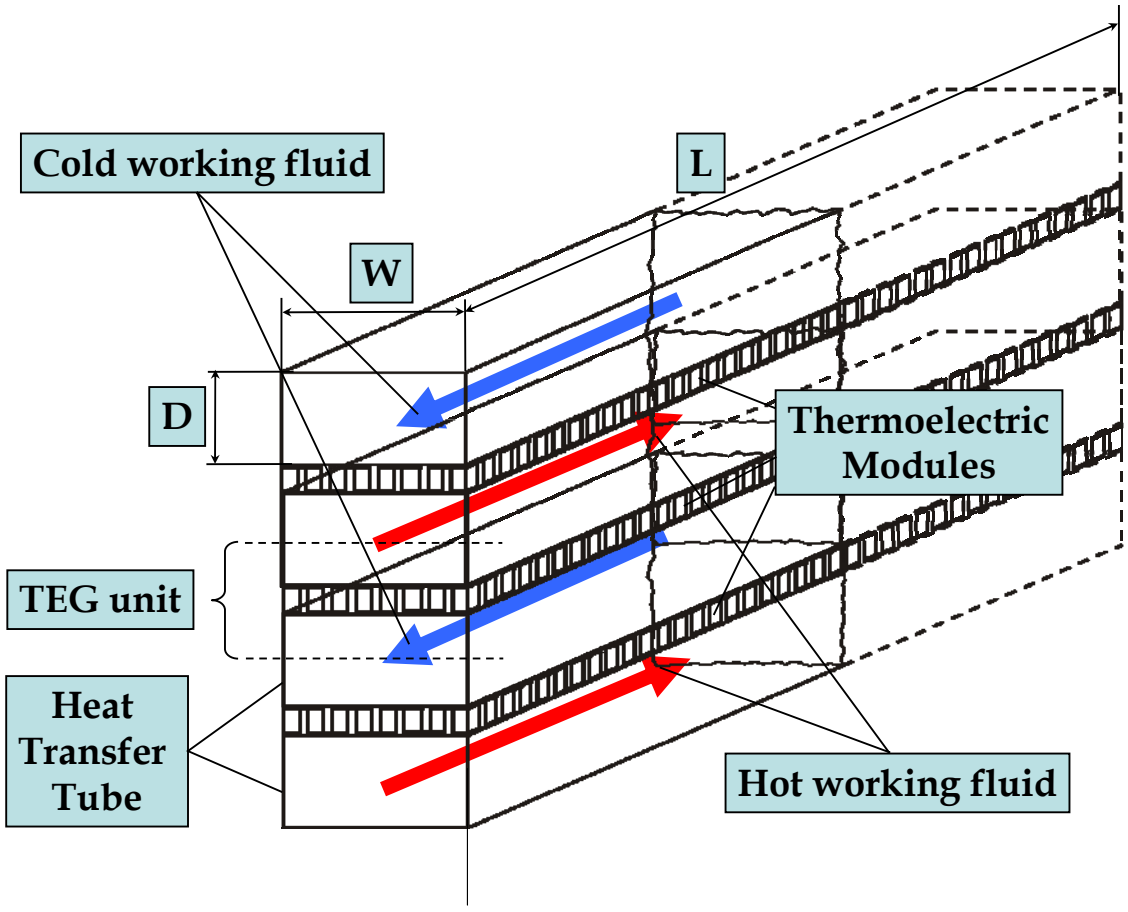

Figure 4.2 : *Configuration of a large scale thermoelectric generator*

As already mentioned in 4.1 h_{Hf} and h_{Cf} are the convective heat transfer coefficients between the fluid and the inside surface of the flow channel

at the hot and cold side and are calculated by *Hausen* [36] for laminar fluid flow and constant heat flux:

$$\frac{h_f d_H}{\lambda_f} = Nu_f = 4.65 + \frac{0.19 \cdot \left(\mathrm{Re}_f \cdot \mathrm{Pr}_f \cdot \frac{d_H}{L} \right)^{0.8}}{1 + 0.117 \cdot \left(\mathrm{Re}_f \cdot \mathrm{Pr}_f \cdot \frac{d_H}{L} \right)^{0.467}} \qquad \text{(equ. 4.15)}$$

the friction factor ξ_f for later calculations of the head losses due to friction for the laminar case is given as:

$$\xi_f = \frac{64}{\mathrm{Re}_f} \qquad \text{(equ. 4.16)}$$

Area of validity and definitions:

$$\mathrm{Re}_f < 2300 \quad \mathrm{Re}_f = \frac{\bar{v}_f \cdot d_H}{\nu_f} \qquad \text{(equ. 4.17)}$$

for turbulent fluid flow the coefficients are given by *Gnielinski* [36]:

$$\frac{h_f d_H}{\lambda_f} = Nu_f = \frac{\frac{\xi_f}{8} \cdot \left(\mathrm{Re}_f - 1000 \right) \cdot \mathrm{Pr}_f}{1 + 12.7 \cdot \sqrt{\frac{\xi_f}{8}} \cdot \left(\mathrm{Pr}_f^{2/3} - 1 \right)} \cdot \left[1 + \left(\frac{d_H}{L} \right)^{2/3} \right] \qquad \text{(equ. 4.18)}$$

with ξ_f as the friction factor by *Filonenko* [36]

$$\xi_f = \frac{1}{\left(1.82 \cdot \log\left(\mathrm{Re}_f \right) - 1.64 \right)^2} \qquad \text{(equ. 4.19)}$$

Area of validity and definitions:

$$\mathrm{Re}_f > 2300 \quad \mathrm{Re}_f = \frac{\bar{v}_f \cdot d_H}{\nu_f} \qquad \text{(equ. 4.20)}$$

N_{uf} is the Nusselt–number, Re_f the Reynolds–number, and Pr_f the Prandtl–number of the particular fluid flow (hot, cold).

d_H (equ.4.19) is the characteristic diameter, defined as 4 times the wetted section divided by the wetted perimeter, and λ_f, ν_f, φ_f, are the relevant fluid properties heat conductivity, kinematic viscosity and density. v_f is the average fluid velocity.

$$d_H = \frac{4 \cdot A_{tube}}{U_{tube}} = \frac{4 \cdot (W \cdot D)}{(2 \cdot W + 2 \cdot D)} \qquad \text{(equ. 4.21)}$$

In the definition of the Reynolds number (equation 4.18) the average fluid velocity is included. Together with the geometrical dimensions of the flow channel and the fluid properties the required mass flow rates (equation 4.22) for the assumed heat transfer coefficients can be found.

$$\dot{m} = \rho \cdot \dot{V} = \rho \cdot A_{tube} \cdot \overline{v} \qquad \text{(equ. 4.22)}$$

The mass flow rates are also an important quantity for the determination of the required pump power, which can not be ignored especially for optimisations according to the minimization of the system volume, what presumably leads to very shallow heat transfer ducts.

4.2.1 Determination of the required pump power

As the power consumption of the pumps is not assumed negligible, the following formulations are used for the determination of the required pump power to circulate the fluid flows.

$$P_{pump} = \begin{bmatrix} \dot{V}_{fH} \cdot \rho_{fH} \cdot g \cdot \left(H_{pH} + H_{fH}\right) + \\ \dot{V}_{fC} \cdot \rho_{fC} \cdot g \cdot \left(H_{pC} + H_{fC}\right) \end{bmatrix} / \eta_{pump} \quad \text{[W]} \qquad \text{(equ. 4.23)}$$

$H_{pH} = H_{pC}$ pressure required to circulate the working fluid outside the TEG [mWC] (equ. 4.24)

$$H_{fH} = \xi_{fH} \cdot L \cdot \frac{v_{fH}^2}{2 \cdot g \cdot d_H} \quad \text{[mWC]} \qquad \text{(equ. 4.25)}$$

$$H_{fC} = \xi_{fC} \cdot L \cdot \frac{v_{fC}^2}{2 \cdot g \cdot d_H} \quad \text{[mWC]} \qquad \text{(equ. 4.26)}$$

where H_{pH} and H_{pC} are the assumed pressures to circulate the hot and cold fluids outside the heat exchanger. H_{fH} and H_{fC} are the head losses in the heat transfer tubes due to friction. η_{pump} is the pump efficiency with an assumed value of 0.9.

For TEG unit shown in figure 4.2 and defined above the left sides of equations 4.3 – 4.6 have to be multiplied by the factor 2 (heat transfer out of the fluid at two sides, top and bottom).

Further on the net generated electrical power is given as:

$$P_{net} = P_{el} - P_{pump}/2 \qquad \text{(equ. 4.27)}$$

with the generated electrical power P_{el} given by

$$P_{el} = 0.5 \cdot \sum_{i=1}^{N} \left(\dot{q}_{H_i} - \dot{q}_{L_i} \right) \qquad \text{(equ. 4.28)}$$

and the total resulting efficiency is

$$\eta_{total} = \frac{P_{el} - P_{pump}/2}{0.5 \cdot \sum_{i=1}^{N} \dot{q}_{H_i}} \qquad \text{(equ. 4.29)}$$

The quantities defined in equations 4.27 - 4.29 will be used in the optimisation and evaluation studies (chapter 6) for the description of the performance of the investigated thermoelectric power generation systems.

The numerical model described by equations 4.1 – 4.29 has been implemented in a MATLAB (www.matlab.com) script applying two solution methodologies. First in an iterative method the mass flow rates for the assumed heat transfer coefficients are determined. Based on these values, in a second step using a finite volume method the temperature profiles along the heat transfer tubes respectively in consequence the performance quantities are calculated. Before using the model with quiet conscience some further clarifications have to be done.

In the approach given in the beginning of this chapter the simplifying assumptions concerning the module modelling have been given. To proof these on compatibility a physical model using the method of the finite elements has been developed and will be explained in the following.

Chapter 5

Modelling small scale thermoelectric devices

To proof the compatibility of the assumptions made in chapter 4 concerning the thermoelectric part (modules) of the large scale thermoelectric generator model and to have a tool for evaluation and optimization of future module designs with various (new) materials an adequate model as a base for the 3-D simulation of the coupled thermal and electrical problem using the method of the finite elements had to be developed and validated.

- **3D-Finite element simulation of thermoelectric devices (small-scale)**

  + **Physical modelling of 4-leg thermoelectric oxide modules (TOMs)**
  + **Validation with measured data from TOM – prototypes**
  + **Physical modelling of the modules used in the large-scale TEG model**
  + **Comparison of the results: Large scale TEG – model vs. FE - model**

Figure 5.1a: *Overview of the modelling and validation procedures on small-scale devices*

A general overview of the procedure concerning modelling, simulation and validation presented in this chapter is given in figure 5.1.

Modelling approach

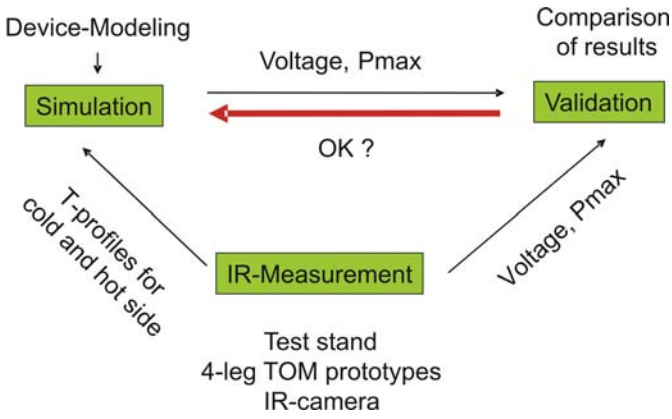

Figure 5.1b: *Overview of the interacting procedures (simulation and measurement)*

Based on the work of Hogan and Shih [11] an appropriate, physical model of a thermoelectric device has been developed and evaluated with COMSOL (www.comsol.de) Multiphysics, a 3D-finite element tool for coupled physical problems (see details in 5.1). The validation was done by the comparison of the quantities load voltage and power output from the simulated results and the experimental data. The experimental data were taken from micro-thermographic measurements of the temperature distribution and standard data logging of the electrical behaviour. Therefore 4-leg TOMs (Thermoelectric Oxide Modules) were assembled and a test stand, consisting of the components for heat supply and removal, the clamping fixture in combination with a scale to obtain well-defined, reproducible results and the measuring equipment (like IR-camera, data logging unit,…), was designed. The interacting of measured data and simulation results is presented schematically in Figure 5.1b.

5.1 Finite element modelling of thermoelectric devices

In the initial derivation of formulas (chapter 2) for the performance of thermoelectric devices it has been assumed that the Seebeck coefficient, the electrical resistivity and the thermal conductivity of thermoelectric elements are independent of temperature. Here these assumptions have been substituted by the general case where all three parameters are arbitrary functions of temperature. Three approaches to the general problem of temperature variation of the parameters are known. The simplest method, as used in chapter 4 for the large scale TEG modelling, is to substitute average values for all the parameters occurring in the equations derived for the constant - parameter case. A rather different approach is to calculate the performance by breaking up the working temperature interval into an infinite number of stages. An analytically exact technique determines the efficiency by setting up the governing equations for the full generator. These methods assume the temperature and electric potential distributions to be one-dimensional. In general this is an arguable assumption, but there are some (boundary) conditions for which these assumptions are not valid. With 3D-finite element (FE) modelling and simulation multidimensional effects caused by heat transfer (e.g. natural convection and/or radiation) can be illustrated. An adequate model using the equations for steady-state multidimensional temperature and electrical potential distributions in thermoelectric materials has been developed. Here the numerical solution has been performed with segregated parametric solvers of the 3D finite elements tool COMSOL Multiphysics.

5.1.1 Governing equations and implementation in the FE-tool COMSOL Multiphysics

The equations governing the multidimensional temperature and electrical potential distributions in TE materials under steady-state conditions and in the absence of an applied magnetic field are the energy equations (equations 5.1a and 5.1b) and the current flow equation with the condition for direct current (equation 5.2). A detailed derivation of these equations can be found in Appendix A.

$$\nabla(\lambda \cdot \nabla T) - T \cdot J \cdot \left(\frac{\partial \alpha}{\partial T}\right) \cdot \nabla T + \rho \cdot J^2 = 0 \qquad \text{(Equ. 5.1a)}$$

$$q = \alpha \cdot T \cdot J - \lambda \cdot \nabla T \qquad \text{(Equ. 5.1b)}$$

$$J = -\sigma \cdot [\nabla V + \alpha \cdot \nabla T],\ \nabla \cdot J = 0 \qquad \text{(Equ. 5.2)}$$

Here the vector J is the electric current per unit area, the vector q is the heat transfer rate per unit area, T is the temperature, λ is thermal conductivity at zero current, $\sigma = 1/\rho$ is electrical conductivity, ρ is electrical resistivity, α is the absolute Seebeck coefficient (thermoelectric power) and V is the electrostatic potential. All the materials properties are functions of temperature. These functions are based here on interpolation of measured data. The equations above form a system of two direct coupled partial differential equations with two dependent variables the temperature T and the electrical potential V. In COMSOL Multiphysics the geometry can easily be modelled by using the internal CAD tool.

Specifiying Physics settings

The implementation of the PDE's is realized by using the physical application modes Conductive Media DC and General Heat Transfer. The description of the physics of the model respectively the various model parts (subdomains) has been done in the subdomain settings. There different values for each subdomain such as material properties, sources and sinks that define the physics in the subdomain can be set. By using the above named application modes the software performs the translation into PDE coefficients automatically. The nonlinear material properties can easily be implemented by defining a function and connect it with the particular data file in the expected format. Further there is the

possibility to deactivate subdomains if they should not be involved in one of the application modes, such as the electrical insulating ceramic plates in the Conductive Media DC application mode. This is important and useful as it helps to minimize memory demand and calculating time without loosing important information.

After defining the physics of the various model parts (subdomains) it is important to define a correct condition to each boundary of the model so that the system converges to a single solution.

Specifiying Boundary conditions (BC's)

The boundary conditions (BCs) for the heat transfer part are as follows:

For all surfaces exposed to the ambient the BC is a combination of convection and heat transfer by radiation (examples see figure 5.3). The only exceptions are the two outer surfaces, where the constant temperatures in combination with a heat transfer coefficient for the hot and cold sides are given. (figure 5.2)

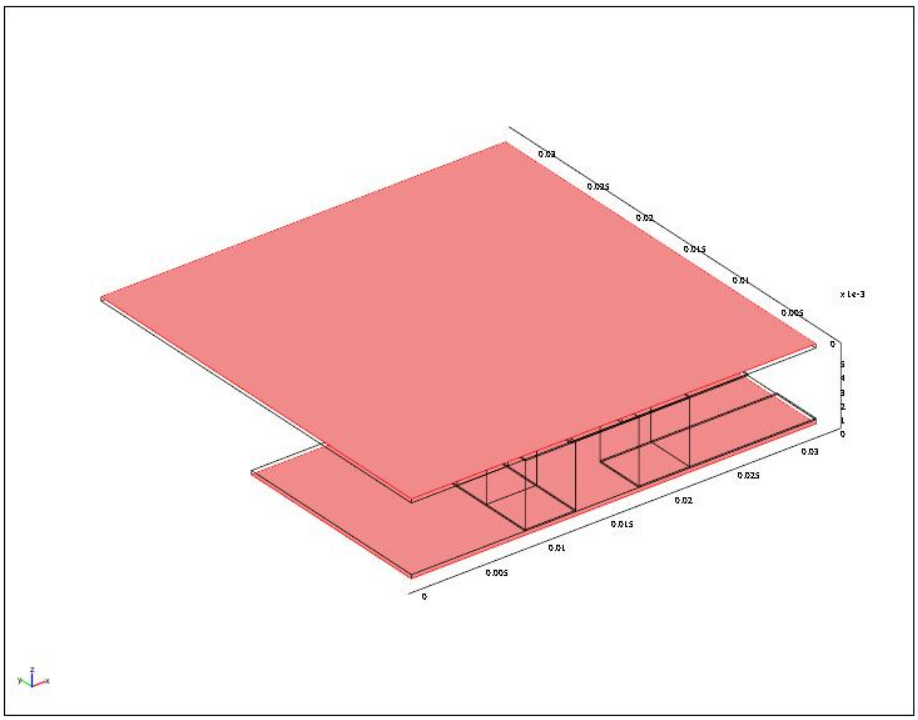

Figure 5.2: *Geometric model of a TOM 5 mm leg length with highlighted boundaries (red) for the hot and cold side*

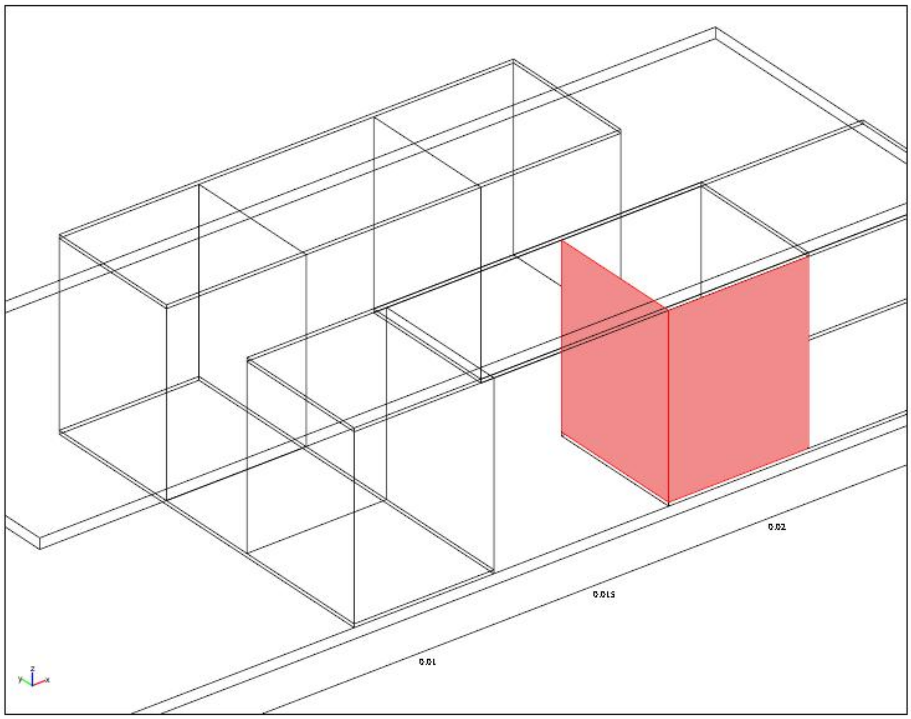

Figure 5.3: *Example surfaces with boundary condition considering heat losses due to convection and radiation*

For the electrical part, the BCs have the meaning of electrical insulation which is defined as $J \cdot n = 0$. This means the current must be parallel to the surface, where n is the unit vector normal to the surface (see figure 5.4). At both ends of the electrical circuit different BCs have to be applied. In the case of the high electrical potential end the BC is called "Distributed resistance" as described by $J \cdot n = \sigma \cdot (V - V_{ref}) / d$ (see figure 5.5). This describes a sheet of resistive material. The sheet which has the thickness d is connected to the voltage V_{ref}. With this BC it is possible to take into account the resistance of the connecting wires to the load resistance network and to vary the load resistance itself as the variable parameter. The voltage V_{ref} and the voltage at the other end of the circuit is set to zero to close the electrical circuit. V is the generated voltage of the module.

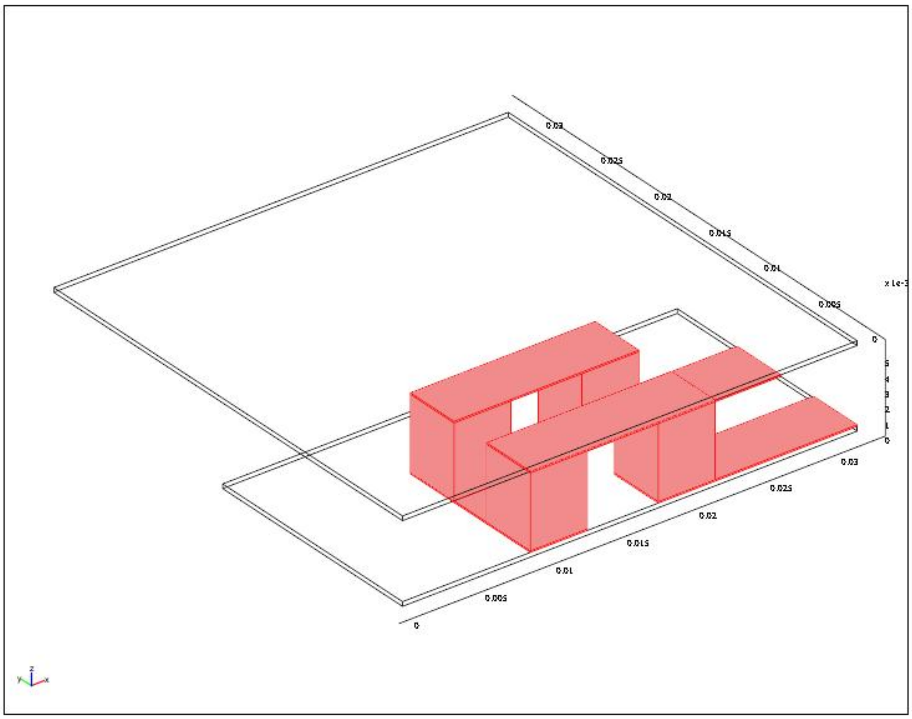

Figure 5.4: *Surfaces with boundary condition "electrical insulation"*

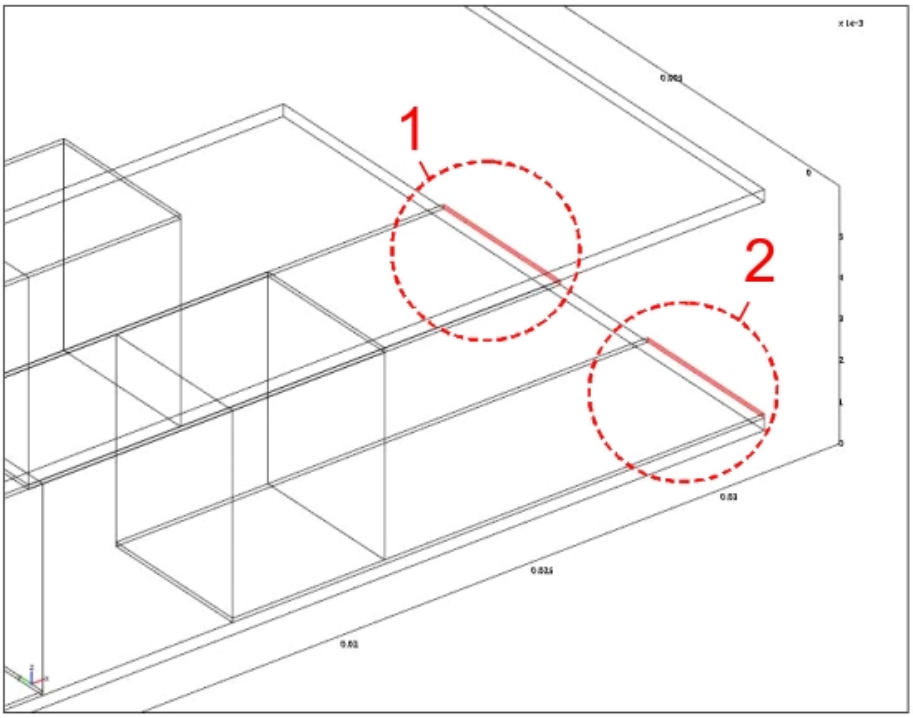

Figure 5.5: *Surfaces with boundary condition*
"Defined voltage (1)" and "Distributed resistance (2)"

For solving the coupled problem an adequate mesh was applied and a segregated parametric solver was used. The variable parameter was the load resistance. The results of the simulations will be shown in the validation part of this chapter (5.3). To obtain adequate measured data for the validation of the FE simulation an experimental setup was created. A description of the main manufacturing processes and the measurement procedure is given in the following.

5.2 Experimental investigation

For the validation of the finite element simulation and the discussion of performance, prototypes of thermoelectric oxide modules (TOMs) have been build up. For the measurements to be performed a test stand was set up. The measured electrical magnitude was the voltage at the varying load resistance. The measurements were done with 5 mm TOM's for varying hot side temperatures T_H. The temperature of the cold side for all measurements was kept at 20°C. This work was done together at EMPA Dübendorf (Laboratory for Solid State Chemistry and Catalysis)

5.2.1 Production of thermoelectric modules

The prototypes consist out of four legs of thermoelectric oxide material synthesized at EMPA Dübendorf. Therefore the legs with a cross-section of 4.5x4.5 mm² and a length (height) of 5 mm were arranged as two pairs of n-type $CaMn_{0.98}Nb_{0.02}O_3$ and p-type $GdCo_{0.95}Ni_{0.05}O_3$ couples. For this bars of 5 mm length were cut from sintered pellets. The thermoelectric elements were electrically connected in series by means of a mixture of silver paste as the bonding agent, silver powder, copper powder and a solvent (xylol thinner). The consistency of the resulting material was paste-like and allowed one to apply it in a thickness of approximately 0.25 mm. The configuration was placed between two 25 x 25 mm² aluminium plates of thickness 0.3 mm. The conducting strips were applied with the help of self-adhesive paper masks on the aluminium oxide plates. The legs were also covered with paste on their front faces and fixed between the aluminium oxide plates, which acted as the electrically insulating part also as the cold and the hot side of the

module. The whole assembly was then subjected to a heat treatment for 2.5 h, where the temperature did not exceed 962°C. At temperatures higher then 962°C the conducting paste started to evaporate. The results were good thermal and electrical contacts of adequate mechanical strength (figure 5.6).

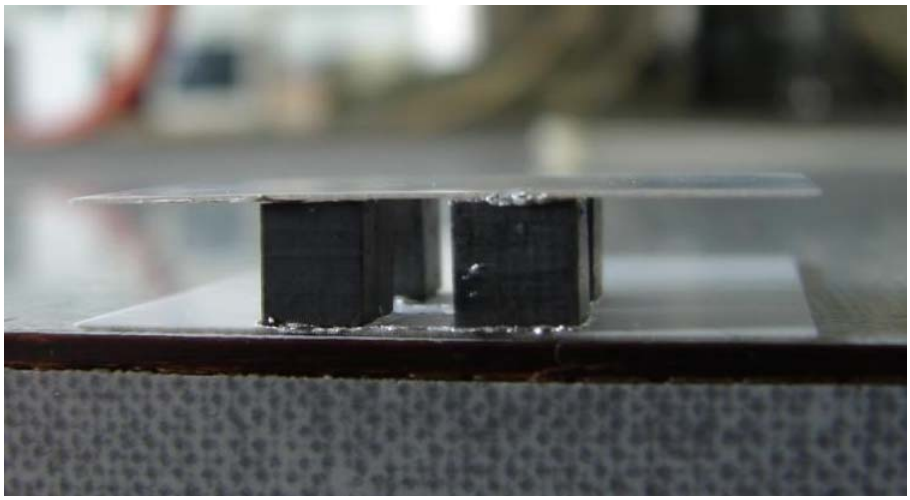

Figure 5.6: *TOM prototype with 5 mm leg length*

5.2.2 Test stand and measurement equipment

For the measurements to be performed a test stand was set up. The main components (figures 5.7 and 5.8) have been a cage including a balance to control the pressure to the module (and so to control the heat transfer conditions to the module) and a fixing mechanism to position the heat source on the top (hot side) of the TOM. The heat source was a controllable electric heating plate, which was insulated and cooled on the upper side, where it was connected with the fixing mechanism. The cold side was a copper block cooled with circulating water inside. The cooling of the upper side to avoid heat transfer to the cage was also done with a controllable water cooler. To improve the heat transfer, a commercially available thin layer of heat conducting paste was applied between the temperature sources and the aluminium oxide plates of the module. For the temperature measurement, thermocouples were arranged directly on the interfaces to the module. Additional thermocouples have been applied inside the copper block of the heat source and to the cooling water. To measure the electrical quantities (power characteristics) the module was connected to an electrical network with 10 different loads

realized by automated parallel switching of 4 high precise resistors. The measured data was viewed and recorded by a LABVIEW applet running on a desktop computer. To get detailed information about the temperature distribution along the legs of the modules an IR-camera for micro-thermographic measurements was installed.

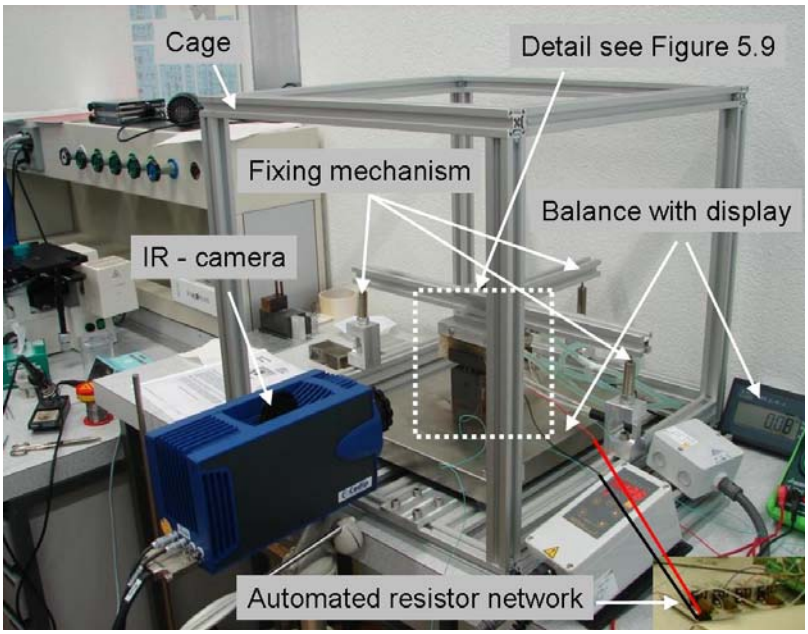

Figure 5.7: *Test stand with measurement equipment and IR camera*

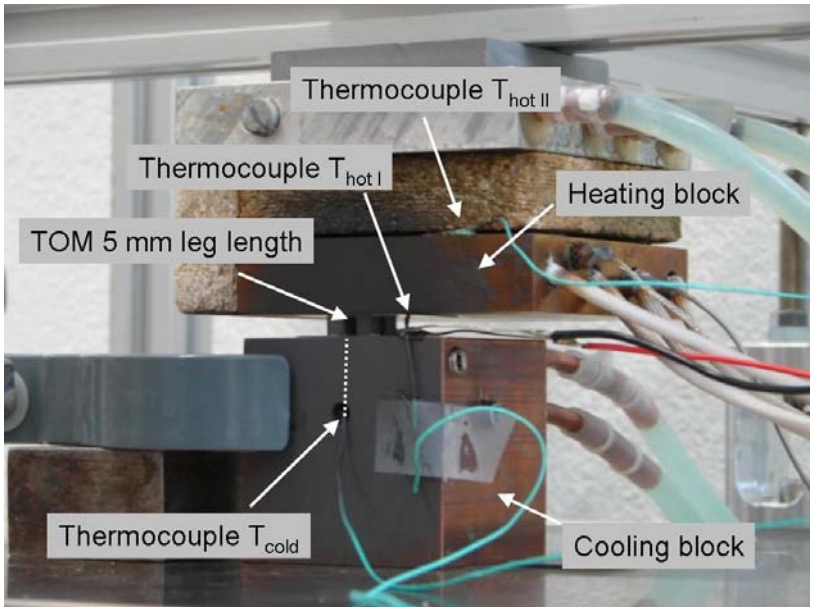

Figure 5.8: *Test stand with measurement equipment and IR camera (detail)*

In the following the measured data is presented and compared with the simulated results of the FE - simulation.

5.3 Experimental results and Validation of the FE-simulation

The measured electrical magnitude was the voltage at the varying load resistance.

The measurements were done with 5 mm TOM's for varying hot side temperatures T_H. The temperature of the cold side for all measurements was kept at 20°C. The power output characteristics (figure 5.11) were calculated out of the measured load voltages (figure 5.10) and the assigned load resistances (Tab. 5.1) according to equation: $P_{OUT} = \frac{V_{LOAD}^2}{R_{LOAD}}$.

Measurement number [-]	1	2	3	4	5	6	7	8	9	10	11
Load resistance [Ω]	∞	3.3	1	0.7674	0.33	0.3	0.2481	0.1	0.0909	0.0767	0.0713

Tab.5.1 Values of the assembled load resistances

The results are shown here in the following and discussed in the following chapter.

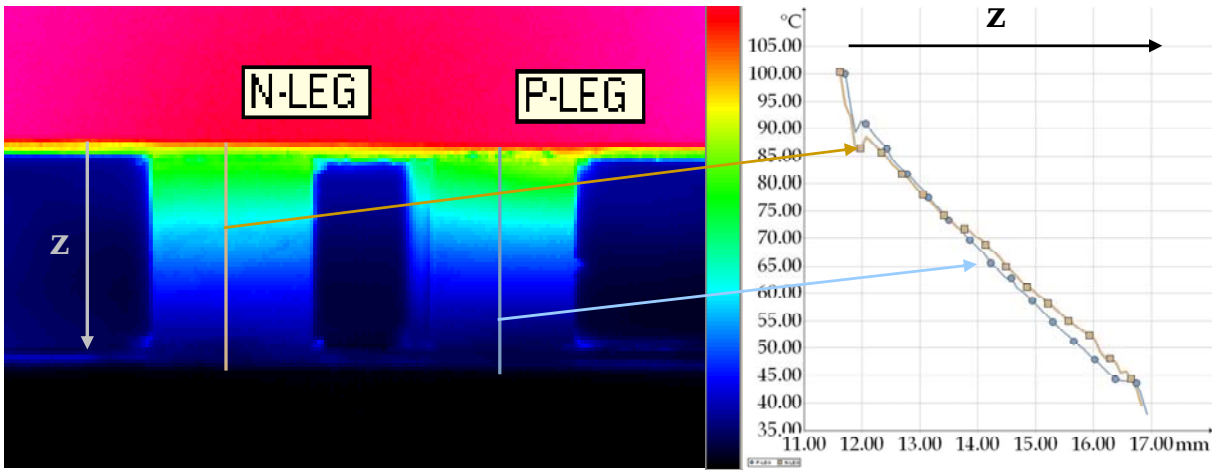

Figure 5.9: *IR-temperature measurement of 5 mm TOM, T_c= 30°C, T_h=100°C*

From the IR – shot it can be seen that the temperature profile along the leg length has a linear character. This is so far important, that it shows that the influences of the losses due to radiation and natural convection are not remarkable at these (low) temperature levels. It was not possible

to take useable IR – shots at higher temperature differences, because of the limited calibration window of the IR-camera.

To provide a better understanding of the quantities used in the following an equivalent circuit diagram for a single thermocouple (1x n-leg and 1x p-leg) is presented (figure. 5.10).

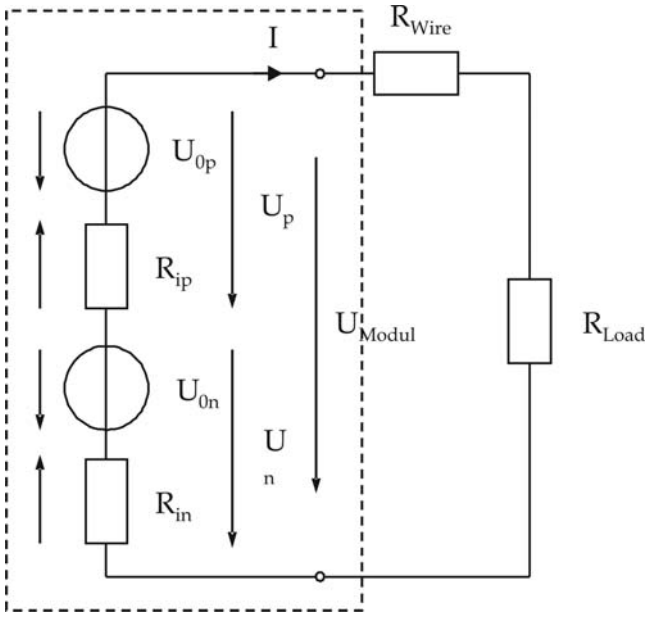

Figure 5.10: *Equivalent circuit diagram for a single thermocouple (1x n-leg and 1x p-leg) connected to a load and considering an additional resistance (eg. connecting wires)*

A thermoelectric generator in its simplest form is made up of one n-leg and one p-leg connected in series. Each leg works as a real voltage source comprising an ideal voltage source and an internal resistance. The generated voltages U_{0p} and U_{0n} are driven by the effective temperature difference and are independent of any electrical current flux through the legs. Added and then multiplied by the number of connected thermocouples they give the open circuit voltage V_0. When a load is connected to the module the electrical current flux causes voltage drops in the internal resistances R_n and R_p and so decreases the terminal voltage U_{Module} of the module. A thermoelectric generator particularly when comprising a small number of thermocouples is in general a low voltage – high current source. Thus the influence of additional resistance from connecting wires is not negligible and can be taken into account by R_{Wire}.

For the validation of the simulation its results were compared with the measured data. The quantities V_0 (open circuit voltage), P_{OUT} (power

output) and the internal resistance R_i are most significant for this task. In figure 5.11 the measured and the calculated (simulated) power output characteristics for varying hot side temperatures are presented for comparison.

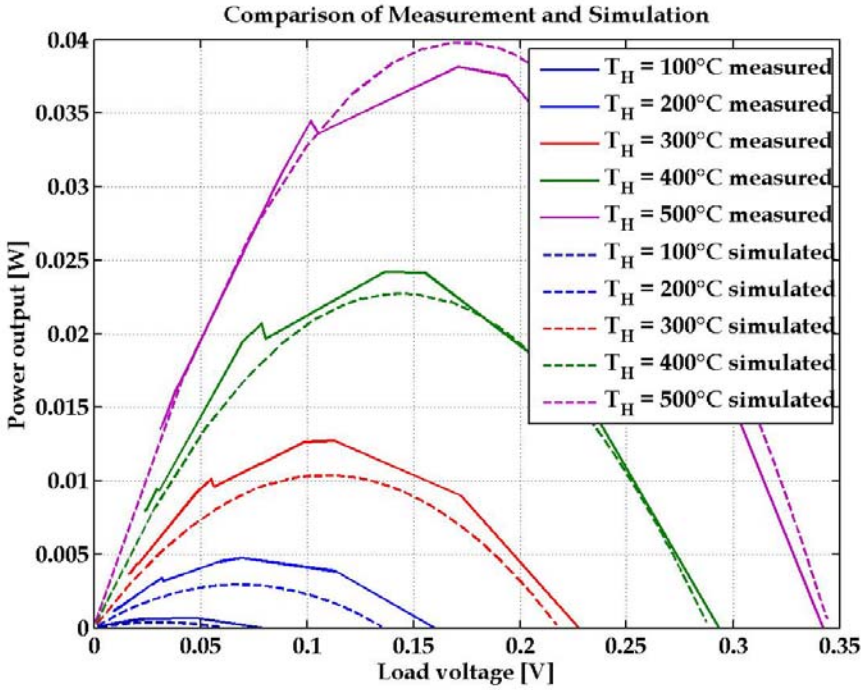

Figure 5.11: *Power output characteristics for different hot side temperatures T_H, T_C=20°C*

It can bee seen that the conformance of the results is quite satisfying, even when the fitting losses quality at lower hot side temperatures. The reason for this may be the assumed heat transfer coefficients at the hot and cold side surfaces, which most likely have not been constant during the measurements respectively changed with temperature.

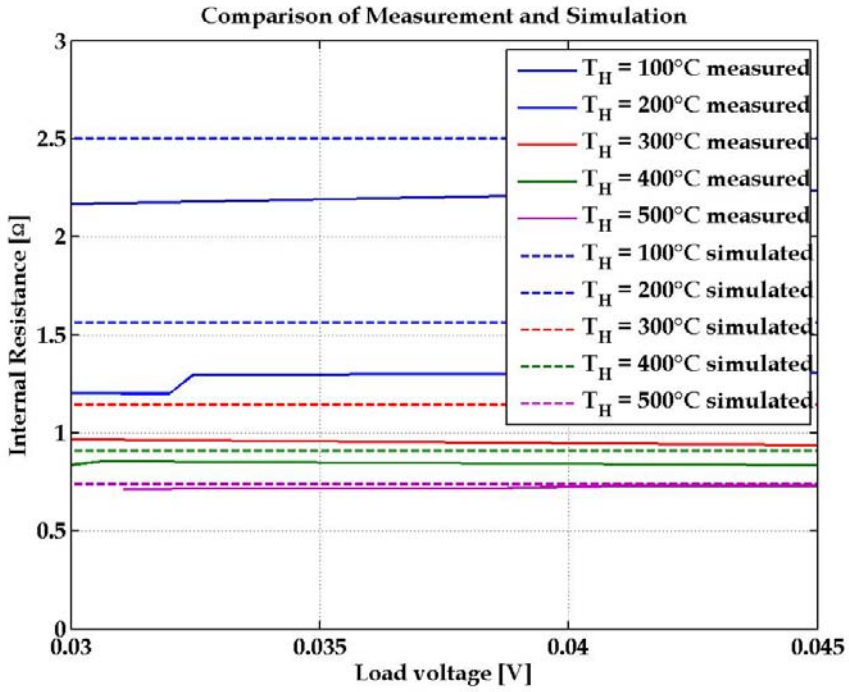

Figure 5.14: *Power output characteristics for different hot side temperatures T_{hot}, T_c=30°C*

The comparison of the internal resistance (figure 5.14) shows a quite similar behaviour, due to the same reasons. Summarized it can be stated that the results of the validation are sufficient and the simulation can be used for further investigations, what has been done in form of a compatibility study of the module used in the large scale model (chapter 4) and is presented in the follwing chapter.

5.4 Compatibility study on the module used in the large scale thermoelectric generator

As already mentioned multiple, in the explanations of chapter 4 the properties of the thermoelectric materials have been assumed constant respectively at average values concerning the temperature dependency were used. Here the FE model is used to proof these assumptions and to give some directives for the handling of material properties.

The specifications and configuration of the modules (commercial available) taken for the following evaluations are given below.

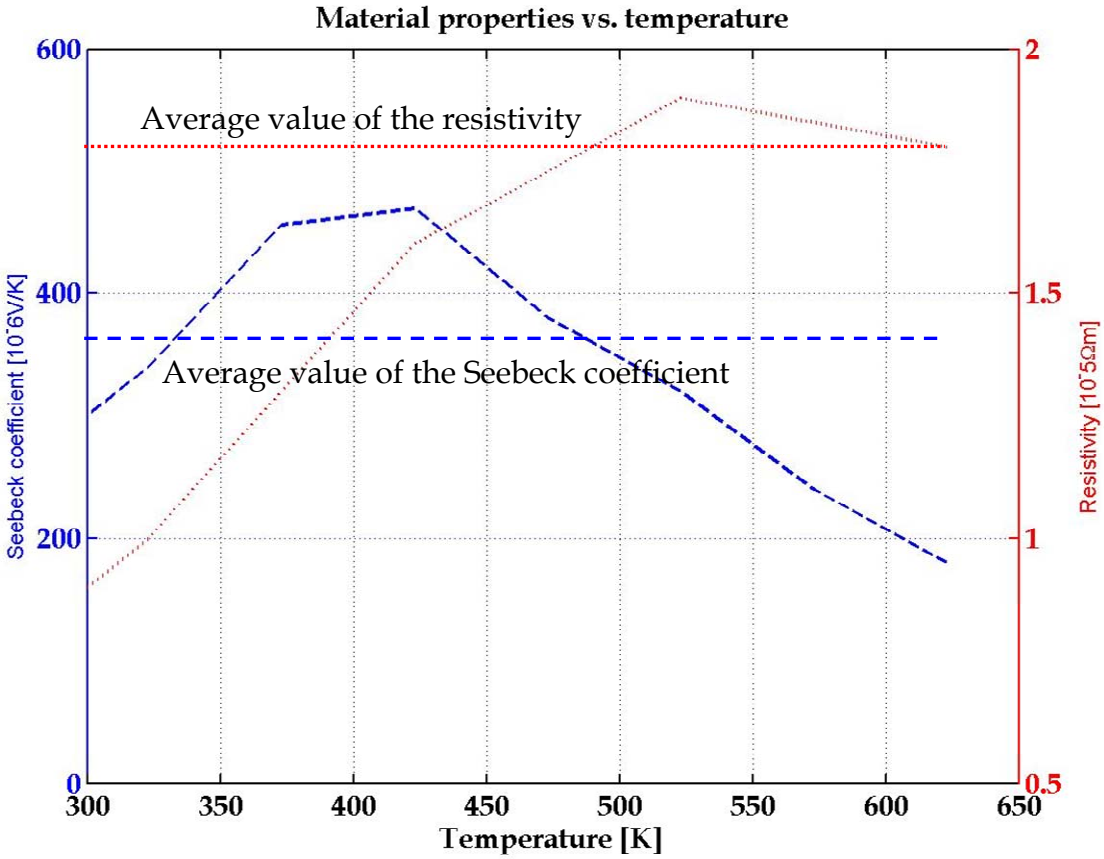

Figure 5.15 :*Thermoelectric properties of the materials of the selected module*

As there was no data available for the thermal conductivity it was set at the constant value of 0.97 W/mK.

Seebeck coefficient (averaged value):	$\alpha_p + \alpha_p = 3.47*10^{-4}$ V/K
Thermal conductivity:	$\lambda_p = \lambda_n = 0.97$ W/mK
Electrical resistivity (averaged value):	$\rho_p = \rho_n = 1.33*10^{-5}$ Ωm
Length of the legs:	1.4 mm
Cross section of the legs:	19 mm^2
Insulator material:	ceramic
Thickness of the insulator:	0.7 mm
Conductor material:	silver
Thickness of the electrical connections:	0.7 mm
Number of couples:	31

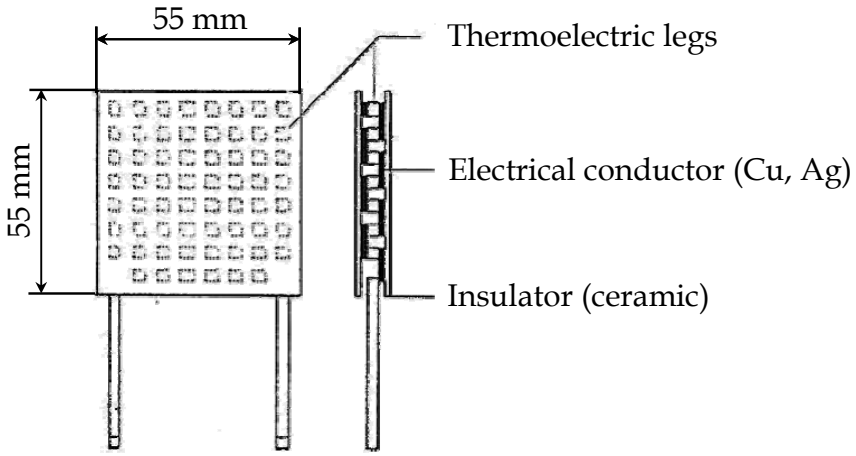

Figure 5.16 : *Configuration and dimensions of a commercial thermoelectric module [18]*

The parameters taken for the calculations are given, such as

T_H	40°C to 340°C,
T_C	20°C constant
$h_h = h_c$	1000 W/m^{2}K

In both models an electrical contact resistance of 0.1mΩ/junction is a assumed. This means that for 31 thermocouples/62 legs in the module an additional resistance of 0.0128 Ω comes to the resistance of the semiconductors and conducting strips. In the large scale TEG model the length and width were set to the dimensions of the module (figure 5.16). The depth D of the heat transfer tubes was chosen to 0.02 m, what

provides nearly isothermal conditions at the hot and cold surface of the module.

To get an idea of the possibilities of FE modelling some exemplary plots (figures 5.17 and 5.18) are presented. Note that they do not present results used in here. For investigation of the several magnitudes you need to have the models opened in the COMSOL Multiphysics tool.

The results, which are needed here have been exported and will be shown below.

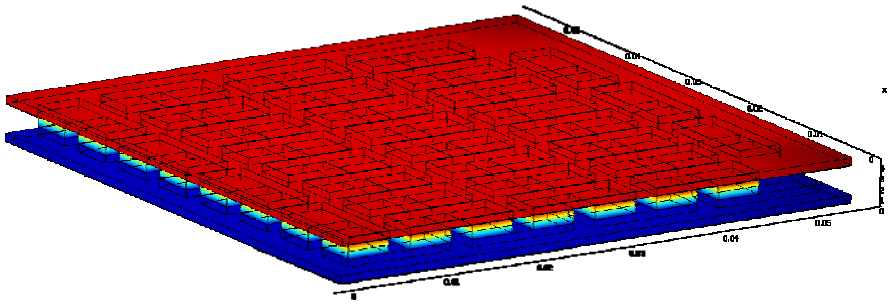

Figure 5.17 : *Temperature distribution in the module calculated with the method of the finite elements*

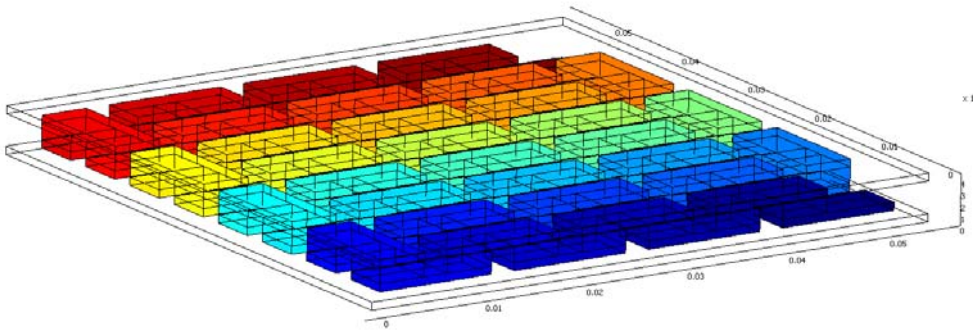

Figure 5.18 : *Voltage distribution in the module calculated with the method of the finite elements*

Comparison of the results from the large scale TEG model and the FE calculations:

The values of the magnitudes power output P_{OUT}, open-circuit voltage V_{OC} , current I and internal resistance R_I will be compared and discussed.

Note that calculations have been done in the case of matched load.

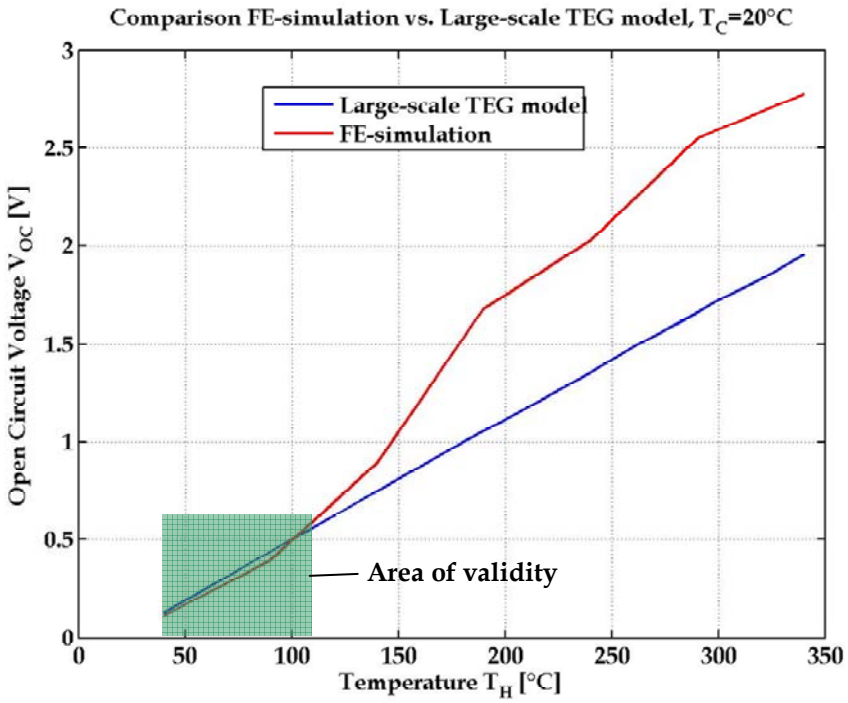

Figure 5.19: *Comparison of the Open Circuit Voltages from FE simulation and TEG model*

The comparison of the open voltage (figure 5.19) shows good agreement at lower hot side temperatures up to 110°C, which therefore can be defined as the area of validity with the averaged values of the material properties given above. At higher temperatures the difference is up to 30% whereas the average values would lead to smaller values. The difference is caused by the influence of the strong temperature dependence of the Seebeck coefficient and the heat transfer coefficient. The constant heat transfer coefficient causes increasing temperature drops between the junctions and the temperature sources. At higher hot side temperatures the legs work in the temperature range where the (non linear) Seebeck coefficient is mostly higher than the average value taken for the large-scale TEG model. This leads to a higher generated open circuit voltage (FE-simulation) at almost equal junction temperatures.

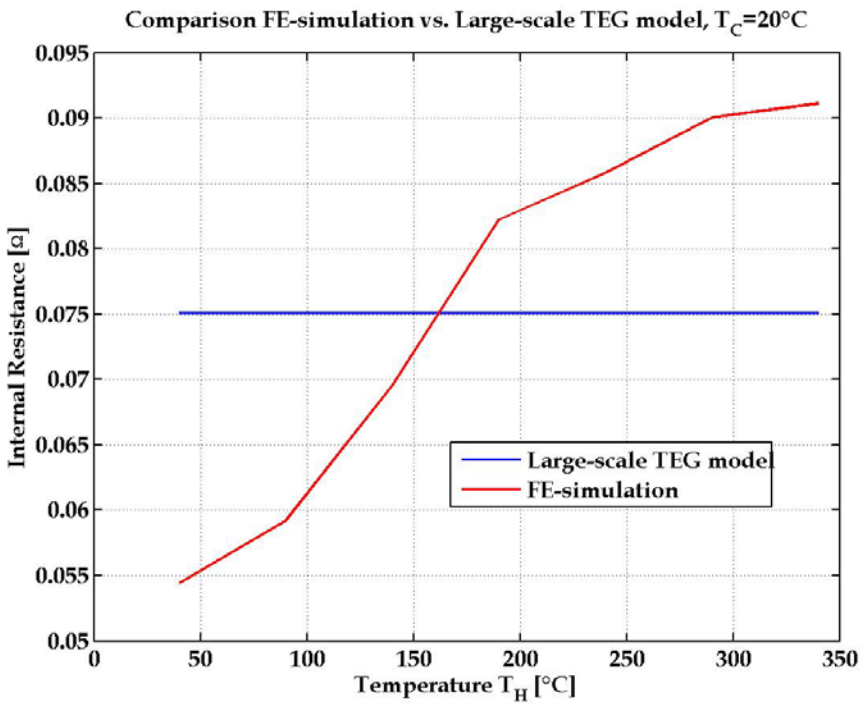

Figure 5.20 : *Comparison of the Internal Resistances from FE simulation and TEG model*

The internal resistance's behaviour is easy explainable with the averaging method of the electrical conductivity.

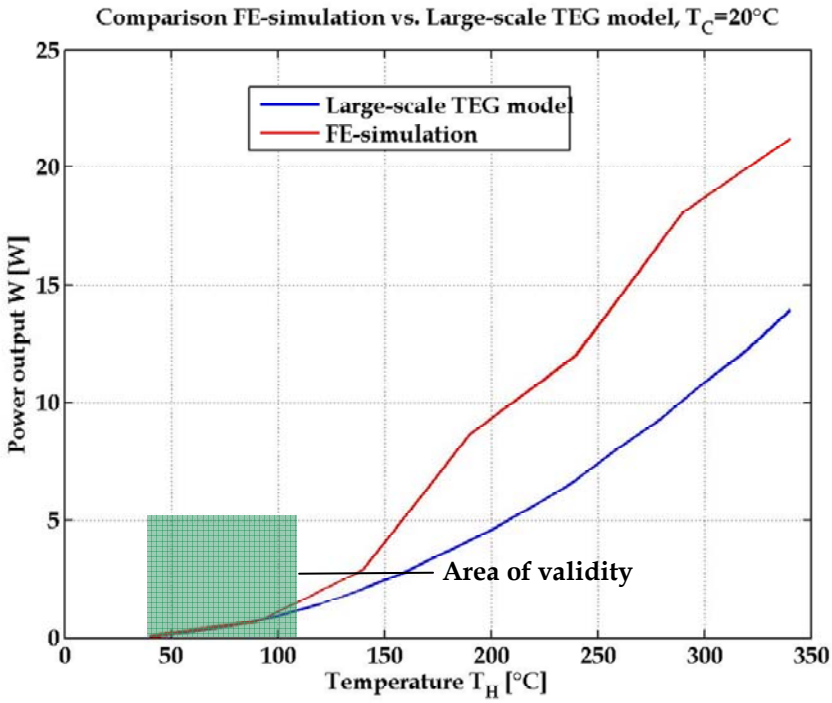

Figure 5.21 : *Comparison of the Power output from FE simulation and TEG model*

The resulting power at matched load shows also a good agreement up to hot side temperatures of T_H = 110°C. For higher temperatures the before

named reasons also cause the differences in power output from more than 25%. Therefore it might be necessary for higher temperatures to work with non-linear functions of the material properties or to adjust the average values to the particular temperature ranges. It is noted that it is known that a real model of this type never would withstand the thermal stress modelled and discussed here.

It can be summarized that the compatibility study showed satisfactory results at lower temperatures, what allows a definition of an area of validity with an upper limit for hot side temperatures of 110°C, which also gives the temperature range for the optimisation and evaluation studies presented next.

Chapter 6

Optimisation studies on the thermoelectric generator

Using the model (large scale TEG, chapter 4), presented and proven in the above chapters, optimisation and performance studies according to the objectives as presented in figure 6.1 have been carried out.

- **Optimisation studies of the heat transfer system corresponding to:**
  - **+ Minimising the specific system volume required to produce 1 kW electrical power**
  - **+ Maximising the system efficiency**
  - **+ Minimising the number of elements required to produce 1 kW electrical power**
- **Evaluation of the influence of module properties on the TEG performance**
  - **+ Leg length**
  - **+ Thermoelectric material properties**

Figure 6.1 : *Overview of the executed optimisation and performance studies*

6.1 Optimisation of the heat transfer system

In the optimisation studies of the heat transfer system the optimum dimensions of the heat transport system to convey the thermal energy to and off the thermoelectric generator have been explored. Further the influence on the performance of various module parameters has been investigated. Before showing some results the assumptions made and the general optimization procedure will be described.

6.1.1 Basic system assumptions and optimization procedure

The fluid flows are assumed as fully developed and the fluid properties are determined at the average temperatures between the inlet and the outlet of the particular heat transfer tubes. For the calculations shown here, water has been taken as the working fluid for the convective heat transfer. For hot side inlet temperatures $T_{Hin} > 100°C$ the fluid properties were taken at pressures, which allow liquid conditions. The media can be changed easily by defining the respective fluid properties.

For the optimisation procedure the temperatures of the hot and cold fluid T_{Hin} and T_{Cin} and the heat transfer coefficients h_W and h_C are set at several constant values. The dimensions of the heat transfer tube have been taken with variable design parameters as:

D: Depth of the heat transfer tube [m]

L: Length of the heat transfer tube [m]

W: Width of the heat transfer tube [m]

Here the width W of the heat transfer tube is given by the width of the selected module and is set to $W = 0.055$ m.

To get the assumed heat transfer coefficients the mass flow rates of the hot and cold fluid were varied iteratively according to equations 4.15 - 4.22. The resulting values of the mass flow rates were used for the determination of the temperature distributions of interest along the heat transfer tubes and further on for the performance data as also described before.

The specifications and configuration (figure 6.2) of the modules (commercially available) taken for the following evaluations are given below:

Seebeck coefficient:	$\alpha_p + \alpha_p = 3.47*10^{-4}$ V/K
Thermal conductivity:	$\lambda_p = \lambda_n = 0.97$ W/mK
Electrical resistivity:	$\rho_p = \rho_n = 1.33*10^{-5}$ Ωm
Length of the legs:	1.4 mm
Cross section of the legs:	19 mm²
Thickness of the insulator:	0.7 mm
Thickness of the electrical connections:	0.7 mm

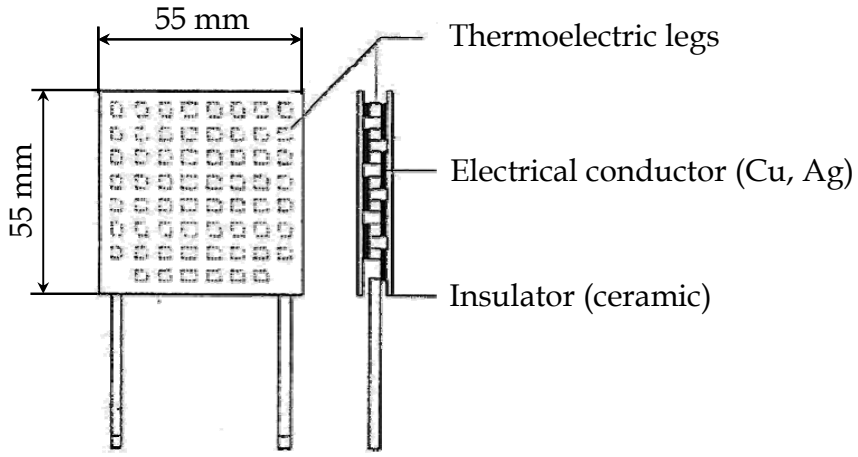

Figure 6.2 : *Configuration and dimensions of a commercial thermoelectric module [18]*

In the following sub-chapters the results of the optimisation strategies are presented. The results are discussed in general for the example with the parameters T_{Hin} = 80°C and $h = h_W = h_C$ = 1000 W/m²K. To show the influence of the parameters T_{Hin} and h additional figures are presented. A complete assembly of all figures for various parameter combinations can be found in Appendix B. The cold side inlet temperature for all evaluations is T_{Cin}= *20°C.*

All magnitudes are displayed as functions of the dimensions length L and/or width D of the heat transfer tubes.

6.1.2 Minimizing the system volume

In the following the specific volume V_{spec} of the thermoelectric generator required to produce 1 kW of P_{net} (equ. 4.27) is calculated and displayed as a function of various variable parameters. Therefore the used terms of volumes are defined as:

$$V = L \cdot W \cdot \left(D + h_{Module}\right) \qquad \text{(equ. 6.1)}$$

$$V_{spec} = \frac{V}{P_{net}} \qquad \text{(equ. 6.2)}$$

First temperature profiles are shown for various lengths and depths of the heat transfer tubes. For each combination of L and D the required mass flow rates to obtain the specific heat transfer coefficient h are also given. Further the specific volume V_{spec} of the thermoelectric generator is displayed as function of the length and depth of the heat transfer tubes.

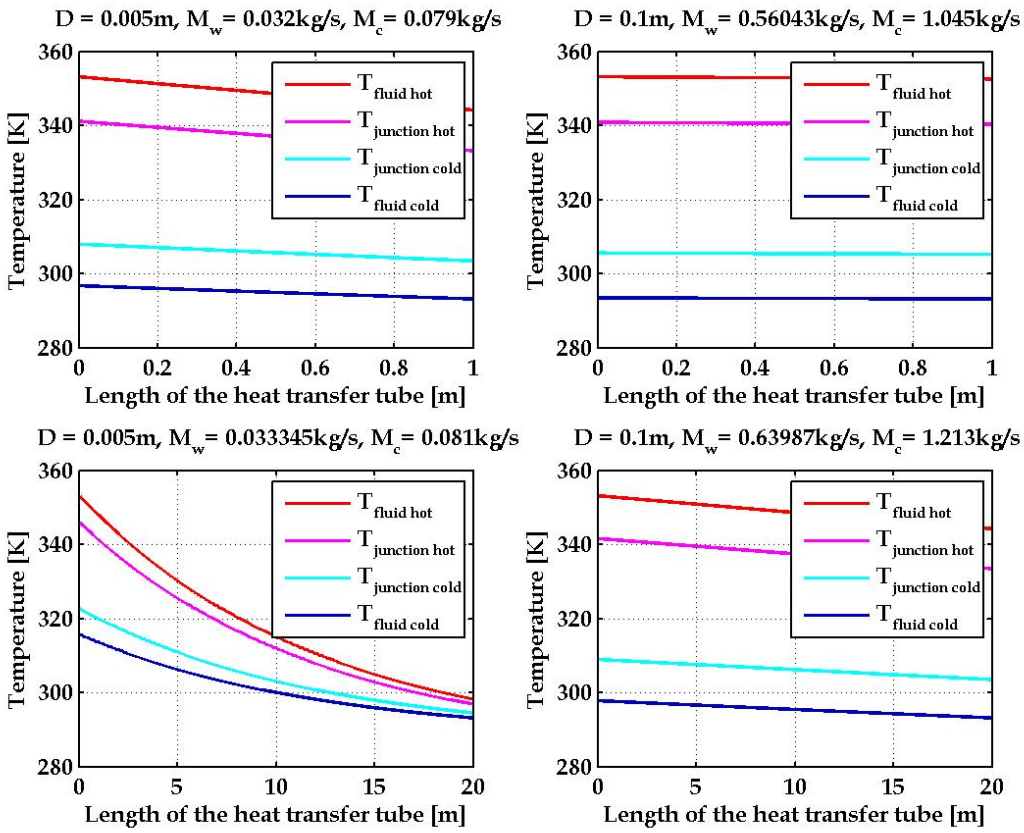

Figure 6.3 : *Temperature profiles for various combinations of the length L and depth D of the heat transfer tubes T_{Hin} = 80°C, T_{Cin} = 20°C, h = h_w = h_c = 1000 W/m²K, W = 0.055m*

Each quadrant of figure 6.3 shows a temperature profile along the heat transfer tubes for a different combination of the length L and the width D

of the heat transfer tubes. The values of the particular dimension can be found in the heading (D) respectively is the parameter of the x-axis (L). Note that the assumed heat transfer unit is a cross-flow heat exchanger, which means the fluid flow direction is in the case of the hot media (red and pink curve) from left to right and in the case of the cold media (light blue and dark blue curves) from right to left.

Comparing the headings of the various temperature profiles in figure 6.3 it can be seen that there is a small increase of the required mass flow rates with increasing tube length, due to the influence of the ratio d_H/L in the equations for the Nusselt numbers (equations 4.16 and 4.19).

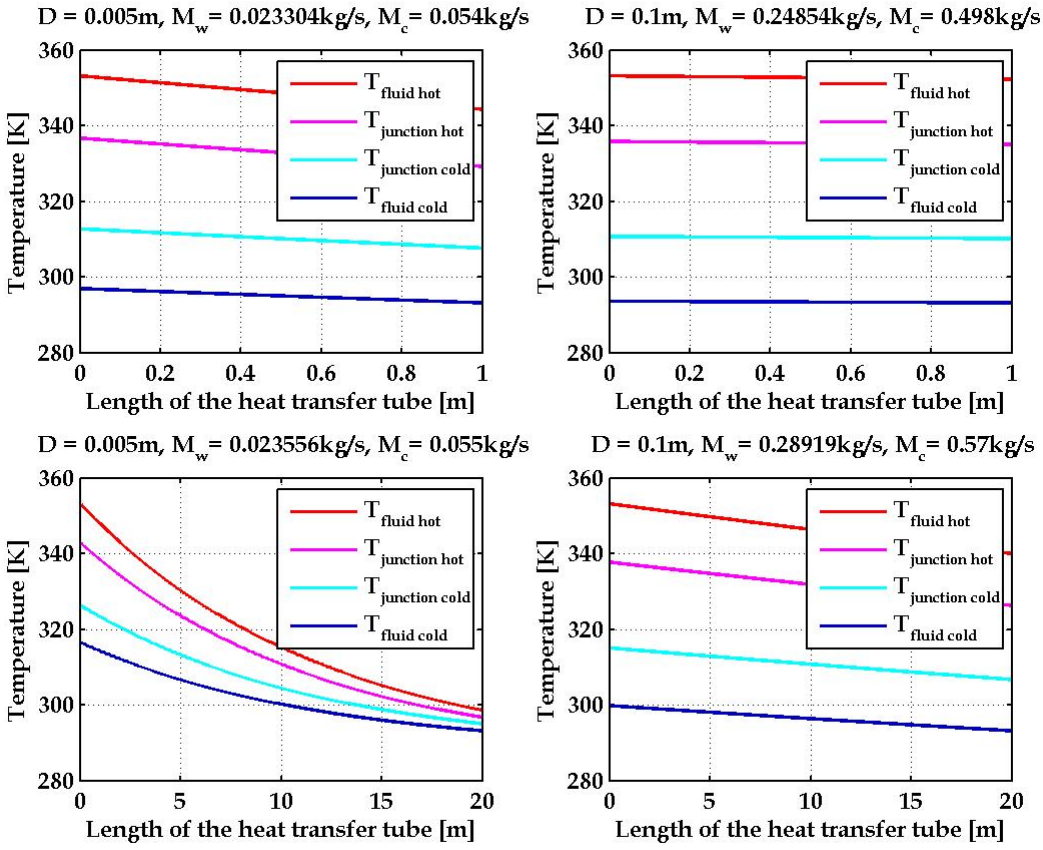

Figure 6.4 : *Temperature profiles for various combinations of the length L and the depth D of the heat transfer tubes T_{Hin} = 80°C, T_{Cin} = 20°C, $h = h_w = h_c$ = 500 W/m²K, W = 0.055m*

Note that the given TEG is considered in the form of a stack structure (Fig.4.2), it means that the given mass flow rates bring and take the heat for two stacked layers of thermoelectric modules. Imaging the defined TEG unit (chapter 4.2) one has to halve the given values to get the required mass flow rates. Comparing figures 6.3 and 6.4, where the latter

it can be seen that at constant inflow temperatures T_{Hin} and T_{Cin}, the mass flow rates M_W and M_C at the hot and cold side of the TEG increase with higher heat transfer coefficients h_w and h_c. This is due to the fact that for higher heat transfer coefficients higher Reynolds numbers are required (according to equations 4.16 - 4.22), which means that at constant cross-section (constant characteristic diameter d_H) of the flow channels and assumed constant fluid properties the flow velocities, respectively the mass flow rates, have to be increased. As h_W and h_C are defined as the overall heat transfer coefficients between the fluid and the thermoelectric junctions, higher heat transfer coefficients cause smaller temperature drops between fluid and junction which in consequence results in a higher effective temperature difference ΔT_{TEG} at the thermoelements. Higher ΔT_{TEG} leads to an increased power output and also to higher efficiency. Higher heat transfer coefficients permit also greater heat consumption /higher heat input at constant heat exchanger area.

Further on it is recognized that for constant heat transfer coefficients with increasing hot side inflow temperatures T_{Hin}, the hot side mass flow rate decreases due to the changing fluid properties (compare figures 6.3 and 6.5). It is noted here that for the calculations at 120°C inflow temperature the fluid properties have been calculated at a pressure of 3 bar. The cold side mass flow rates M_C remain constant.

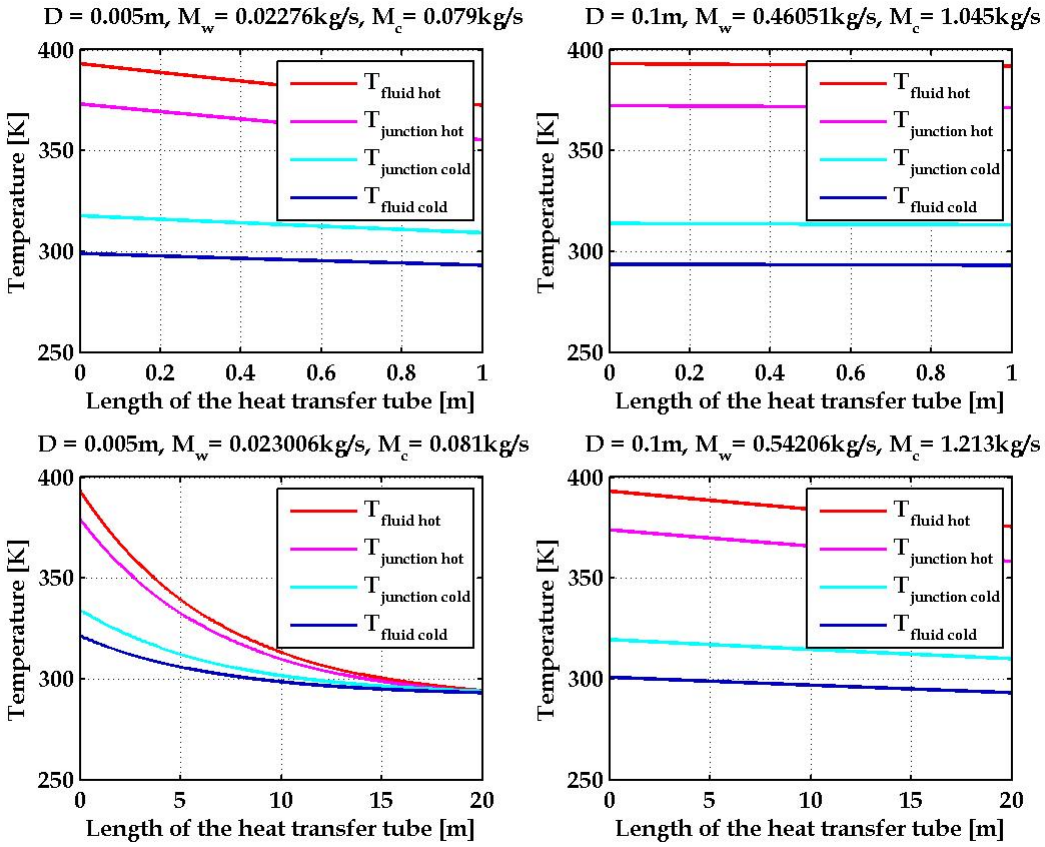

Figure 6.5 : *Temperature profiles for various combinations of the length L and depth D of the heat transfer tubes T_{Hin} = 120°C, T_{Cin} = 20°C, h = h_w = h_c = 1000 W/m²K, W = 0.055m*

All figures presenting temperature profiles (figures 6.3 to 6.5) show that at constant depth *D* and constant mass flow rates (constant *h's*) with increasing length *L* the temperature drop along the heat transfer tube increases due to greater heat exchanger area respectively higher heat consumption due to a higher number of thermoelectric modules. The generated power therefore increases with the length of the tubes but with decreasing efficiency.

For very small depth *D* the temperature profiles (figures 6.3-6.5 – left/bottom) show strong drops along the tube length respectively decreasing effective ΔT_{TEG}. Under these conditions the maximum energy is taken out of the heat transfer medium. As the temperature profiles lose linearity the heat exchanger area is so big that in combination with the small amount of thermal energy (small mass flow rate M_W) brought into the TEG, the effective temperature differences approach zero and almost no electrical power is generated at the duct end part of the TEG.

Increasing depth at constant length (figures 6.3-6.5 – right/top) needs higher mass flow rates for the desired *h's*. The heat uptake (heat input Q_H) is constant with constant length as also the heat exchanger area. If *D* is big (high mass flow rate) a lot of thermal energy is available, but cannot be taken up by the modules, due to their thermal resistivity, and so goes unused through the heat exchanger, increasing the required pump power.

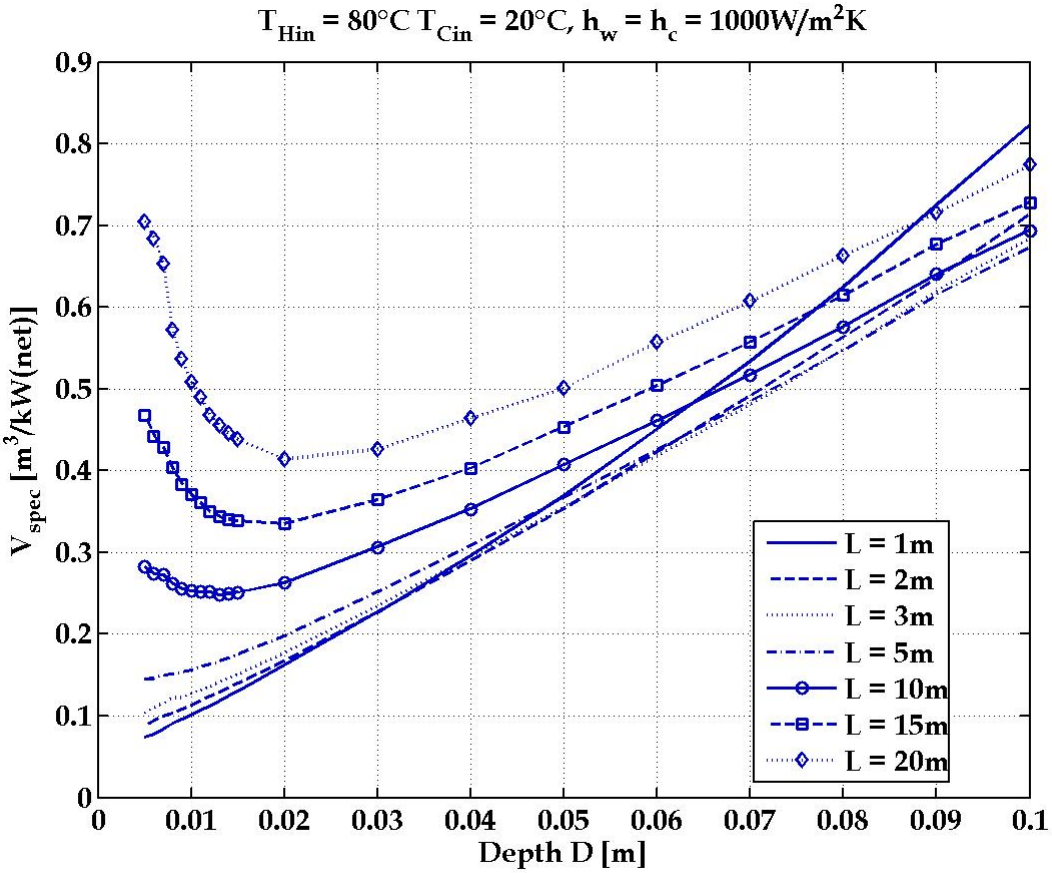

Figure 6.6 : *Required system volume to generate 1kW (net) as a function of the length of the heat transfer tube T_{Hin}= 80°C, T_{Cin} = 20°C, h = h_w = h_c = 1000 W/m²K, W = 0.055m*

As the system volume increases linearly with *L* at constant *W* and *D* and the net produced power has a non-linear behaviour, due to the required pump power increasing with length, there can be found a minimum of the specific volume for each combination of the *L* and *D* (see figures 6.6 and 6.7).

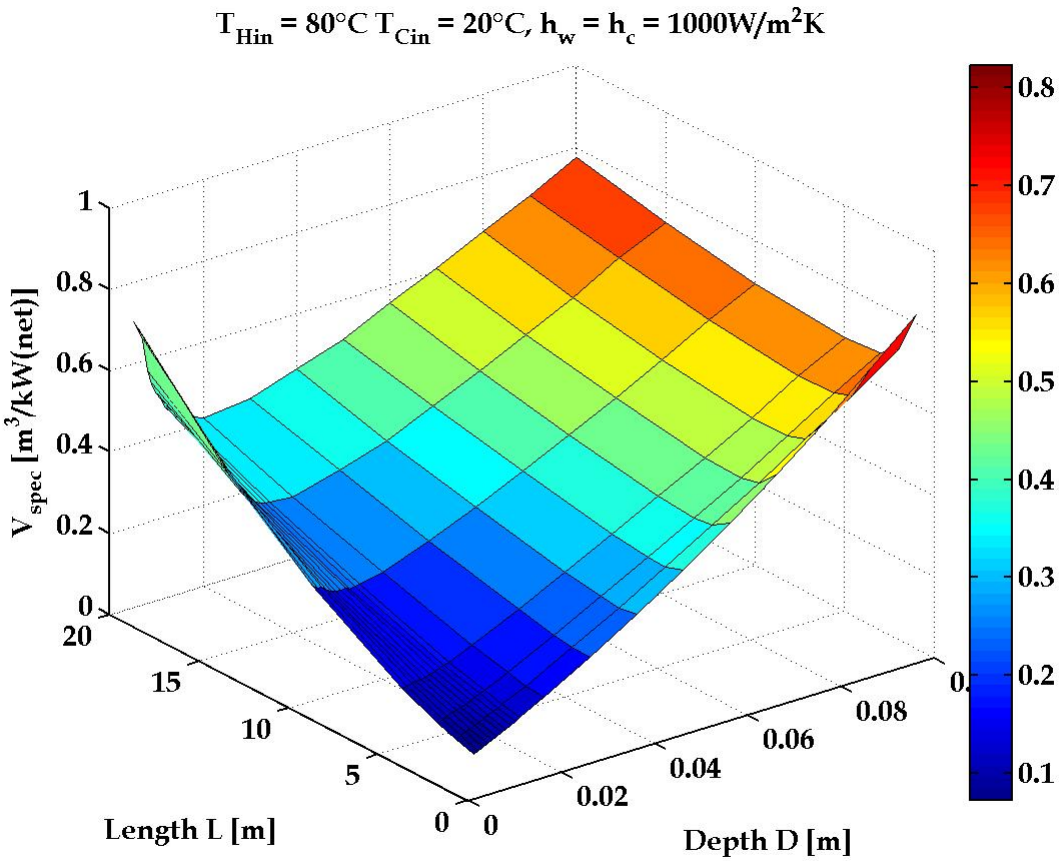

Figure 6.7 : *Required system volume to generate 1kW (net) as a function of the length L and depth W of the heat transfer tube T_{Hin}= 80°C, T_{Cin} = 20°C, h = h_w = h_c = 1000 W/m²K, W = 0.055m*

Especially when harvesting low temperature heat sources the limits for the depth *D* should be carefully considered (see figures 6.7 and 6.8). Both limits, the minimum and the maximum of *D* are given by the increasing pump power, which in the extreme amounts to the entire generated power. The required increase of the pump power is caused in the minimum case by the drastically increasing friction losses and in the maximum case by the big amount of heat transfer media, which has to be pumped and does not increase the power output due to the restrictions mentioned above.

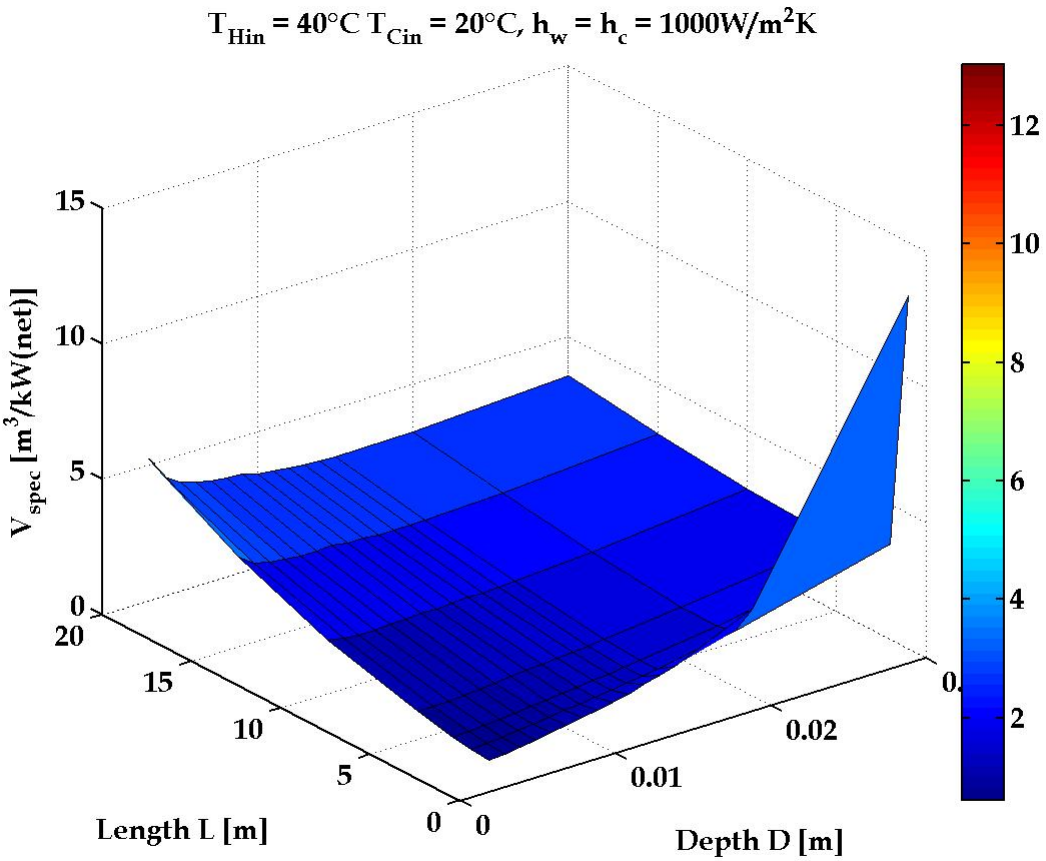

Figure 6.8 : *Required system volume to generate 1kW (net) as a function of the length and of the depth of the heat transfer tube* T_{Hin}*= 40°C,* T_{Cin} *= 20°C, h =* h_w *=* h_c *= 1000 W/m²K, W = 0.055m*

6.1.3 Maximising the system efficiency:

In the following the total system efficiency is displayed as a function of depth *D* and length *L* of the heat transfer tubes and discussed for selected parameter combinations.

The explanations for this are as follows: As already explained before higher heat transfer coefficients (compare figures 6.3 and 6.4) lead to higher junction temperatures (for constant inflow temperatures) and so also to higher efficiencies. (see figures 6.9 and 6.10)

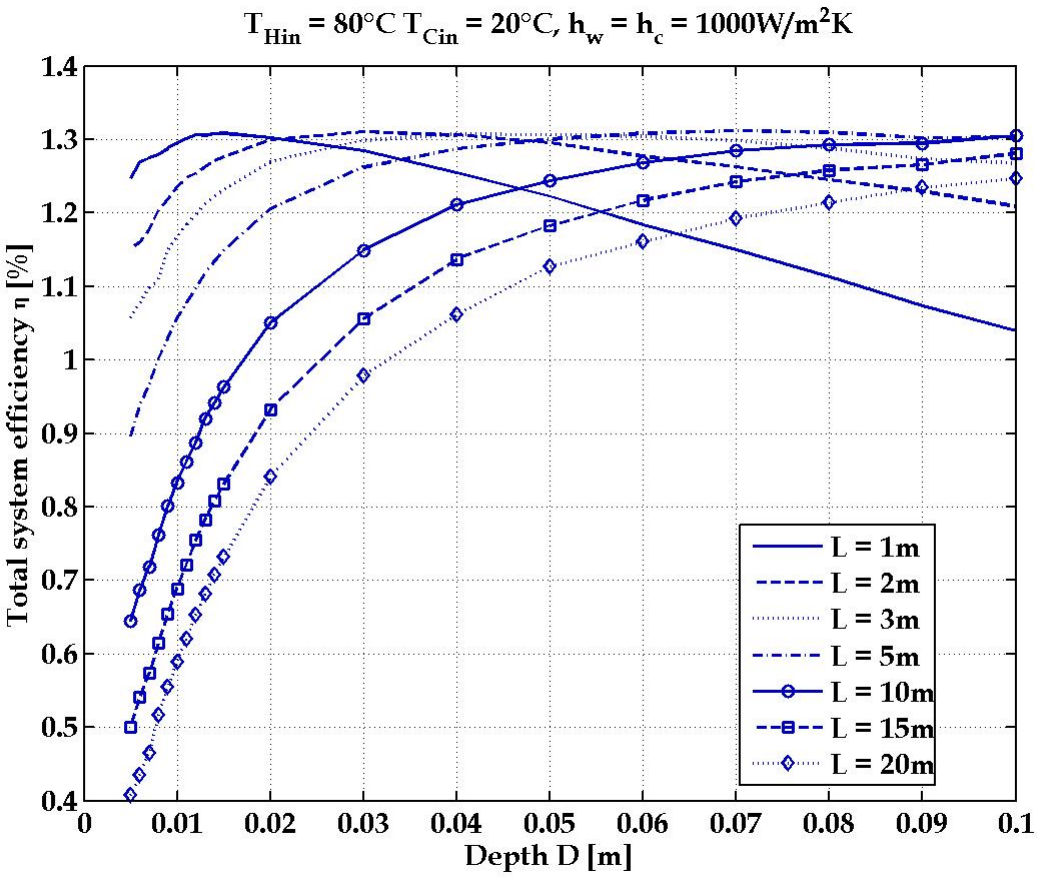

Figure 6.9 : *Total system efficiency as a function of the depth D of the heat transfer tubes T_{Hin}= 80°C, T_{Cin} = 20°C, h = h_w = h_c = 1000 W/m²K, W = 0.055m*

The system efficiency theoretically would find its maximum, when the temperatures along the length of the heat transfer tubes would be at a constant level. In this case (isothermal case) no power would be generated. In the more realistic model the minimal need of generated power is the required pump power. If there are still almost constant temperatures (the reason for this is, as mentioned before, the depth is very big and so the mass flow rates are also very high), this leads in combination with relatively short tubes (small heat exchanger area) to a lot of unconsumed thermal energy going through the heat exchanger tubes. Of course the thermoelectric generator is working at maximum power output, but the net generated power is reduced by the bigger pump power required, which with constant heat input results in smaller efficiencies (see figures 6.9 and 6.10).

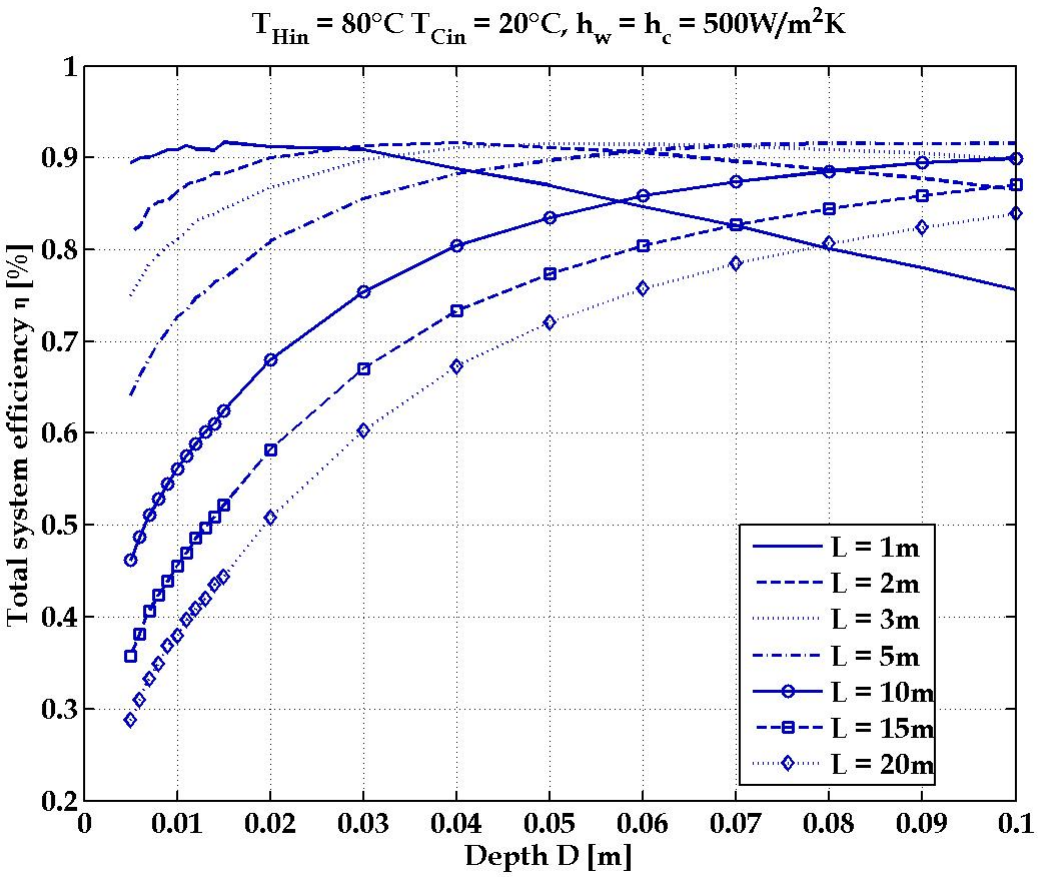

Figure 6.10 : *Total system efficiency as a function of the depth D of the heat transfer tubes, T_{Hin}= 80°C, T_{Cin} = 20°C, h = h_w = h_c =500 W/m²K, W = 0.055m*

At small depth and so also low mass flow rates, which leads in combination with big length of the tubes to strong temperature drops in the temperature profiles, the maximum power is taken out of the heat transfer medium, but the average junction temperature difference is small, which explains the decreasing efficiencies (see figure 6.11). By taking the maximum energy out of the heat transfer medium the temperature profiles lose linearity and ΔT_{TEG} decreases along the tubes. In this case the influence of the nonlinearity of the thermoelectric material properties can become very pronounced. (see temperature profiles left/bottom)

This has to be investigated individually for the particular modules respectively for the module materials.

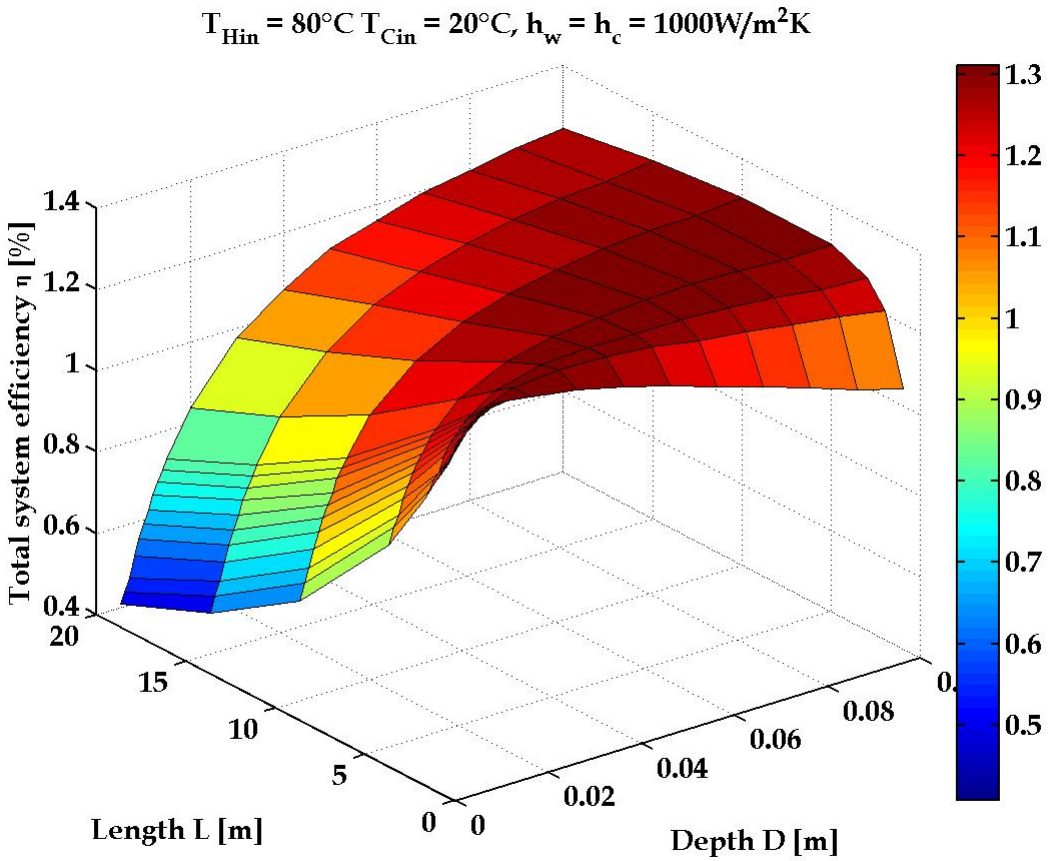

Figure 6.11 : *Total system efficiency as a function of the length L and of the depth D of the heat transfer tubes T_{Hin}= 80°C, T_{Cin} = 20°C, h = h_w = h_c = 1000 W/m²K, W = 0.055m*

6.1.4 Minimising the number of thermoelectric modules:

As the thermoelectric material contributes the dominant part of the construction costs, the number of required modules should be minimized. Here the numbers of modules required to generate 1kW(net) as a function of the depth and the length of the heat transfer tubes are presented and discussed for selected parameter combinations.

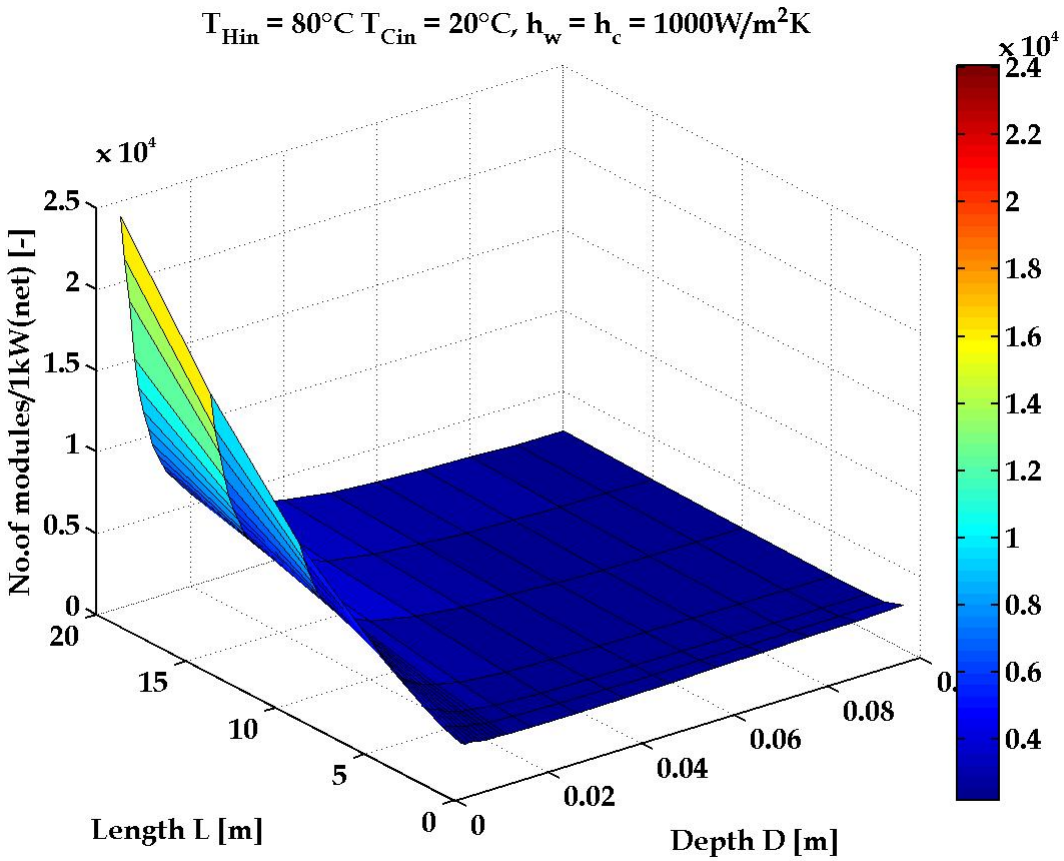

Figure 6.12 : *Number of required modules to produce 1kW(net) as a function of the length and of the depth of the heat transfer tubes* T_{Hin}*= 80°C,* T_{Cin} *= 20°C,* $\boldsymbol{h = h_w = h_c = 1000\ W/m^2K}$**, W = 0.055m**

The optimisation of the number of modules does not really show defined extrema when a certain point of value of the depth (depending on the length of the tubes) is exceeded for hot side inflow temperatures T_{Hin} > 80 °C (see figure 6.12). It is preferable to set the value of the depth D to the minimum permissible size. For low temperatures a well defined minimum for the number of modules can be found, as the smaller ratio of generated power to required pump power is more pronounced (see figure 6.13).

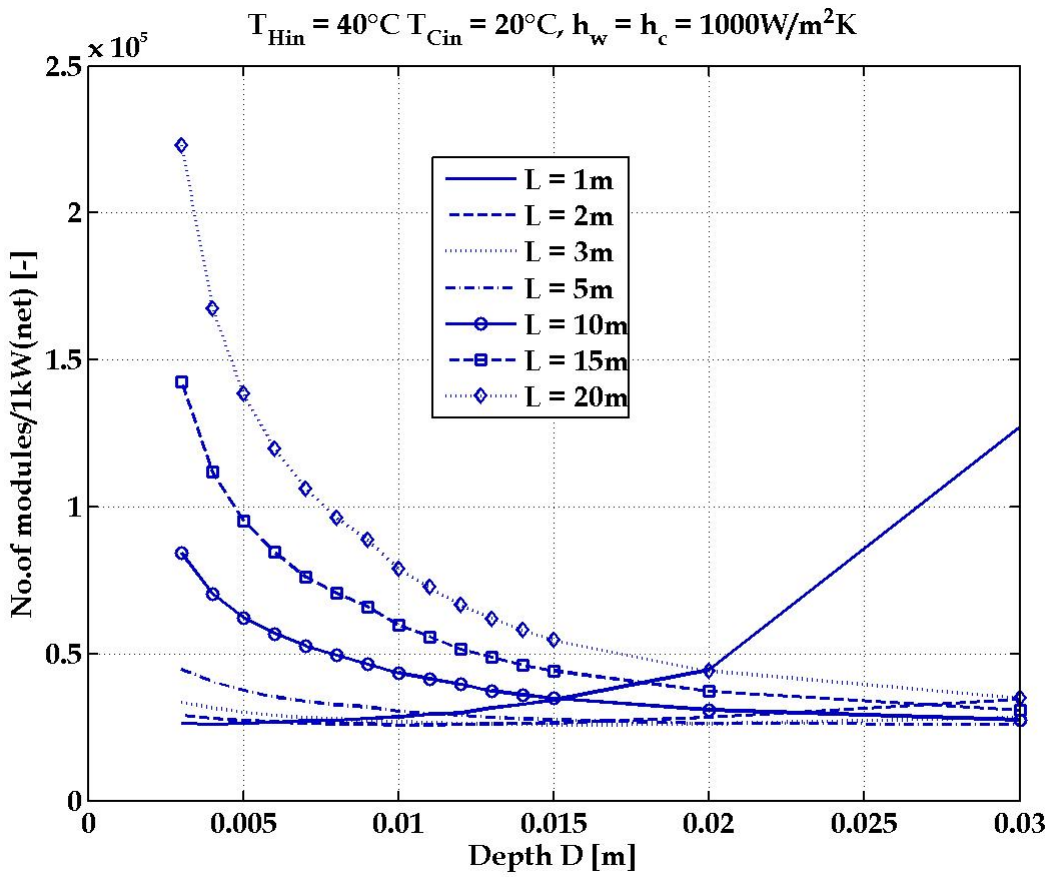

Figure 6.13: *Number of required modules to produce 1kW(net) as a function of the depth of the heat transfer tubes T_{Hin}= 40°C, T_{Cin} = 20°C, $h = h_w = h_c$ = 1000 W/m²K, W = 0.055m*

It is assumed that the dimension *W* of the heat transfer tubes is dictated by the dimensions (width) of the selected modules. Bigger values of *W'* should be multiples of this *W*, so that the whole width of the duct is covered with modules, as it is not reasonable to waste heat exchanger surface, by having any area not in contact with either the heat transfer medium or the surface of the module. This should also help to keep the number of modules and the total system volume small.

6.2 Influence of the module properties on the performance of the TEG

The influence of the dimensions and properties of the materials used in the thermoelectric modules is widely discussed in the specific literature [3, 5 ,7, 14, 18, 20, 24, 25, 30, 38]. There is the influence of the leg length of the thermoelectric modules and of the material properties themselves. The main statement according to the length of the legs is that longer legs, due to lower thermal conductance, yield higher efficiency than short legs, which due to lower internal resistance yield larger power output.

The material properties, which can be summarized in the figure of merit ZT already mentioned, can also be allotted to the two potential areas of performance improvement. From the definition of ZT (equation 6.1) it can be seen easily that higher ZT can be reached by two ways.

$$ZT = \frac{\alpha^2 \cdot \sigma}{\lambda}, \qquad \text{(equ. 8.1)}$$

one is to increase in the numerator the product of the square of the Seebeck coefficient α and the electrical conductivity σ, which is self-explanatory, also called the power-factor, and two is to decrease the thermal conductivity λ, which leads to higher efficiencies. It should, however, be noted that varying one is not without influence on the other and but even then, if the total ZT is increased, bigger power outputs and higher efficiencies are the result.

These statements are absolutely valid for observations on a single couple or module at isothermal conditions. The aim of the following is to show the influence of the parameters above named in a complete thermoelectric energy conversion system.

All calculations have been carried out at the same operating conditions, such as:

T_H = 80°C, T_C = 20°C, $h = h_w = h_c$ = 1000 W/m²K

D (depth of the heat transfer tubes) = 0.02 m and

W (width of the heat transfer tube) = 0.055 m

The length of the thermoelectric legs has been varied from 1 to 5 mm in combination with:

- the variation of the length L of the heat transfer tubes from 1 to 20 m with constant depth D = 0.02 m.
- the variation of the depth D of the heat transfer tubes from 0.001 to 0.1 m with constant length L = 1 m.

The material properties have been varied independently in the range of 0,5…2,5 W/mK for the thermal conductivity and from $7*10^{-3}...35*10^{-3}$ W/mK^2 for the power factor. In the case of the power factor this was done in equal parts to the relevant material properties, this means e.g. to double the power factor, the values of the Seebeck coefficient and the electrical conductivity have been multiplied by the factor 1.25. As the Seebeck coefficient appears quadratic in the definition of the power factor this brings about the doubling of the power factor

In the following the influence of the particular parameters on the specific volume, which is an indicator for the power output and the total system efficiency, are presented. For the discussion temperature profiles are also presented.

Influence of the leg length:

For the following explanations the length of the thermoelectric legs has been varied from 1 to 5 mm in combination with the variation of the length L of the heat transfer tubes from 1 to 20 m with constant depth D = 0.02 m.

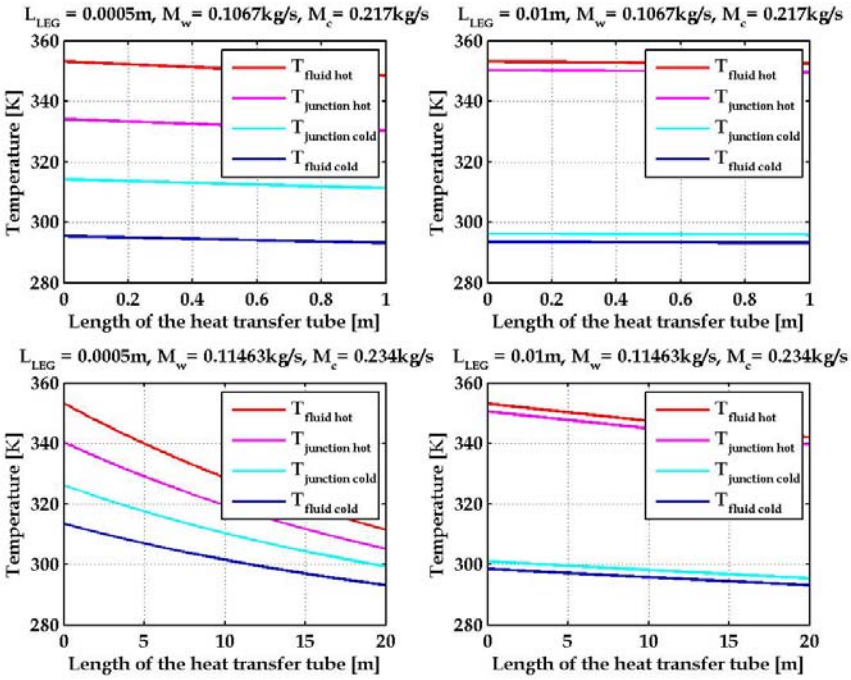

Figure 6.14 : *Temperature profiles for various combinations of the length L of the heat transfer tubes and the leg length of the modules, T_{Hin} = 80°C, T_{Cin} = 20°C, $h = h_w = h_c$ = 1000 W/m²K, W = 0.055m, D = 0.02 m*

Looking at figure 6.14 it can be seen that with increasing leg length the effective temperature difference at the junction increases, this explains also the increasing efficiency (see figure 6.16). When the thermal resistance increases the heat input (consumption) decreases and correspondingly the output power decreases and the specific volume increases (see figure 6.15). At a certain point, the product of increasing efficiency and decreasing heat input results in a maximum of the power output, which can be seen in figure 6.15 as the minimum of the specific volume V_{spec} at a leg length of about 1 mm for the selected parameters and a tube length of L = 1 m.

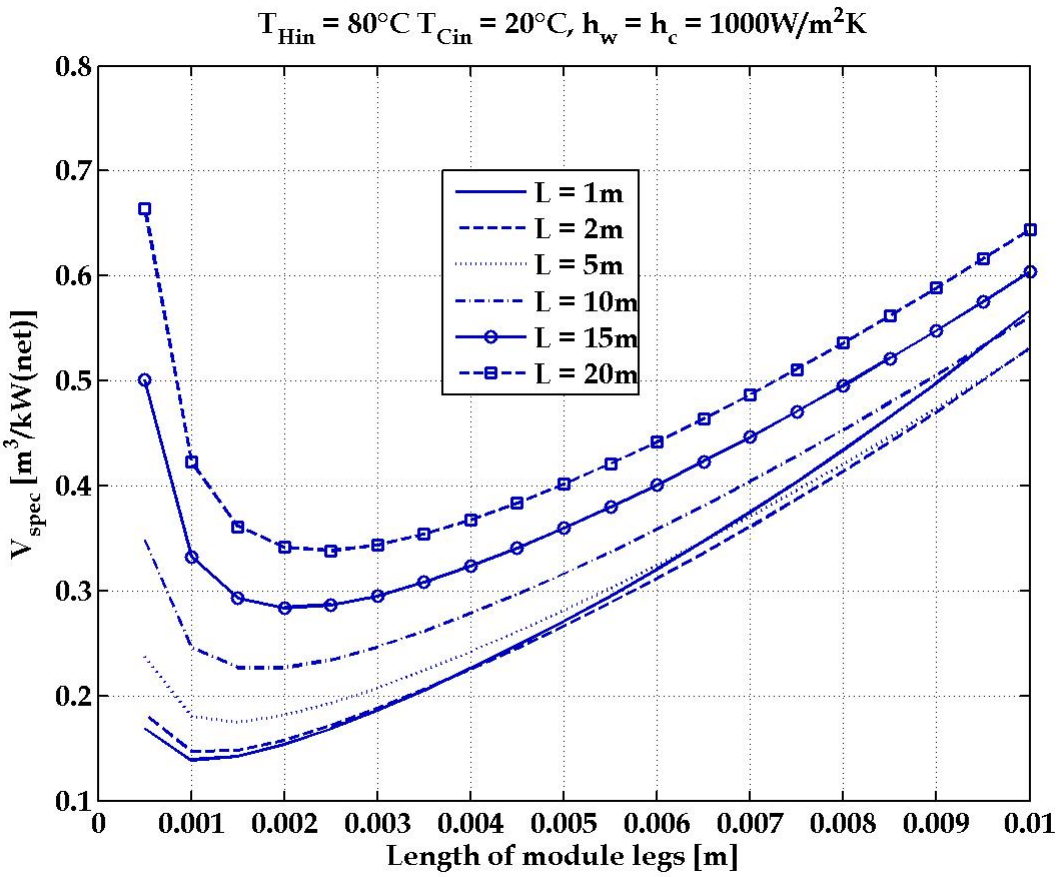

Figure 6.15 : *Required specific volume as a function of the length of the module legs, T_{Hin}= 80°C, T_{Cin} = 20°C, $h = h_w = h_c$ = 1000 W/m²K, D = 0.02 m*

For constant input of thermal energy (constant mass flow rate M_W and constant h) the value of this extremum increases and moves with increasing tube length to bigger leg length with increasing tube length (see figure 6.15). The system efficiency in general increases with increasing leg length. But it is also recognized that for short tubes the maximum efficiency is reached at smaller leg length compared to a a system with long heat transfer tubes. (see figure 6.16).

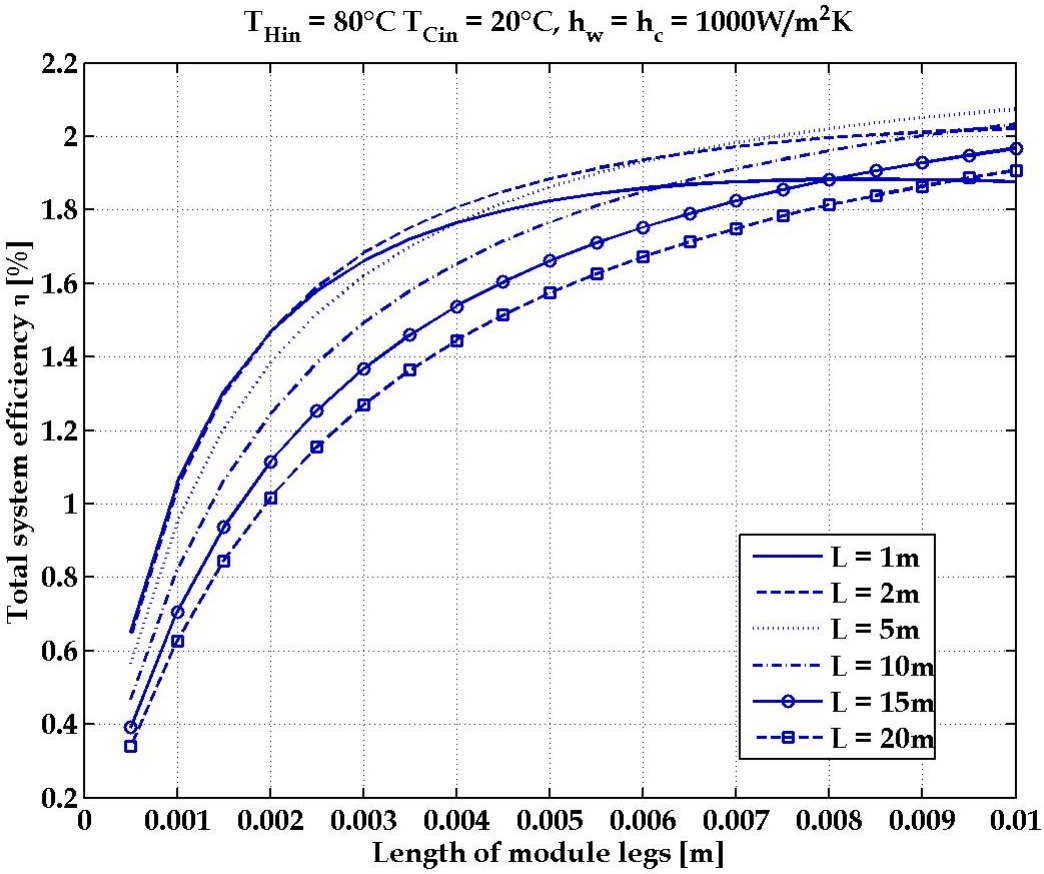

Figure 6.16 : *Total system efficiency as a function of the length of the module legs, T_{Hin}= 80°C, T_{Cin} = 20°C, $h = h_w = h_c$ = 1000 W/m²K, D = 0.02 m*

Next the length of the thermoelectric legs has been varied from 1 to 5 mm in combination with the variation of the depth *D* of the heat transfer tubes from 0.001 to 0.1 m with constant length *L* = 1 m. These results are presented in figures 6.17 to 6.19 and discussed below.

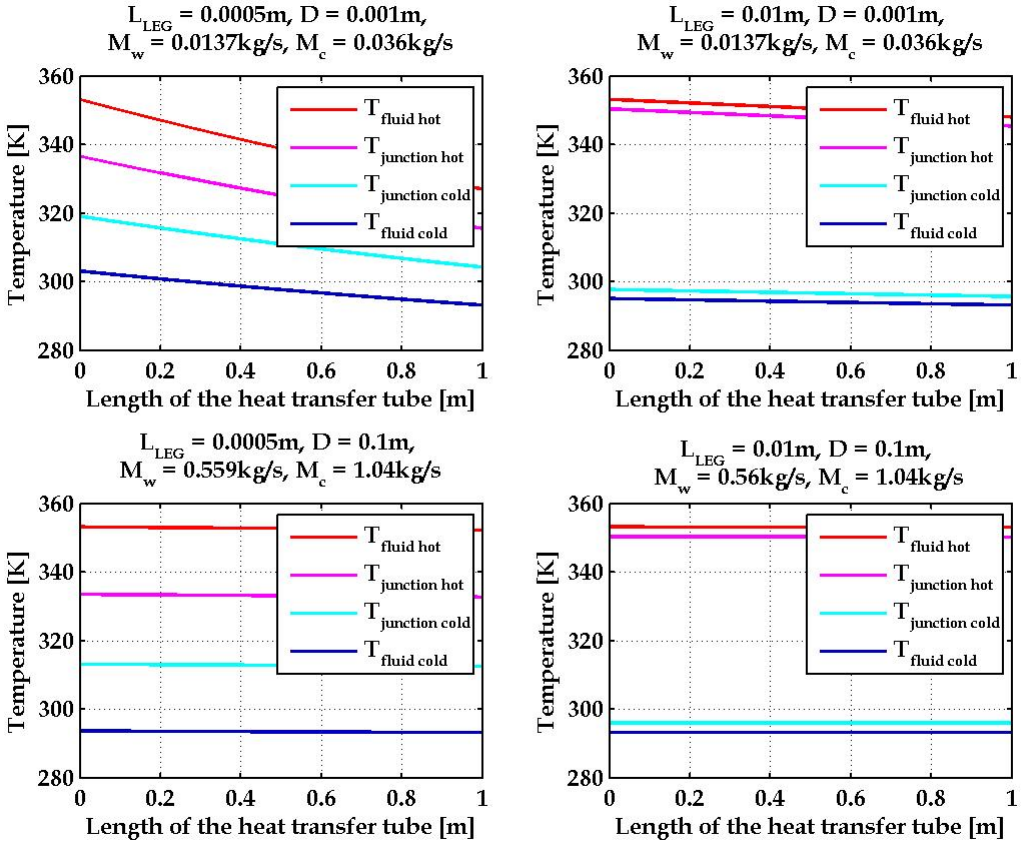

Figure 6.17: *Temperature profiles for various combinations of the depth D of the heat transfer tubes and the leg length of the modules, T_{Hin} = 80°C, T_{Cin} = 20°C, $h = h_w = h_c$ = 1000 W/m²K, W = 0.055m, L = 1m*

For constant tube length *L* and constant depth *D*, increasing leg length also yields higher effective temperature differences at the junctions (see figure 6.17). The specific volume V_{spec} increases with increasing leg length for all sizes of *D* (see figure 6.18). The influence is weak for small values of *D*, but grows exponentially with higher values of *D*. The explanation therefore is that longer legs have a higher thermal resistivity and so the heat consumption decreases. For small depths this is almost compensated by the efficiency increasing with leg length (figure 6.19). For large depths again a big amount of thermal energy requiring high pump power is supplied and cannot be utilized due to the high thermal resistivity of the long legs. The pump power remains constant and this leads to decreasing efficiency and increasing specific volume V_{spec} (figures 6.18 and 6.19)

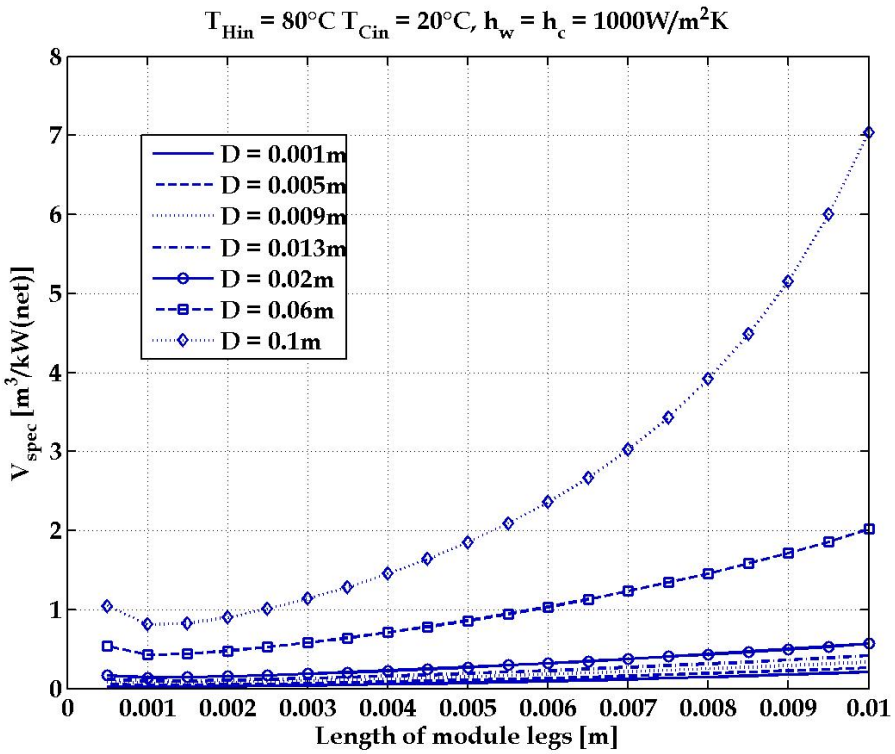

Figure 6.18: *Required specific volume as a function of the length of the module legs, T_{Hin}= 80°C, T_{Cin} = 20°C, h = h_w = h_c = 1000 W/m²K, L = 1m*

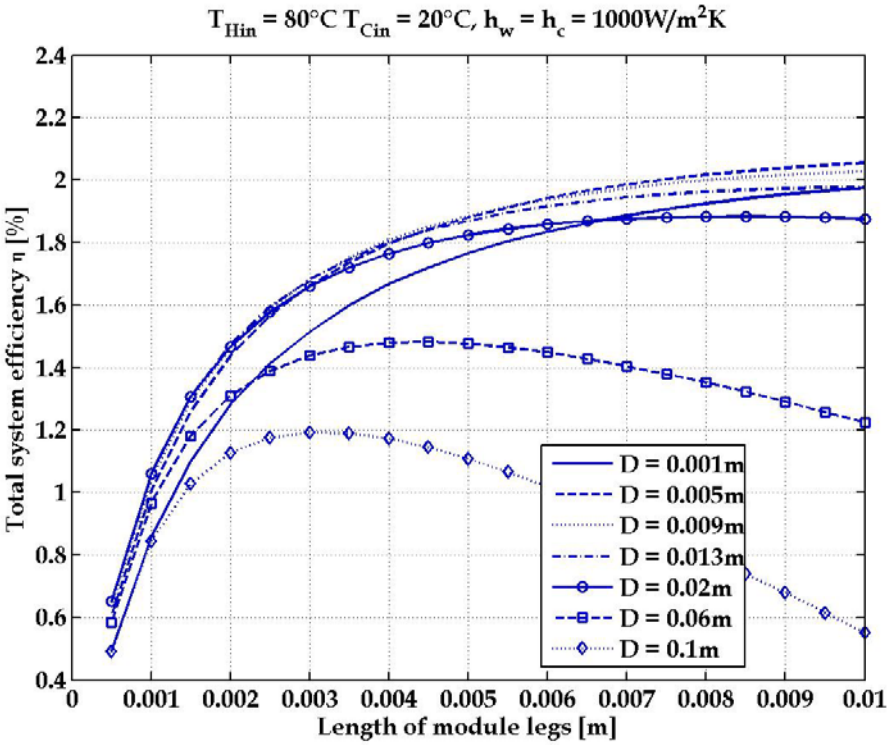

Figure 6.19: *Total system efficiency as a function of the length of the module legs, T_{Hin}= 80°C, T_{Cin} = 20°C, h = h_w = h_c = 1000 W/m²K, L = 1m*

Influence of material properties:

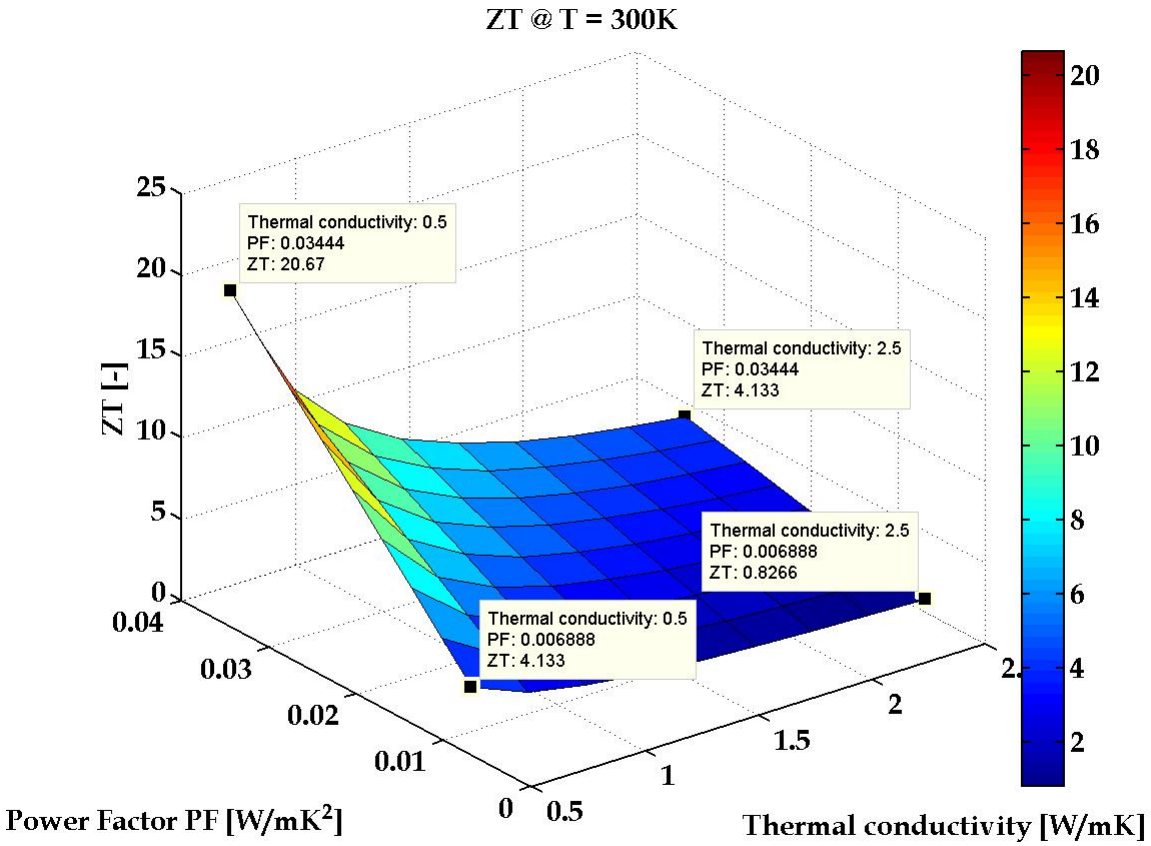

Figure 6.20 : *Figure of Merit as a function of material properties, T =300K*

In figure 6.20 the resulting ZTs according to the variation of the power factor and the thermal conductivity are displayed. The values grow from $ZT = 0.826$ for lowest power factor and highest thermal conductivity to a hypothetical 20.66 for highest power factor and lowest thermal conductivity.

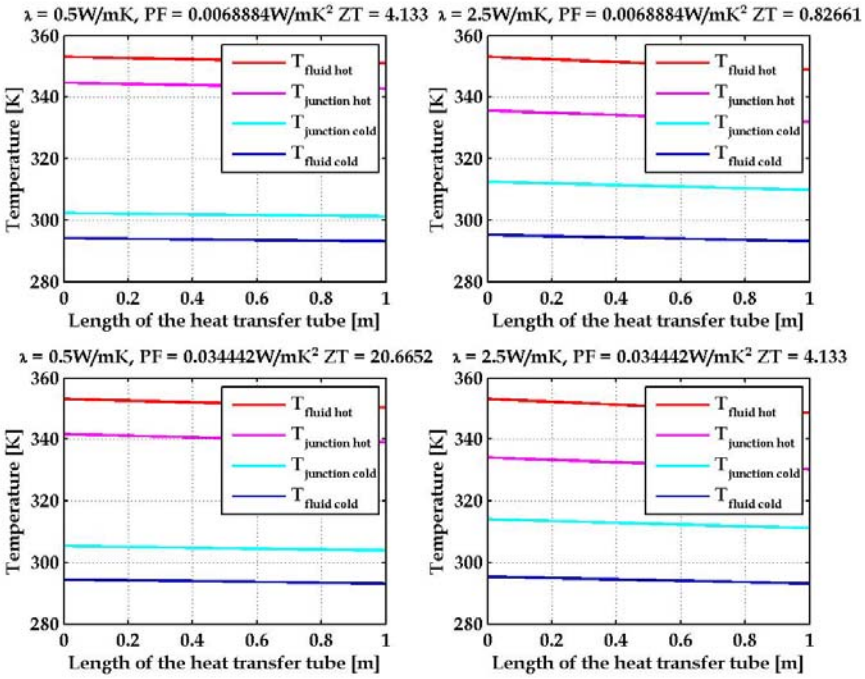

Figure 6.21 : *Temperature profiles for various combinations of material parameters, T_{Hin} = 80°C, T_{Cin} = 20°C, $h = h_w = h_c$ = 1000 W/m²K, W = 0.055m, L = 1 m, D = 0.02 m*

In the temperature profiles (compare columns of figure 6.21) it can be seen that for constant λ and increasing power factor *PF* (increasing *ZT*) the effective temperature difference at the junctions decreased. This becomes clear, when one considers that increasing the power factor in the way described above means higher heat consumption, due to higher Peltier heat and smaller Joule losses (equ. 4.4), this leads with constant heat transfer coefficients to higher temperature differences between the working fluid at the junction. In a similar way the behaviour at the cold side can be explained. Although the effective temperature difference at the junctions is smaller, both the power output and the system efficiency increase (see figures 6.19-6.20) as is explained by the higher values of *ZT*. Increasing the thermal conductivity at constant power factor also leads to higher heat consumption and a smaller effective temperature difference.

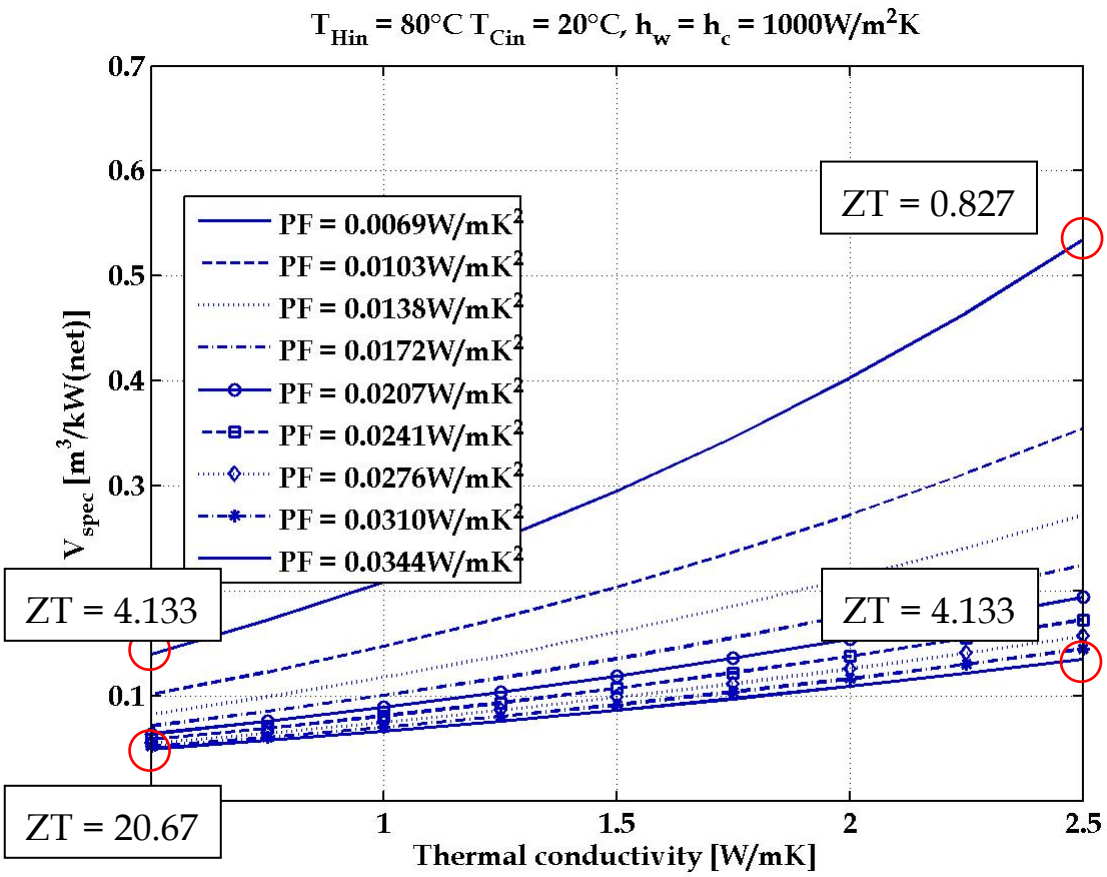

Figure 6.22 : *Specific volume as a function of the thermal conductivity*
T_{Hin}= 80°C, T_{Cin} = 20°C, h = h_w = h_c = 1000 W/m,L =1 m, D = 0.02 m, W=0.055m

Looking at figure 6.22 it can be recognized that for high power factors the influence of lowering the thermal conductivity on V_{spec} decreases. This is the same for small thermal conductivities and increasing power factors (figure 6.23). In both cases when ZT was increased to the highest value, there were only relatively small improvements concerning the power output. For the specific volume and thus also for the power output it is not too important which combination of the material properties is chosen for a specific *ZT* (figures 6.19 and 6.20).

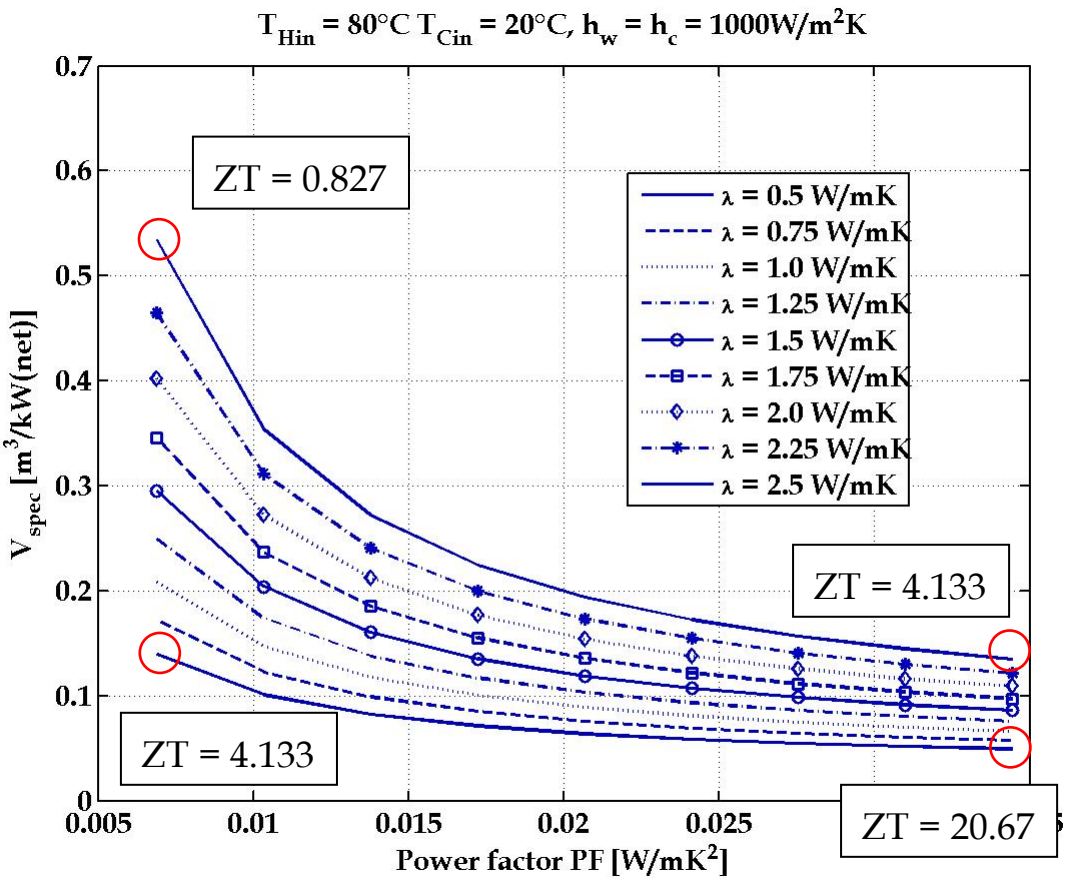

Figure 6.23 : *Specific volume as a function of the Power factor PF, T_{Hin}= 80°C, T_{Cin} = 20°C, $h = h_w = h_c$ = 1000 W/m, L =1 m, D = 0.02 m, W=0.055m*

This is different, when we look at figures 6.24 and 6.25, where the system efficiency as a function of the material properties is given. Here it can easily be seen that for the same values of *ZT* the system efficiency is much higher for low thermal conductivity. The explanation for this can also be found in the temperature profiles. For lower thermal conductivity the thermoelectric generator works across a higher temperature difference, according to the definition of Carnot this yields in general a higher efficiency (compare figure 6.18 top/left and bottom/right).

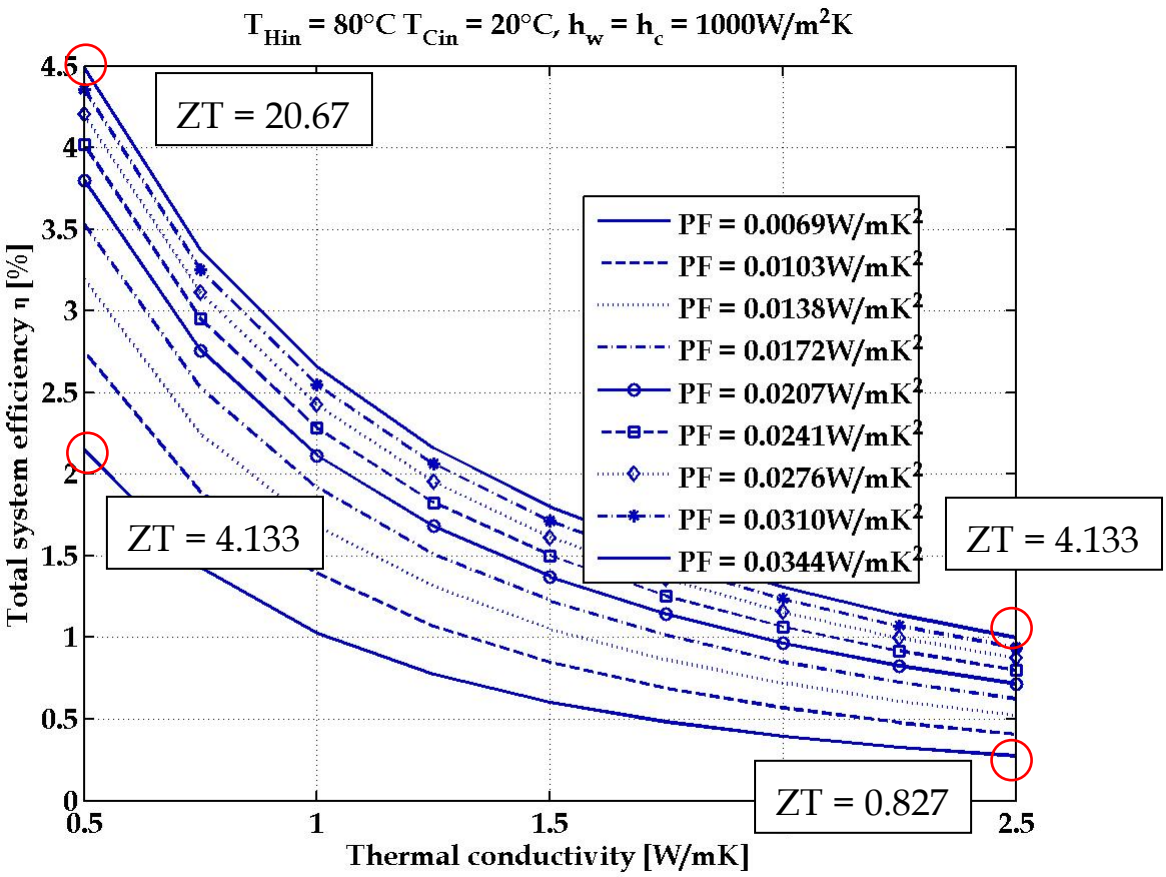

Figure 6.24 : *Total system efficiency as function of the thermal conductivity, T_{Hin}= 80°C, T_{Cin} = 20°C, $h = h_w = h_c$ = 1000 W/m, L =1 m, D = 0.02 m, W=0.055m*

It can also be stated that improving *ZT* by lowering the thermal conductivity λ has a strong influence (exponential) on the system efficiency, as has the power factor.

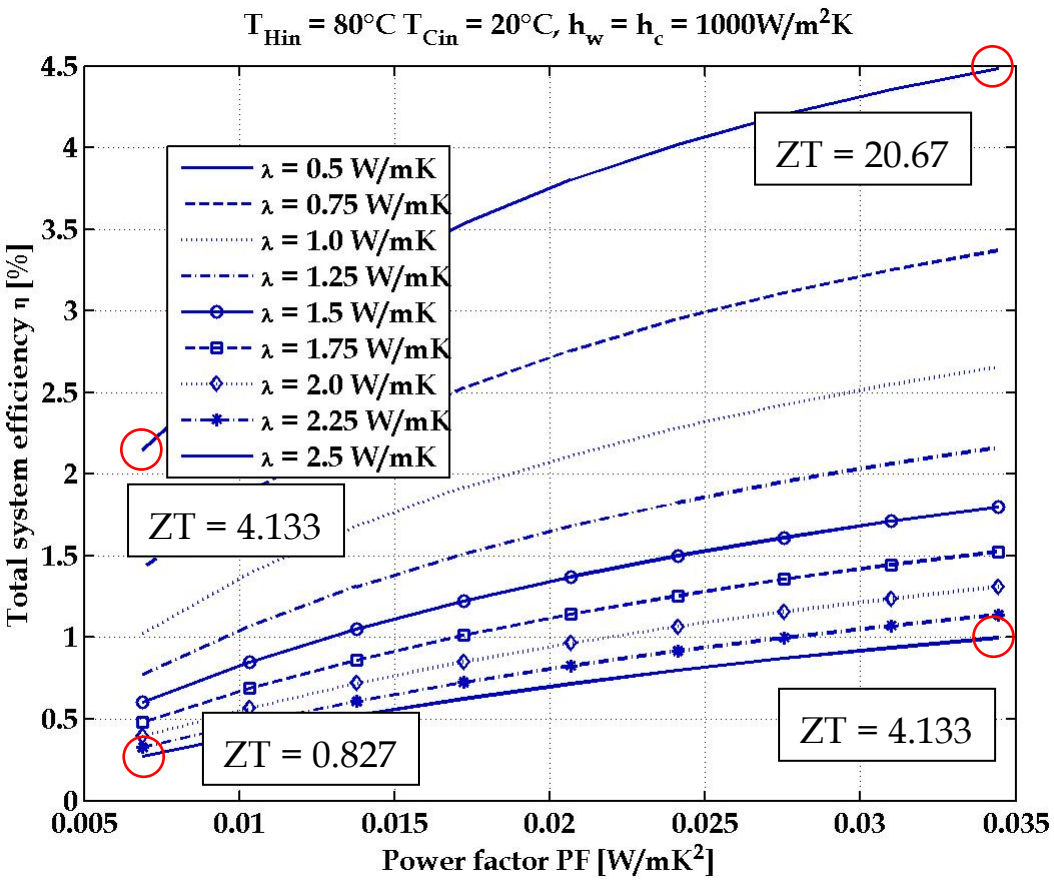

Figure 6.25 : *Total system efficiency as function of the Power factor PF, T_{Hin}= 80°C, T_{Cin} = 20°C, h = h_w = h_c = 1000 W/m, L =1 m, D = 0.02 m, W=0.055m*

As it is seen that for the specific volume respectively the power output only the total value of ZT is crucial and on the other side the system efficiency is more sensitive to the lowering of the thermal conductivity, the efforts of the materials science will go in this direction; this is already a main aim of many research groups.

To give a better insight into the results and to adapt the models to a specific application a readily understood example for thermoelectric power generation is presented next.

6.3 Example for thermoelectric power generation

As the explanations given hitherto were of a more general nature in the following the procedures developed will now be applied to a specific example titled:

Electric power generation utilizing geothermal heat sources

Geothermal energy in general can be subdivided in two main areas (for illustrations and more basics see http://www.unendlich-viel-energie.de/en/geothermal/deep-geothermics.html).

These are depending on the length of the boreholes respectively on the depth of the exploited geothermal reservoir:

- Near surface geothermal energy: (ref. as above)

  Near-surface geothermal energy utilizes the energy stored in the top layers of the earth down to 400 metres or in the groundwater. The prevailing temperatures of only 8 to 15 degrees Celsius can be used in different ways to provide space heating and hot water as well as for cooling buildings. Heat pumps, geothermal energy collectors (slinkys), ground probes, energy piles or even concrete structural elements in contact with the soil are used to utilize the energy that exists in the shallow subsoil. Switzerland is Europe's primus in the utilization of near surface geothermal energy sources.

- Deep geothermal energy: (ref. as above)

  Deep geothermics is the term used to describe utilization of geothermal energy at depths between 400 and 5000 metres. The temperatures there are far higher than those used in near-surface energy extraction. Apart from heat supply, deep geothermal energy can be used for electricity generation. Economic electricity generation is possible from a temperature of around 90 degrees Celsius. The main advantage of geothermal energy is its permanent availability. All geothermal power plants in operation are exploiting hydrothermal sources, this means that large reservoirs of hot water at depth have been tapped. Suitable reservoirs can predominantly be

found in the vicinity of volcanic areas and are thus not universally available.

Electrical power production out of geothermal sources is still in the initial stages in Switzerland. The deep heat mining project in Basel is stopped after unacceptable seismic activities during the stimulation process and is still waiting for a decision to continue. The site at Basel is together with Soultz/France a pioneer project for Enhanced Geothermal Systems (EGS) also known as Hot dry rock systems (HDR), Hot-Fractured-Rock (HFR) systems or Petrothermal systems. Enhanced geothermal systems (EGS) enable the exploration of the Earth's interior heat outside known geothermal provinces. In contrast to a geothermal field in one of these volcanic/tectonic anomalies, an EGS is based on the artificial stimulation of naturally tight, cleft, hot formations. Fluid will be circulated in a closed circuit mode, whereby reservoir pressures and fluid throughputs are managed by balanced production and injection rates in multiple well arrays.

For the example presented in the following an EGS system has been selected to extract geothermal heat out of the subsurface. A characteristic and also a disadvantage of EGS systems are their relatively high pressure drops along the artificial underground heat exchanger, which requires additional pump power and so degrades the total system performance. Anyway or even hence this configuration seems to be an interesting and representative example to be investigated and discussed.

The conditions and selected parameters for the investigation are:

- T_H = 120°C, usable water temperature at the surface out of a 3500 m depth bore hole
- T_C = 12°C, average water temperature of a the river Rhine in Switzerland

The required pressure to pump the water through the EGS is assumed very optimistically as

- 15 bar and for the cold water supply
- 1 bar

The varied parameters and the ranges of variation are:

- Heat transfer coefficients h_W = h_C = h = 2000 W/m²K and 5000 W/m²K
- Figure of Merit ZT = 0.817 (commercial modules available) and 4.95 (future materials ?),

ZT is varied as follows:

for a ZT of 0.817 the material properties of the module specified in chapter 5.4 are used. To improve the ZT to the hypothetical value of 4.95 the Seebeck coefficient has been increased by the factor 1.25, the electrical conductivity by the factor 2 and the thermal conductivity has to be halve.

- Widths of the heat transfer tubes W = 0.055 m (1 module) and W = 0.55 m (10 modules in a row)

The lengths L and depths D of the heat transfer tube have been varied in a way to find the extrema for power output and efficiency.

The results of the optimizations are presented in tables where each quantity for the varied parameters can be compared.

The quantities presented and discussed in the following are:

- Temperature profiles along the heat transfer tubes
- Generated power P_{el}
- Required pump power P_{pump}
- Net produced power $P_{net} = P_{el} - 0.5 * P_{pump}$
- Specific volume V_{spec}
- Consumed heat Q_H
- Total system efficiency η_{total}
- Number of modules to generate 1 kW of P_{net}

The structure of the tables is explained in figure 6.26.

W = 0.055m (1 module) **I** **h = 2000W/m²K** **ZT = 0.817** **Leg length = 0.0014m**	**W = 0.055m (1 module)** **IV** **h = 2000W/m²K** **ZT = 4.95** **Leg length = 0.0014m**
W = 0.055m (1 module) **II** **h = 2000W/m²K** **ZT = 0.817** **Leg length = 0.0025m**	**W = 0.055m (1 module)** **V** **h = 5000W/m²K** **ZT = 4.95** **Leg length = 0.0014m**
W = 0.055m (1 module) **III** **h = 2000W/m²K** **ZT = 0.817** **Leg length = 0.005m**	**W = 0.55m (10 modules)** **VI** **h = 5000W/m²K** **ZT = 4.95** **Leg length = 0.0014m**

Figure 6.26 : *Structure of the tables presenting the values of the varied parameters*

The temperature profiles presented first do not follow the structure of figure 6.26. Each quartet of T-profiles belongs to a combination (set) of the parameters varied respectively to one cell of the table in figure 6.26.

The depth D and length L are selected for the points of:

- maximum net produced output power - top/left of the quartet
- maximum system efficiency – bottom/right of each quartet
- minimum specific system volume V_{spec} - top/right of each quartet
- minimum no. of modules to produce 1kW net output power - bottom/left of each quartet

Additionally the mass flow rates through the heat transfer tubes are given. Note again that here a cross flow heat exchanger is considered and therefore the fluid flows go left to right at the hot side and right to left at the cold side.

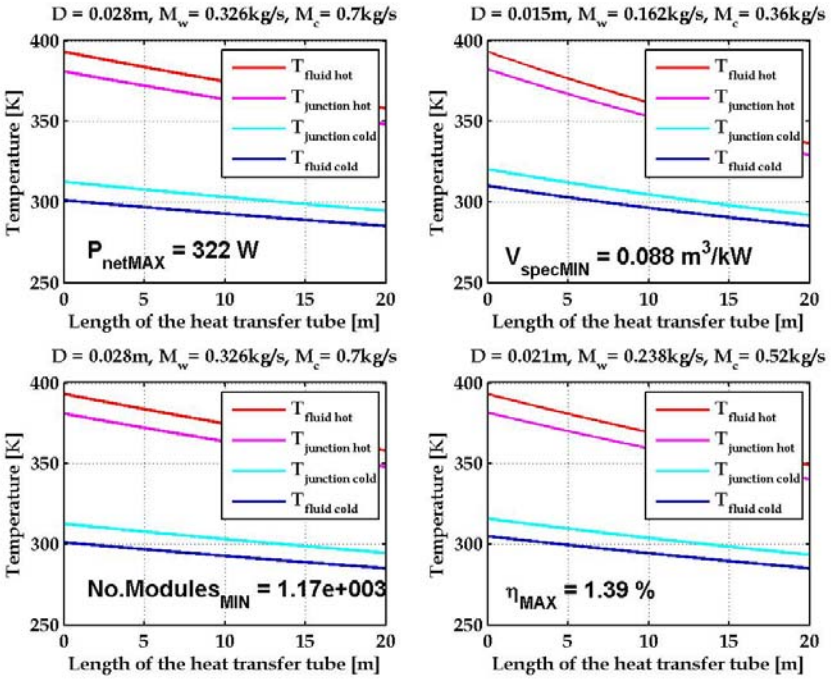

Figure 6.27 :*Temperature profiles of parameter set I*

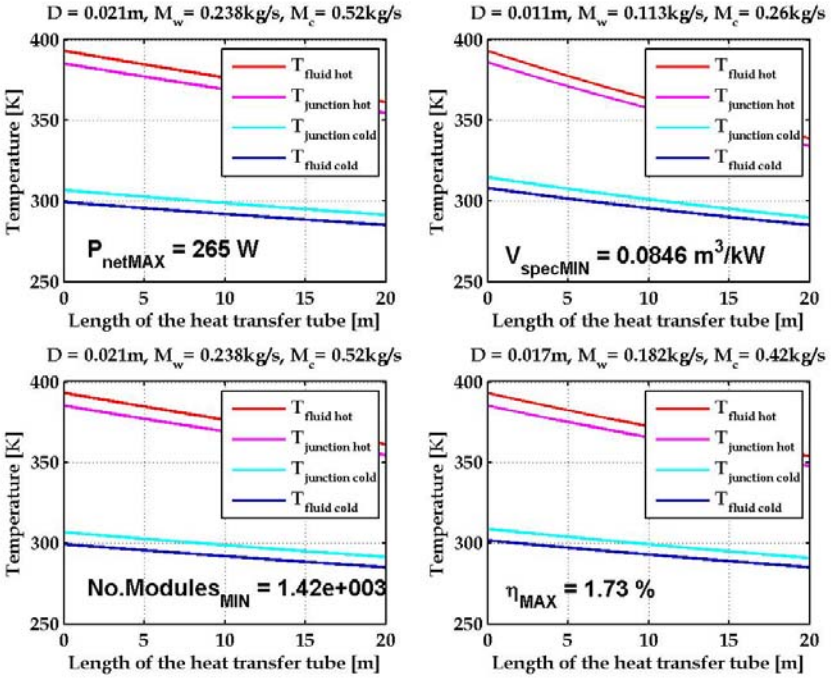

Figure 6.28 :*Temperature profiles of parameter set II*

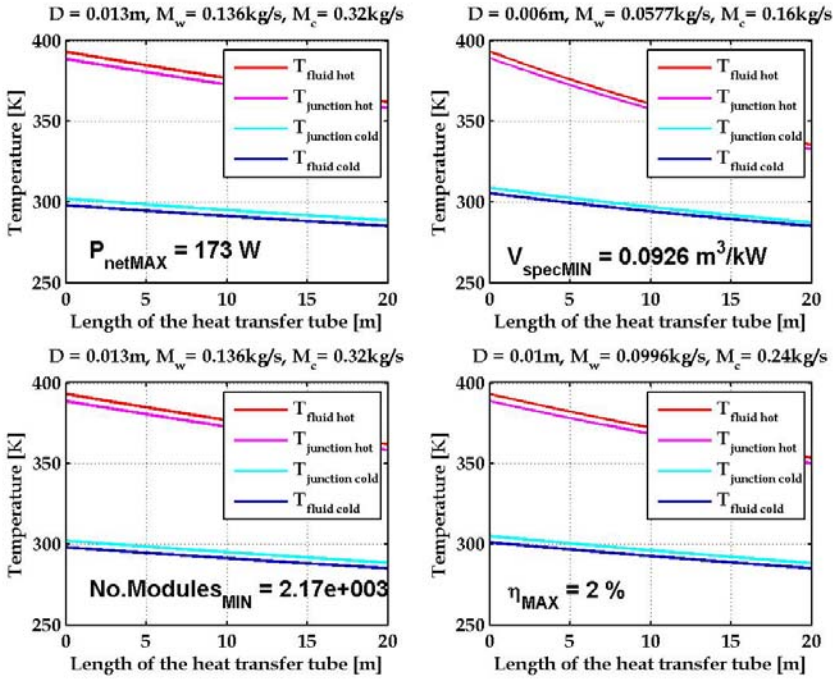

Figure 6.29 :*Temperature profiles of parameter set III*

Comparing the temperature profiles belonging to the parameter sets I, II and III, (figures 6.27-6.29) where the length of the module legs is the parameter varied it can be seen that with increasing leg length the effective temperature difference increases due to the higher thermal resistance of the module legs, which is an already known fact. For the temperature profiles of maximum efficiency (right/bottom) it would be expected that the distribution shows the highest average temperature difference compared to other points of extrema e.g. maximum net generated power (left/top). Here the influence of the required pump power causes that the system is more efficient by having smaller mass flow rates due to smaller depth *D* which leads to smaller required pump power (figure 6.34). Smaller mass flow rates yield stronger cooling of the working fluid as the heat input (figure 6.37) also decreases with smaller heat exchanger area. The maximum efficiency can be found at relatively small depths *D*, while the associated absolute values of *D* increase with increasing *L* (figure 6.38). The minimum number of modules is related with the maximum generated power this means that identical heat transfer tube dimensions and can be found at higher depths for the same length *L* (compared to maximum efficiency). The minimum specific system volume can be found at the smallest depths and is reached when the gradient of the net generated power *D* increasing with *D* comes to

saturation and gets smaller than the linear gradient of the volume V growing with D (at constant length).

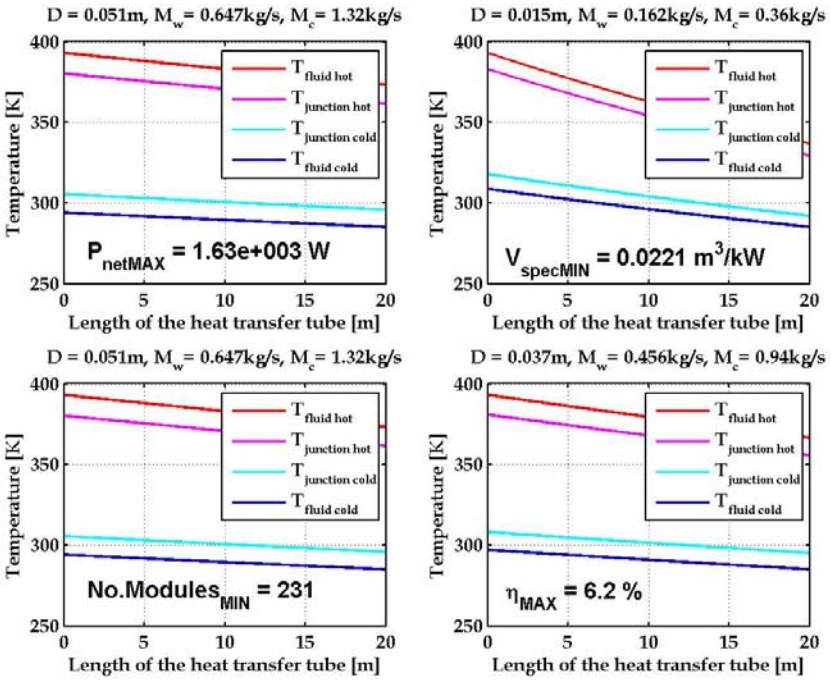

Figure 6.30 :*Temperature profiles of parameter set IV*

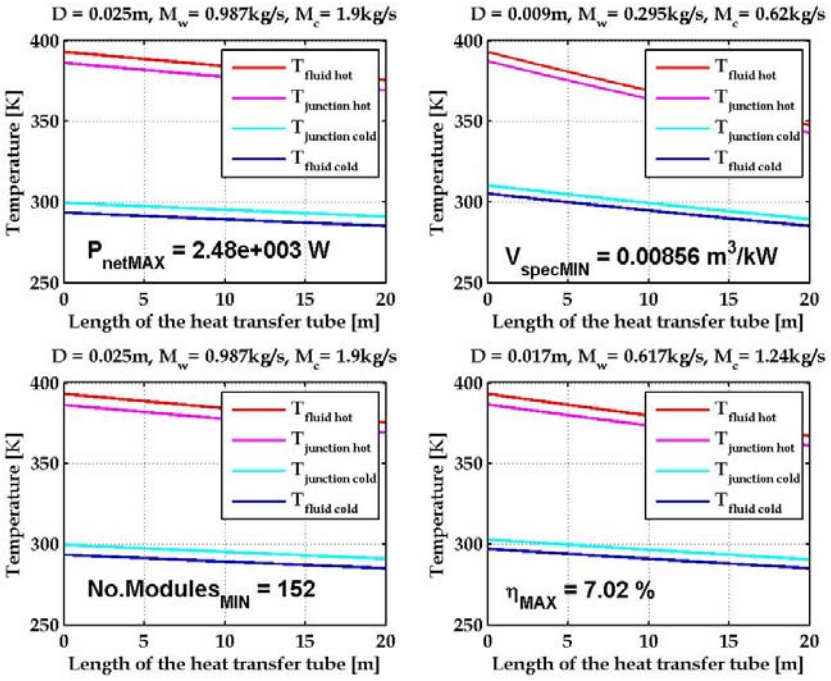

Figure 6.31 :*Temperature profiles of parameter set V*

Comparing figures 6.27 and 6.31, where the thermoelectric material properties have been varied in the way explained above, what results from an increase of ZT from 0.817 to 4.95 is that there are only small differences in the temperature distributions along the heat transfer tubes. The real difference can be found in the also displayed numbers. The improved material properties permit a wider range for the combinations of the heat transfer tube dimensions (e.g see figure 6.35 – upper row) that permits the utilization of larger amounts of thermal energy (higher mass flow rates). The values of the extrema are therefore improved by factors 4 to 5.

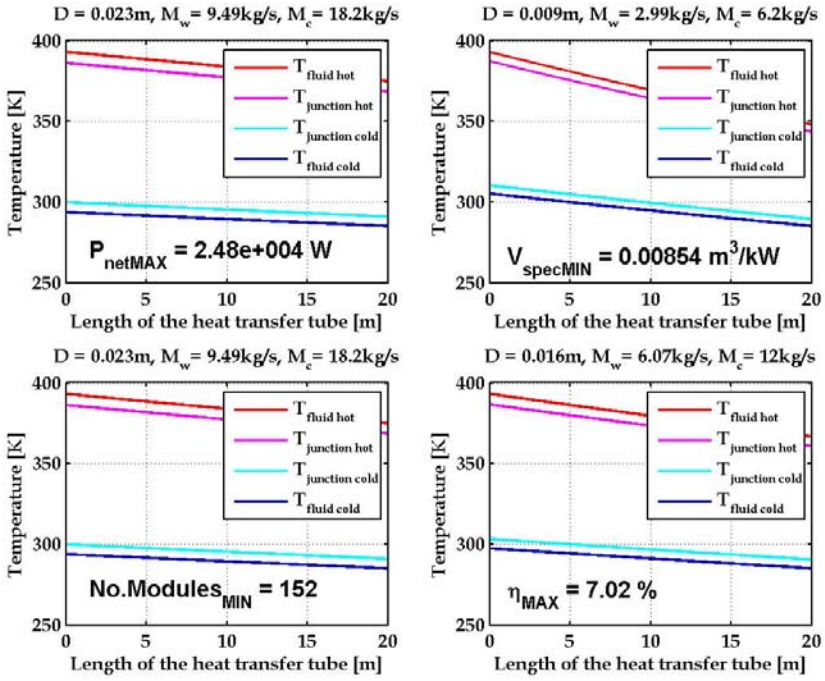

Figure 6.32 :*Temperature profiles of parameter set VI*

Comparing figures 6.30 and 6.31 the increased heat transfer coefficient *h* (from 2000 to 5000 W/m²K) results in a higher effective temperature difference between the junctions and thus in improved values of the extrema considered. The field of reasonable combinations for the dimensions of the heat transfer tubes is smaller compared to the case of parameter set IV, due to the increased mass flow rates (higher required pump power) for the assumed higher heat transfer coefficients (e.g figure 6.35 – top/right – middle right).

In figure 6.32 the width *W* of the heat transfer tubes is increased by factor 10. This means that in this dimension 10 modules are arranged

transversely to cover the total heat exchanger area. The results show, as expected, that the absolute values as e.g. net generated power also increase by the factor 10 and that the specific quantities as e.g. the efficiency remain constant compared to the numbers displayed in figure 6.31.

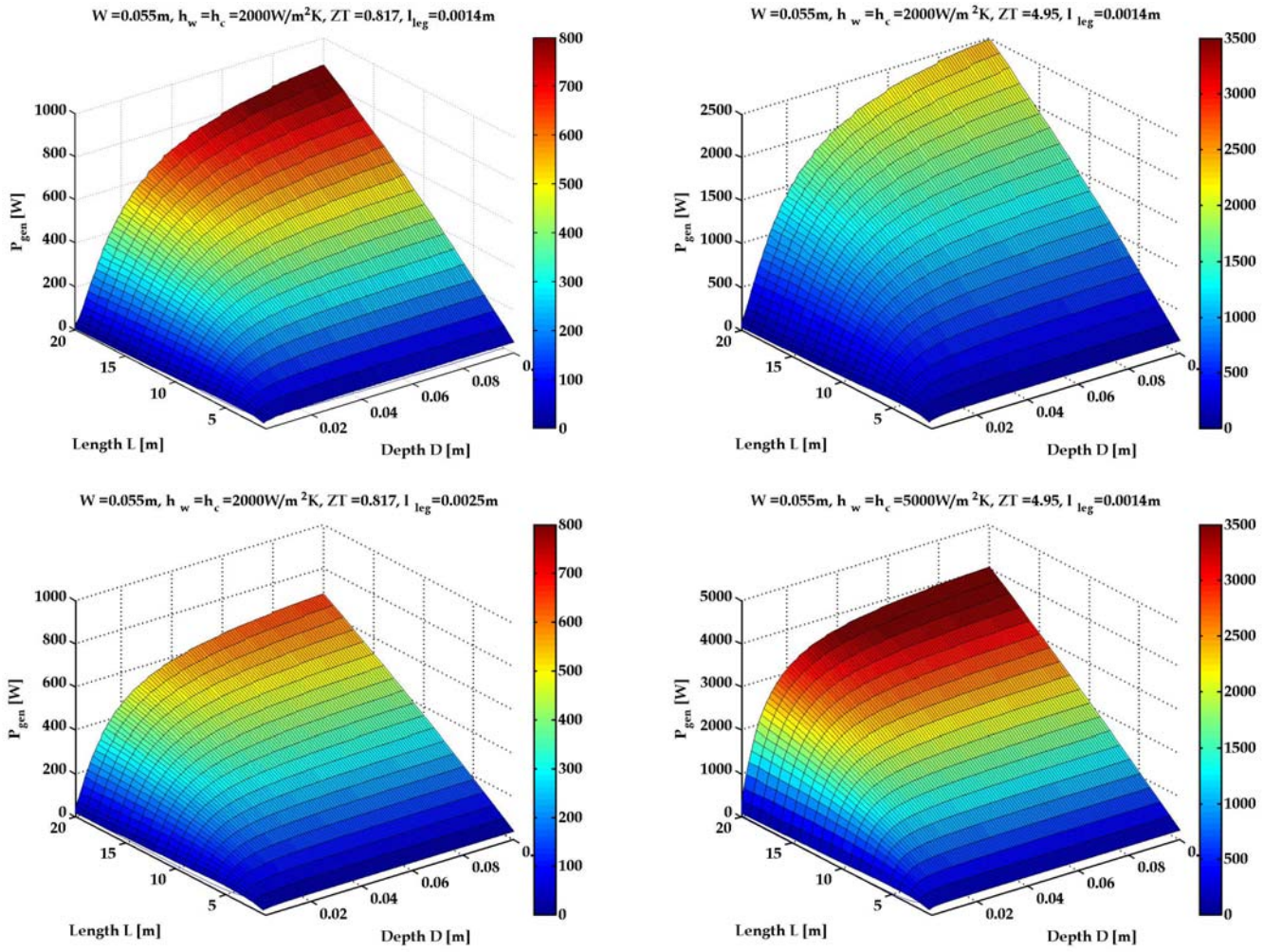

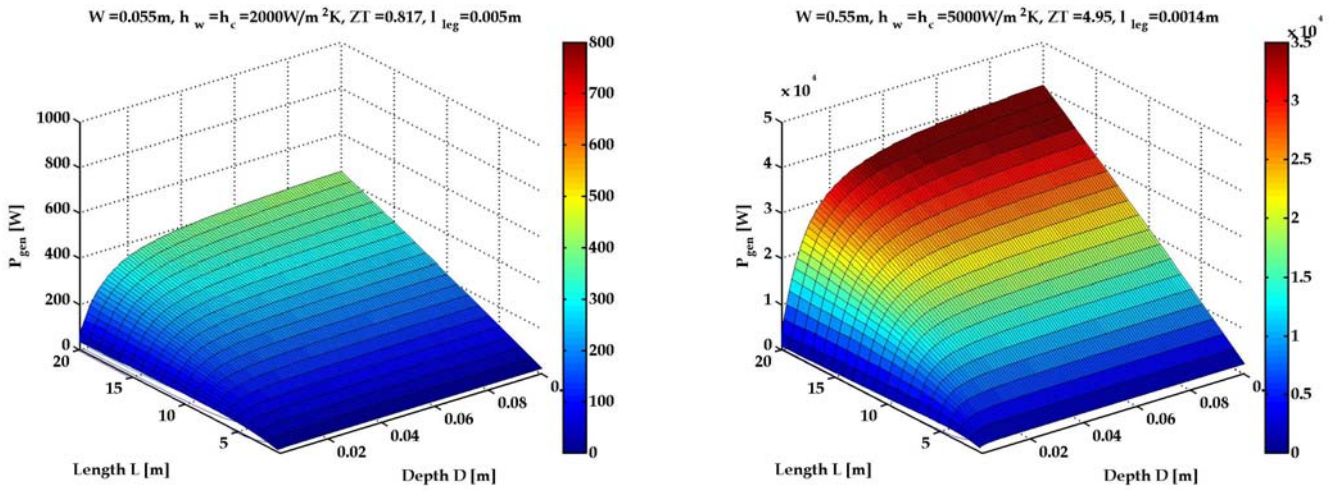

Figure 6.33 : *Generated power as a function of the length L and the width D of the heat transfer tubes for various parameter sets*

The generated power displayed in figure 6.33 is the generated electrical power of the thermoelectric modules. Therefore it grows with increasing heat transfer dimensions asymptotically to the values of the isothermal case. Considering a defined length *L* (defined heat exchanger area) of the heat transfer tubes and a specific parameter set the heat uptake (figure 6.37) increases with increasing depth (increasing mass flow rates with constant heat transfer coefficient). For a better explanation an additional temperature profile for parameter set VI is given (figure 6.33b). At small depth *D* the heat uptake leads to strong cooling (non-linear T-distribution) of the heat transfer media (figure 6.33b – top/left) according to the size of the heat exchanger area respectively the thermal energy uptake of the modules. Exceeding a particular value of *D* the heat consumption comes to saturation, as can be seen in the temperature profiles assuming their typical linear character (figure 6.33b – top/right). Further increment of *D* leads to constant effective temperature differences along the heat transfer tubes (figure 6.33b – bottom/left) finding its end in the almost isothermal case mentioned above. (figure 6.33b – bottom/right)

The influence of the varied parameters is as follows:

- Decreasing leg length shows higher maxima for P_{gen} (figure 6.33 – left column)
- Increasing ZT from 0.82 to 4.95 increases the generated power by a factor of about 4 (figure 6.33 – upper row)

- Increasing the heat transfer coefficient from 2000 to 5000 W/m²K increases the P_{gen} up to 25% (figure 6.33 – top/right – middle/right)

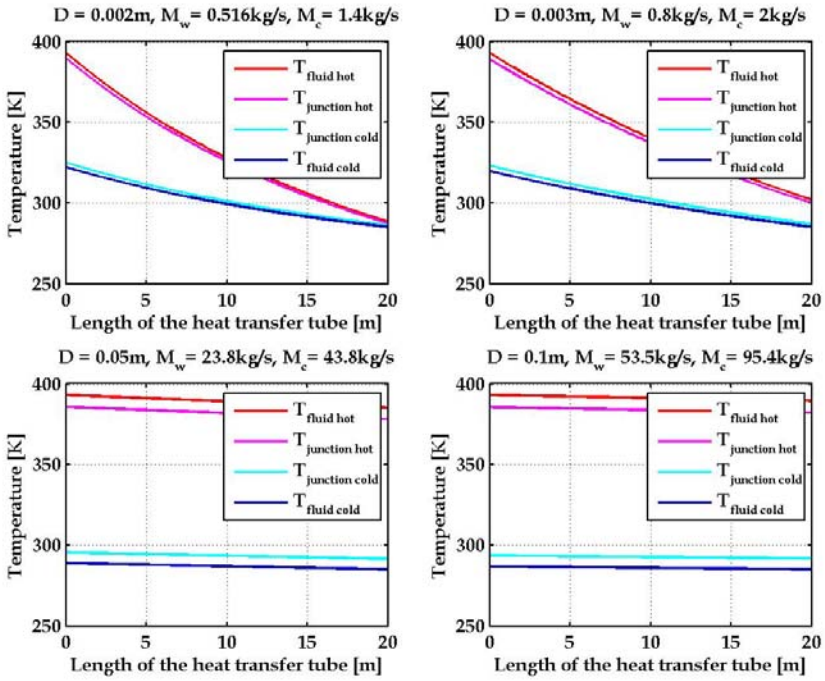

Figure 6.33b : *Temperatur profiles for L = 20 m and various D (parameter set VI)*

In figure 6.34 the required pump power is displayed for the various parameter sets. The pump power increases almost linear with depth *D* respectively with the mass flow rates as the pressure (15 bar) needed to circulate the water through the bore hole is the dominating factor for the required pump power, which also increases slightly with *L* due to increasing friction losses. At small depths an exponential increase of the pump power due to friction losses according to equ. 4.25 has also to be considered. The selected range for *D* in this large-scale application shows this influence very weak at the smallest depths (figure 6.34).

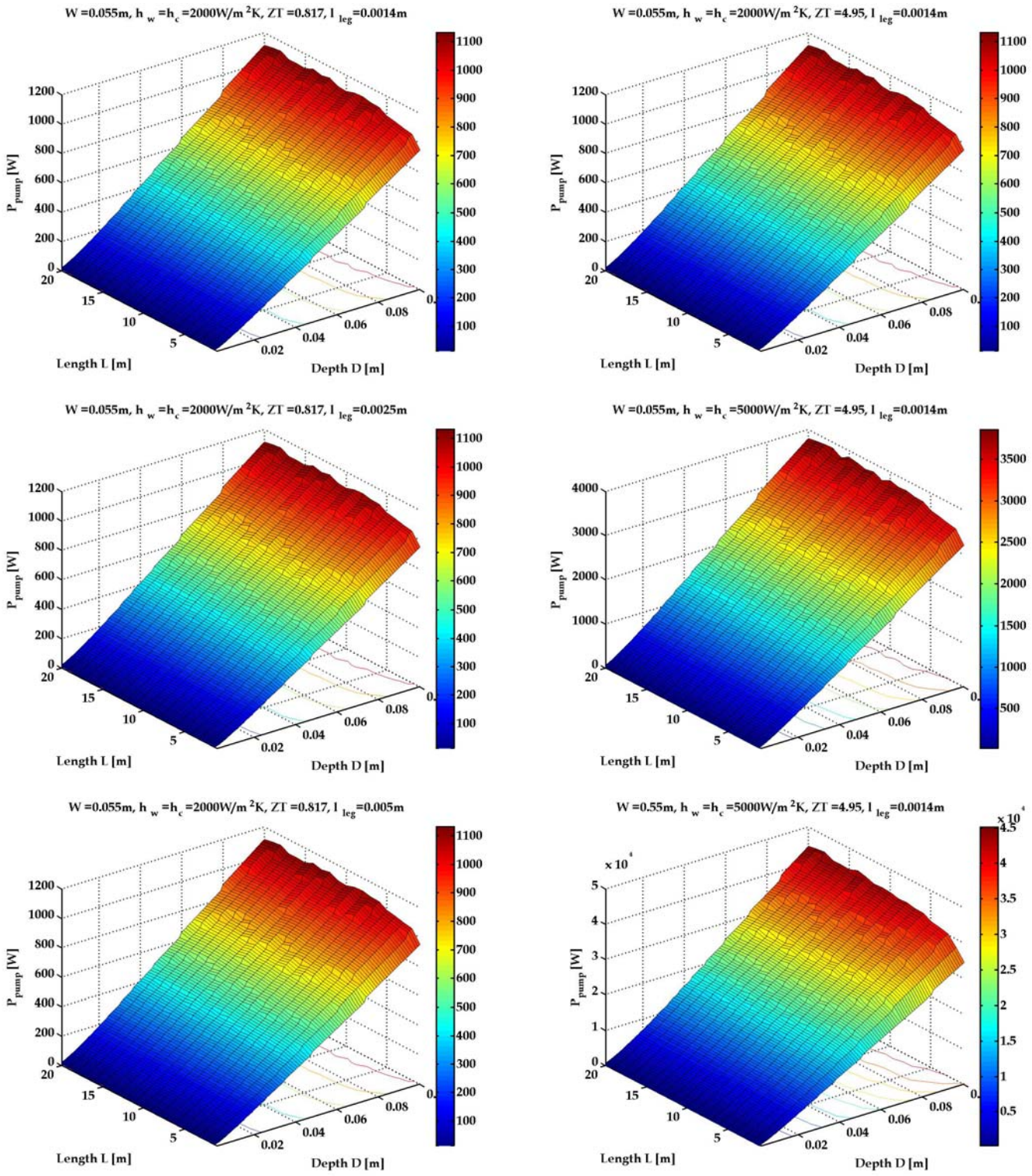

Figure 6.34 : *Required pump power as a function of the length L and the width D of the heat transfer tubes for various parameter sets*

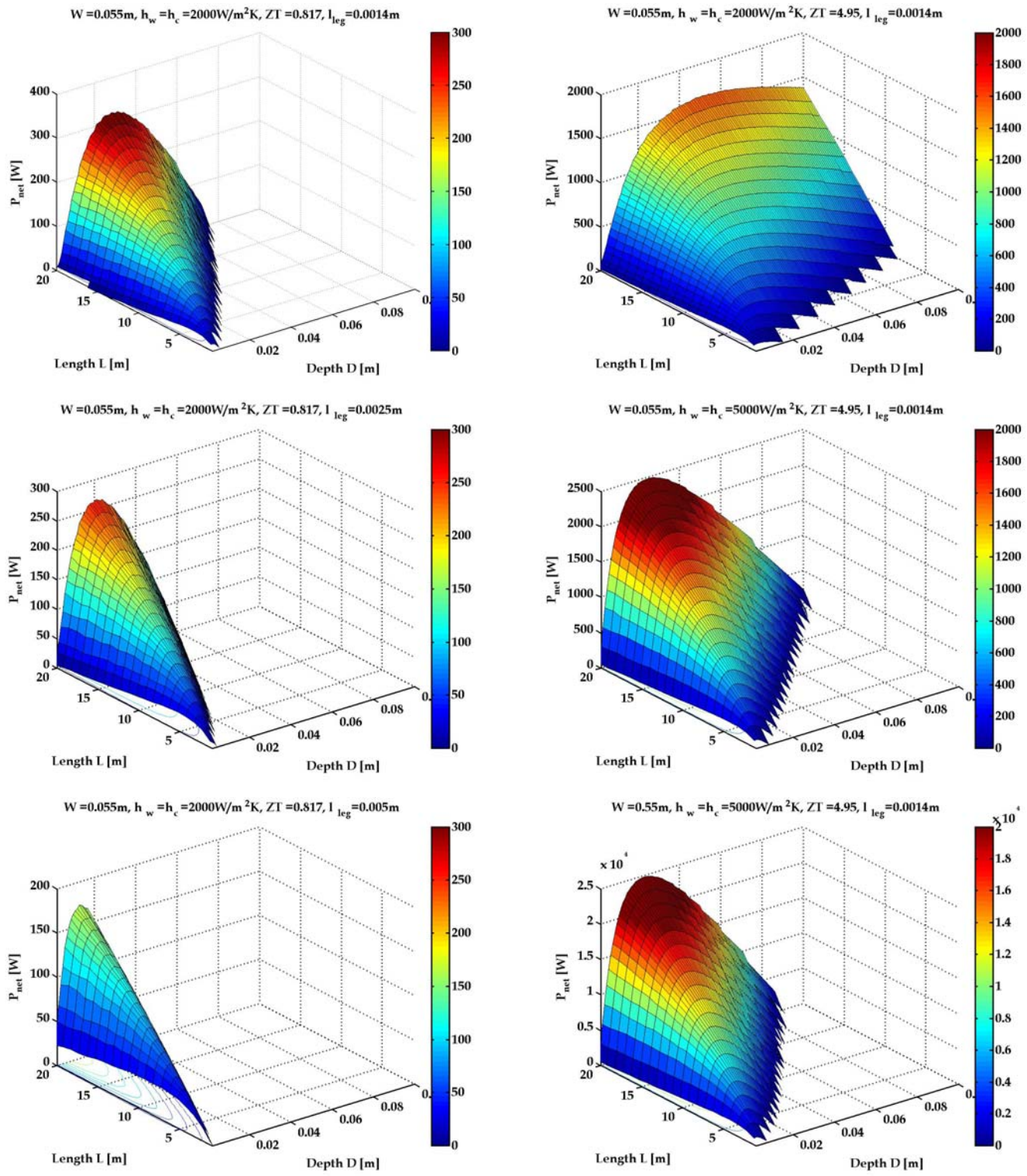

Figure 6.35 : Net *produced electrical power as a function of the length L and the width D of the heat transfer tubes for various parameter sets*

Figure 6.35 shows the (positive) values of the net generated power. It can be seen that the parameters varied have influences on the absolute value

of the net generated power and also on the field of reasonable combinations for the heat transfer tube dimensions such as:

- Smaller leg length increases the maxima of P_{net} and increases the field of useful combinations slightly (figure 6.35 - left column)
- Increasing ZT increases the maxima of P_{net} and increases the field of useful combinations strongly (figure 6.35 – upper row)
- Increasing heat transfer coefficients increases the maxima of P_{net} and decreases the field of useful combinations (figure 6.35 – right/top – right/middle)

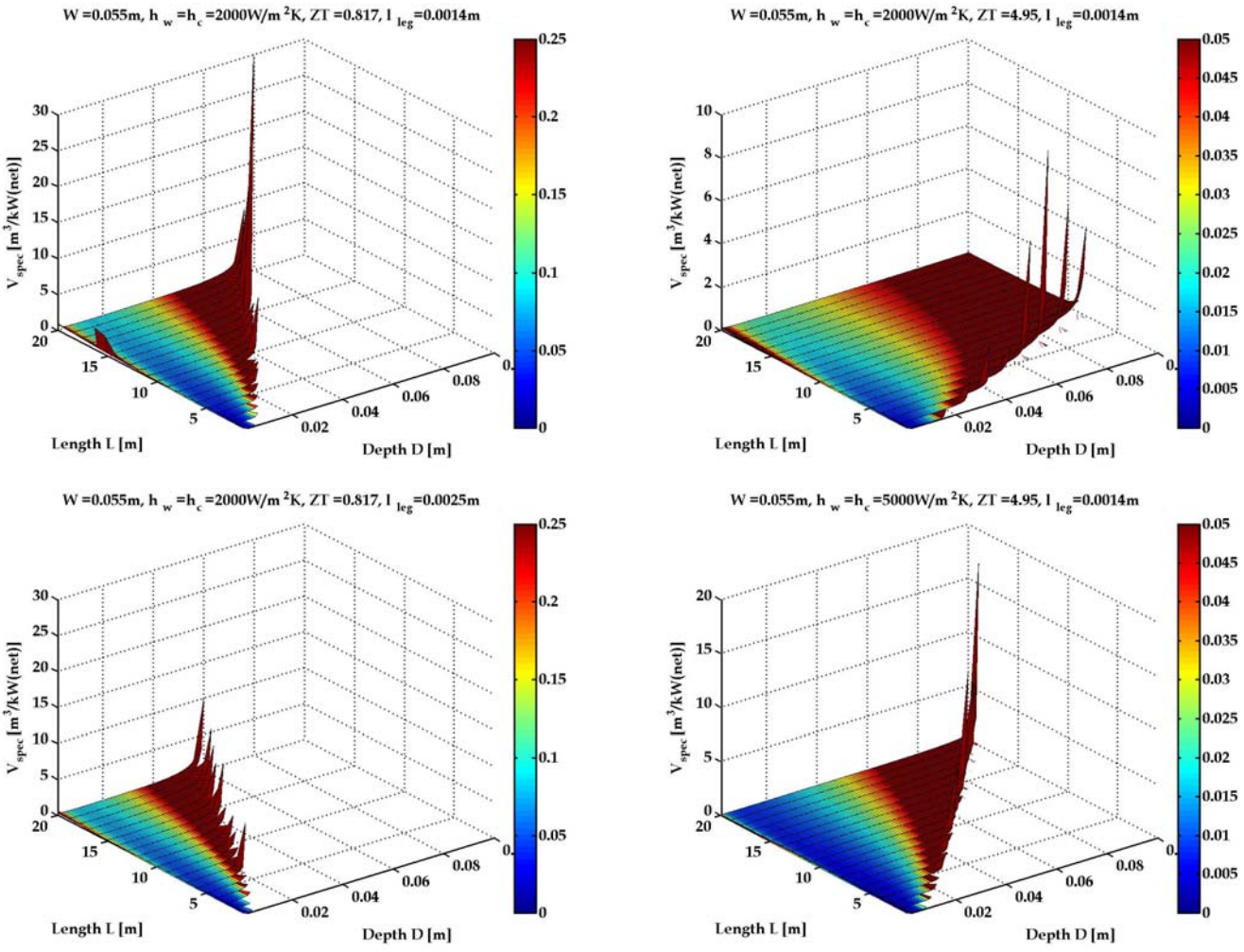

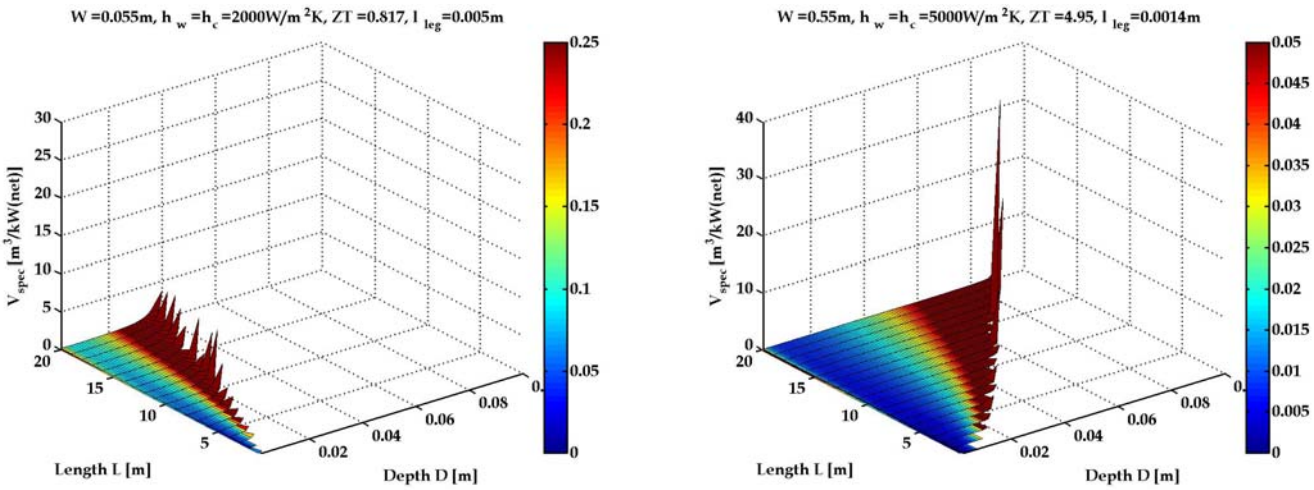

Figure 6.36 : *Specific system volume as a function of the length L and the width D of the heat transfer tubes for various parameter sets*

The specific system volume (figure 6.36) is a convenient unit for optimization strategies. It links the influence of the above mentioned quantities, generated power, pump power with the system dimensions and gives a value for the energy density of the system, which is together with the system efficiency an often used quantity for comparison of different energy systems.

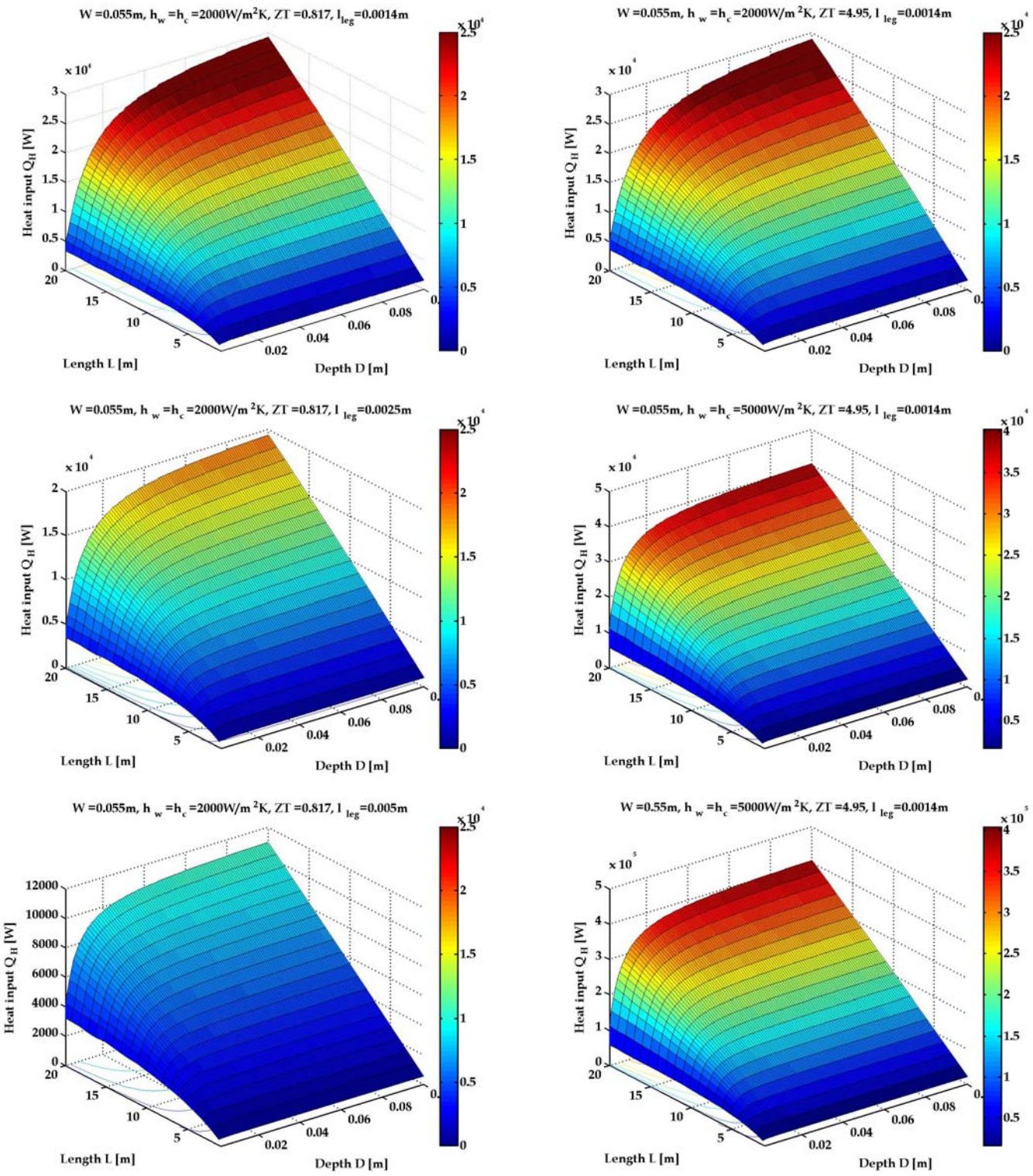

Figure 6.37 : *Heat input Q_H as a function of the length L and the width D of the heat transfer tubes for various parameter sets*

The heat input (figure 6.37) has already been mentioned and discussed in the explanations of the temperature profiles and the generated power. It

is presented here as it leads to the next important performance quantity: the total system efficiency.

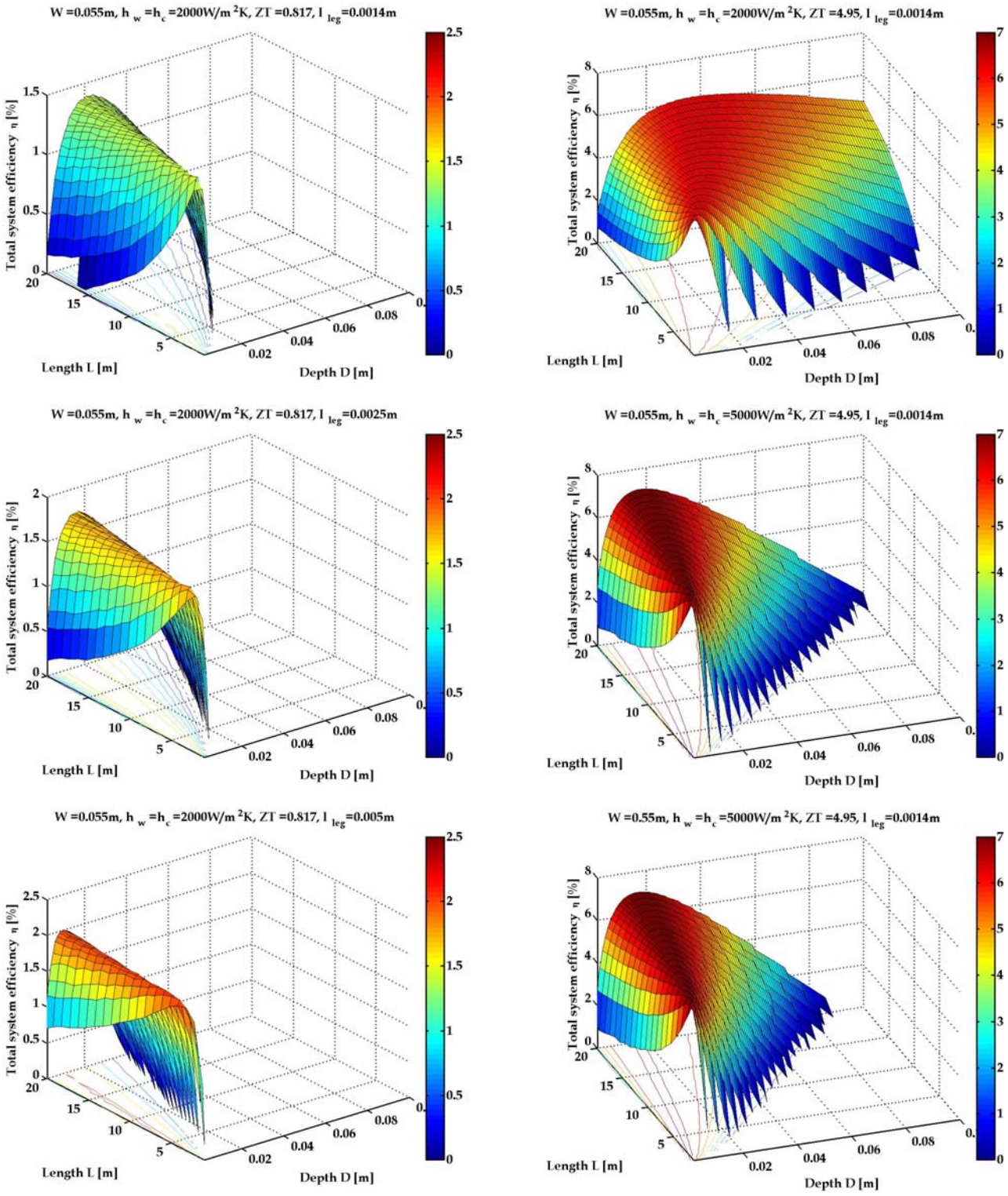

Figure 6.38 : *Total system efficiency as a function of the length L and the width D of the heat transfer tubes for various parameter sets*

The behaviour of the total system efficiency (figure 6.38) can be explained as follows:

- Increasing leg length increases the efficiency due to higher thermal resistance resulting in higher effective temperature differences at the junctions. (figure 6.35 - left column)
- Increasing ZT increases the efficiency due to lower thermal conductivity and increased power factor PF of the materials (figure 6.35 – upper row)
- Increasing heat transfer coefficients increases the efficiency and gives better defined maxima (figure 6.35 – right/top – right/middle)

The development of new materials with higher ZT would lead to a drastic improvement of the characteristic parameters V_{spec}, η and *number of modules* particularly when the strong influence of the leg length is also considered.

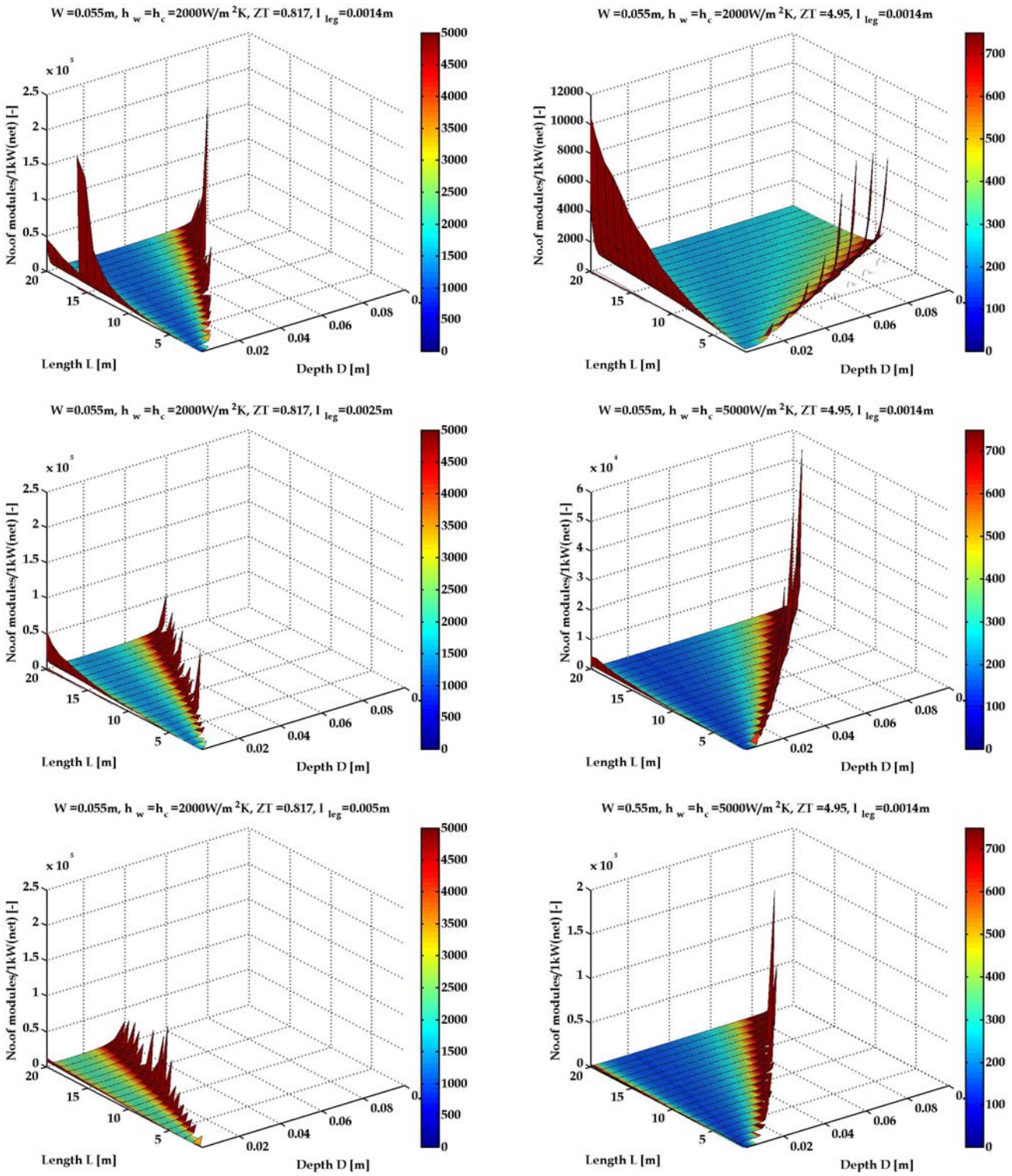

Figure 6.39 : *Number of Modules/1kW net produced electrical power as a function of the length L and the width D of the heat transfer tubes for various parameter sets*

As the number of modules as already mentioned is directly related to the net generated power output, the same explanations for the influence of the parameters varied are valid in the inverted way.

With modules available today and realistic mass flow rates out of the bore hole of 30 kg/s the maximum net generated power would not come up to 60 kW at a poor efficiency of about 1.2%. Additionally the required number of modules/1kW in this case is 1170: This leads with a price of about 100 Sfr./Module to specific investment costs of 117000 Sfr./kW which is 4-5 times higher compared to photovoltaic power generation. Besides this the volume of the system would be 3.6 m^3 (parameter set I).

With the assumed hypothetical materials (ZT=4.95) the situation would change remarkably. Under the same conditions the net generated power output would increase to 152 kW at a efficiency of about 6%. The specific investment costs would come down to 23100 Sfr./kW and the volume would be 2.65 m^3 (parameter set IV).

It is noticed here that in all cases (except $V_{specMIN}$) the outflow temperatures of the fluid flows are maximally different by 20°C referred to the inflow temperatures. Therefore the hot side media can be used further as process heat or for district heating, this would increase the economics.

In general the example underlines the importance of developing better and less costly materials.

Chapter 7

Conclusions and outlook

In this work modelling and simulation of thermoelectric systems has been carried out on two different size levels: First for the minimal functional element, then for an array of a multitude of such devices integrated into a cross flow heat exchanger system.

The simulations show, that the choice of the geometric parameters has to be a compromise between best efficiency and highest power output as these quantities show opposite tendencies with parameter variation. Considerations of size and capital costs may impose further criteria influencing eventual parameter selection.

Stacks with long heat transfer units will extract the greatest amount of energy given from a given thermal input, but the average temperature difference will be small and thus the overall system efficiency low. Long heat transfer tubes may also demand higher pump power which would tend to reduce the overall efficiency even further.

High efficiency demands high heat transfer coefficients which can only be obtained with turbulent flow in relatively shallow ducts. This increases the pump power requirement – once more a compromise has been sought.

With typical parameter values of a temperature difference of 60 K, a heat transfer coefficient of 1000 W/m^2K and considering heat transfer tubes of 10 m length and a cross sectional area of a 55x15 mm^2 an overall system efficiency of 1.1% and a characteristic minimal volume of 0.25 m^3/kW appears achievable with the type module (ZT~1) investigated here.

The configuration of the individual modules can be optimized to fulfil the design objectives: Reduced thermocouple leg length increases the power output but decreases the efficiency, however the increase in power output may outweigh the loss of efficiency.

Development of new materials will be aimed at reducing the thermal conductivity while retaining an adequate “power factor”. Figures of merit of the materials will have to be considerably improved, otherwise a large scale implementation of thermoelectrics will not be commercially justified.

Thermoelectric power generation with today’s technology (materials) utilizing geothermal energy seems not to be a competitive solution for power generation. Even with the hypothetic materials, which would bring the performance of the energy conversion system to a strongly competitive level it is additionally important to have module prices, which are almost ten times smaller than these for today available ones.

Models developed here permit streamlined general performance studies of thermoelectric energy conversion systems using fluid heat transfer media with only modest expenditure of time. On small scale level the 3D model using the method of finite elements also allows insight into current density distributions and heat fluxes within smaller devices.

Appendix A

Equations for thermoelectric effects in solid materials

Following the procedures from Schmidt [29] the derivation of the governing equations is based on the energy conservation equation and the Gibbs fundamental equation. For the change of the internal energy of U in a volume element with density ρ in the time slice dt the energy conservation equation is given by:

$$\rho \cdot \frac{\partial U}{\partial t} = -div\ \vec{u} \qquad \text{(Equ. A.1)}$$

Considering the 1st law of thermodynamics the internal energy flux density $\vec{u}$ is connected with the heat flux $\vec{q}$ and the electrical energy flux $V \cdot \vec{J}$ in the following way:

$$\vec{u} = \vec{q} - V \cdot \vec{J} \qquad \text{(Equ. A.2)}$$

Under the rules of vector analysis and consideration of the definition of the electrical potential

$$E \equiv -grad\ V \qquad \text{(Equ. A.3)}$$

follows with (Eq. A.1) and (Eq. A.2):

$$\rho \cdot \frac{\partial U}{\partial t} = -div\ \vec{u} + \vec{E} \cdot \vec{J} - \vec{V} \cdot div\ \vec{J} \qquad \text{(Equ. A.4)}$$

The extension of the Gibb's fundamental equation for homogenous systems with negative charged particles is:

$$T \cdot dS = du + p \cdot dv - (\mu - F \cdot V) \cdot dn \qquad \text{(Equ. A.5)}$$

where S is the entropy and the expression $\mu - F \cdot V$ stands for the electrochemical potential, including μ as the chemical potential and $F = 96485.3399\ C\ mol^{-1}$ as the Faraday constant. Assuming that the change of the specific volume dv is negligible the expression for the change of entropy is.

$$\rho \cdot T \cdot \frac{\partial S}{\partial t} = \rho \cdot \frac{\partial U}{\partial t} - \rho \cdot \frac{\partial}{\partial t}\left[(\mu - F \cdot V)\, dn\right] \qquad \text{(Equ. A.6)}$$

The change of the electric charge in the volume element corresponds to the divergence of the current density J:

$$F \cdot \rho \cdot \frac{\partial n}{\partial t} = div\ \vec{J} \qquad \text{(Equ. A.7)}$$

Combination of the equations A.5 to A.7 results in an expression for the change of total entropy:

$$T \cdot \rho \cdot \frac{\partial S}{\partial t} = -div\, \vec{q} + \vec{E} \cdot \vec{J} - \frac{\mu}{F} \cdot div\ \vec{J} \qquad \text{(Equ. A.8)}$$

The total change of entropy has to be separated into the reversible and in the irreversible part. According to the 2nd law of thermodynamics the entropy stays only constant with reversible process control. The conservation law therefore is:

$$\rho \cdot \frac{\partial S}{\partial t} = -div\, \frac{1}{T} \cdot \left(\vec{\dot{q}} + \frac{\mu}{F} \cdot \vec{S} \right) \qquad \text{(Equ. A.9)}$$

According to the 2nd law of thermodynamics the entropy increases because of irreversible processes. The quantity of entropy generation is the difference between the reversible entropy flux according to equation A.9 and the total entropy change according to equation A.8. In consideration of the equation for heat conduction

$$\dot{Q}_W = \lambda \cdot A \cdot \frac{dT}{ds} \qquad \text{(Equ. A.10)}$$

the transformation of equation A.8 results in:

$$\rho \cdot \frac{\partial S}{\partial t} + div\, \frac{1}{T} \cdot \left(\vec{\dot{q}} + \frac{\mu}{F} \cdot \vec{J} \right) = \frac{1}{T} \cdot \vec{\dot{q}} \cdot \left(-\frac{1}{T}\, grad\, T \right) + \frac{1}{T} \cdot \vec{J} \cdot \left(\vec{E} + T\ grad \frac{\mu}{F \cdot T} \right) \qquad \text{(Equ. A.11)}$$

where the right side describes the entropy generation. The entropy generation can expressed by the phenomenological relations, where the

fluxes $\vec{q}, \vec{J}$ with the gradients $-\frac{1}{T} grad\, T$ and $\vec{E} + T \cdot grad \frac{\mu}{F \cdot T}$ are connected in linear equations.

$$\vec{q} = -\frac{l_{11}}{T} grad\, T + l_{12} \cdot \left(\vec{E} + T\, grad \frac{\mu}{F \cdot T} \right) \qquad \text{(Equ. A.12)}$$

$$\vec{J} = -\frac{l_{21}}{T} grad\, T + l_{22} \cdot \left(\vec{E} + T\, grad \frac{\mu}{F \cdot T} \right) \qquad \text{(Equ. A.13)}$$

The factors l_{11} to l_{22} are designated as the phenomenological coefficients. For the interpretation of these quantities based on the thermoelectric effects the current density $\vec{J}$ is chosen as the independent variable:

$$\vec{q} = \frac{l_{12}}{l_{22}} \vec{J} - \frac{l_{11} - l_{21} \cdot l_{12} / l_{22}}{T} grad\, T \qquad \text{(Equ. A.14)}$$

$$\vec{E} = \frac{1}{l_{22}} \vec{J} + \frac{l_{21} / l_{22} + \mu / F}{T} grad\, T - grad \frac{\mu}{F} \qquad \text{(Equ. A.15)}$$

Thomson relations:

To analyze the phenomenological relations (Equ. A.14 - A.15) the thermoelectric properties were examined for two border cases. In the case of no current ($\vec{J} = 0$) the Fourier equation (Equ. A.10) applies for the heat transport in homogeneous materials. Comparing with equation A.14 the connection between the phenomenological coefficients and the thermal conductivity becomes

$$\lambda = \frac{l_{11} - l_{21} \cdot l_{12} / l_{22}}{T} \qquad \text{(Equ. A.16)}$$

Equation A.15. implicates the electric field that arises in the thermoelectric material due to the temperature gradient:

$$\left[\vec{E}\right]_{\vec{J}=0} = \frac{l_{21} / l_{22} + \mu / F}{T} grad\, T - \frac{1}{F} \frac{d\mu}{dT} grad\, T \qquad \text{(Equ. A.17)}$$

This relationship includes the transformation

$$grad \frac{\mu}{F} = \frac{1}{F} \frac{d\mu}{dT} grad\, T \qquad \text{(Equ. A.18)}$$

which implies the homogeneity of the materials. With equation A.17 the open loop electromotive force can be determined. Because the electric field (*E =-grad U)* is irrotational the line integral is used for the calculation of the voltage generated along the thermoelectric materials (n- and p-leg).

$$U_p - U_n = \int_{k_n}^{k_p} \left[\vec{E}\right]_{\vec{J}=0} d\vec{s} \qquad \text{(Equ. A.19)}$$

Note that the inhomogeneous areas at the cold and warm contacts cause the generation of a contact potential:

$$\left(U_p - U_n\right)_{grad\,T=0} = -\int_{k_n}^{k_p} \left[\vec{E}\right]_{\vec{J},gradT=0} d\vec{s} = \frac{1}{F}\left(\mu_p - \mu_n\right)_{gradT=0} \qquad \text{(Equ. A.20)}$$

The integration of equation A.19 leads by comparison with the definition equation

$$U_p - U_n = -\int_{T_k}^{T_w} \left(\frac{l_{21}}{l_{22}} + \frac{\mu}{F}\right)_{p,n} \cdot \frac{1}{T} \cdot dT \qquad \text{(Equ. A.21)}$$

to the connection of the absolute Seebeck coefficient with the phenomenological quantities.

$$\alpha = -\left(\frac{l_{21}}{l_{22}} + \frac{\mu}{F}\right) \cdot \frac{1}{T} \qquad \text{(Equ. A.22)}$$

For the isothermal case ($grad\,T = 0$) Ohm's law determines the voltage drop in homogeneous materials:

$$\left[\vec{E}\right]_{grad\,T=0} = \frac{1}{\sigma} \cdot \vec{J} \qquad \text{(Equ. A.23)}$$

The comparison with equation A.15 gives

$$\sigma = l_{22} \qquad \text{(Equ. A.24)}$$

Furthermore the entropy relation (A.11) changes for the isothermal case ($grad\,T = 0$) to the form:

$$\rho \cdot \frac{\partial S_{th}}{\partial t} + div\,\frac{\vec{S}}{T} \cdot \left(\frac{l_{12}}{l_{22}} + \frac{\mu}{F} \right) = \frac{1}{T} \cdot \frac{S^2}{\sigma} \qquad \text{(Equ. A.25)}$$

On the right side is the entropy generation due to irreversible Joule heating, when the divergence (second term on the left side) represents the reversible entropy generation. The discharged heat is the reversible Peltier heat, which gives the connection between the absolute Peltier coefficient π and the phenomenological quantities:

$$\pi = -\left(\frac{l_{12}}{l_{22}} + \frac{\mu}{F} \right) \qquad \text{(Equ. A.26)}$$

Considering equations (A.16), (A.22), (A.24), und (A.26) the phenomenological coefficients can be eliminated from the basic equations (A.12 and A.13):

$$\vec{\dot{q}}_{th} = -\left(\pi + \frac{\mu}{F} \right) \vec{S} - \lambda \cdot grad\,T \qquad \text{(Equ. A.27)}$$

$$\vec{E} = \frac{1}{\sigma} \vec{S} - \alpha \cdot grad\,T - grad\,\frac{\mu}{F} \qquad \text{(Equ. A.28)}$$

The Thomson effect is illustrated by inserting equation (A.27) into the expression (A.11) for the reversible entropy flux, considering the condition for DC current $div\,\vec{S} = 0$.

$$div\,\frac{1}{T} \cdot \left(\vec{\dot{q}}_{th} + \frac{\mu}{F} \cdot \vec{S} \right) = div\,\frac{1}{T} \cdot \left(-\lambda \cdot grad\,T \right) - \frac{1}{T} \left(\frac{d\pi}{dT} - \frac{\pi}{T} \right) \cdot \vec{S} \cdot grad\,T \qquad \text{(Equ. A.29)}$$

The second term on the right side shows the additional entropy flux due to reversible Thomson heat.

The Thomson coefficient τ is defined as:

$$\tau = -\left(\frac{d\pi}{dT} - \frac{\pi}{T} \right) \qquad \text{(Equ. A.30)}$$

This expression is known as the 1st Thomson equation, which gives a connection between the thermoelectric coefficients. According to the

fundamental theorem of irreversible thermodynamics the matrix of the phenomenological coefficients is symmetric.

$$l_{12} = l_{21} \qquad \text{(Equ. A.31)}$$

Consideration of equations (A.20), (A.26), (A.28) and (A.30) results in the important relation between Seebeck- and Peltier coefficient, which is known as the 2nd Thomson equation.

$$\pi = \alpha \cdot T \qquad \text{(Equ. A.32)}$$

It also follows from equations (A.30) and (A.32) that:

$$\tau = -\frac{d\alpha}{dT} \cdot T \qquad \text{(Equ. A.33)}$$

The equations governing the multidimensional temperature and electrical potential distributions in TE materials under steady-state conditions and in the absence of an applied magnetic field are the energy equation (A.34) and the current flow equation (A.36) resulting from equations (A.2) under consideration of (A.28), (A.30), and (A.32).

$$\nabla(\lambda \cdot \nabla T) - T \cdot J \cdot \left(\frac{\partial \alpha}{\partial T}\right) \cdot \nabla T + \rho \cdot J^2 = 0 \qquad \text{(Equ. A.34)}$$

$$\nabla \cdot J = 0 \qquad \text{(Equ. A.35)}$$

$$J = -\sigma \cdot [\nabla V + \alpha \cdot \nabla T] \qquad \text{(Equ. A.36)}$$

$$q = \alpha \cdot T \cdot J - \lambda \cdot \nabla T \qquad \text{(Equ. A.37)}$$

Appendix B

Complete assembly of figures presenting the quantities for various parameter combinations as summarized in table B.1

			T_H		
[°C]	40	80	80	80	120
			$h=h_w=h_c$		
[W/m²K]	1000	500	1000	2000	1000
T-profiles along the heat transfer tubes	B.1	B.2	B.3	B.4	B.5
Specific system volume/1kW(net) 2D	B.6	B.7	B.8	B.9	B.10
Specific system volume/1kW(net) 3D	B.11	B.12	B.13	B.14	B.15
Total system efficiency η_{total} 2D	B.16	B.17	B.18	B.19	B.20
Total system efficiency η_{total} 3D	B.21	B.22	B.23	B.24	B.25
No.of Modules for 1Kw(net) 2D	B.26	B.27	B.28	B.29	B.30
No.of Modules for 1kW(net) 3D	B.31	B.32	B.33	B.34	B.35

Tab.B.1 Assignment of figure numbers to the displayed magnitudes (left colum) and the varied parameters (upper rows)

T_{Hin} = 40°C, T_{Cin} = 20°C, $h = h_w = h_c$ = 1000 W/m²K

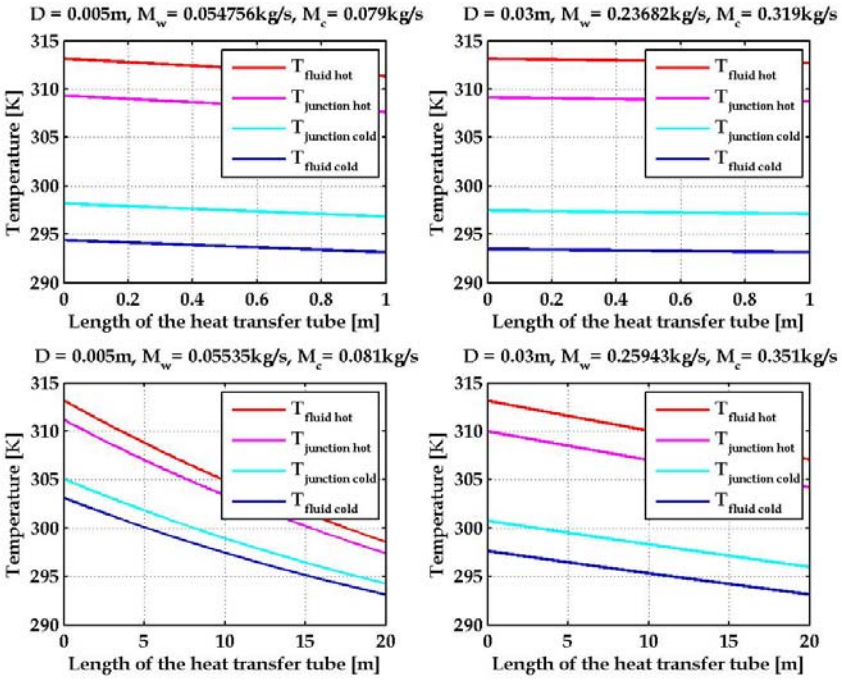

Figure B.1 : *Temperature profiles for various depth and length of the heat transfer tubes*

T_{Hin} = 80°C, T_{Cin} = 20°C, $h = h_w = h_c$ = 500 W/m²K

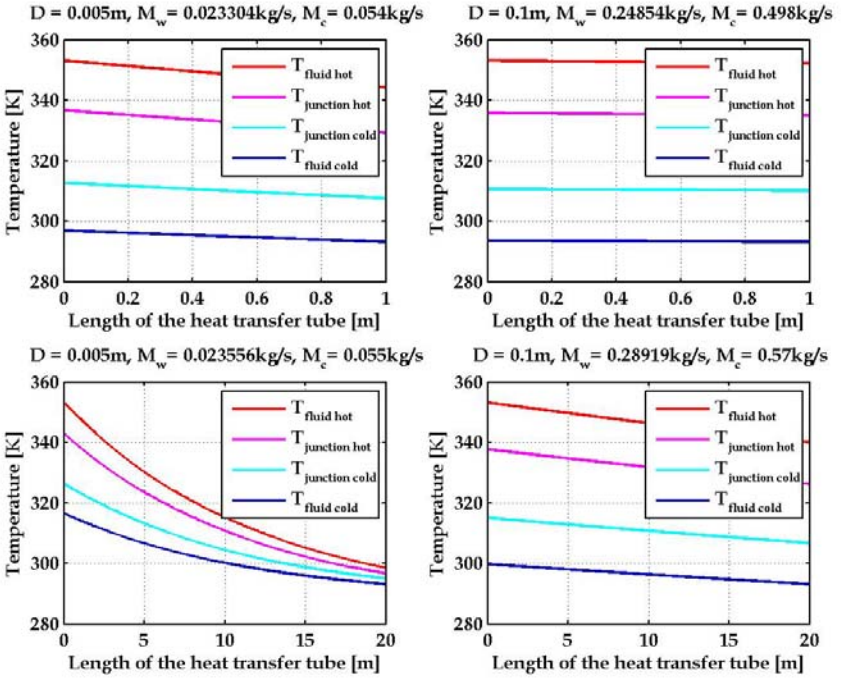

Figure B.2 : *Temperature profiles for various depth and length of the heat transfer tubes*

T_{Hin} = 80°C, T_{Cin} = 20°C, $h = h_w = h_c$ = 1000 W/m²K

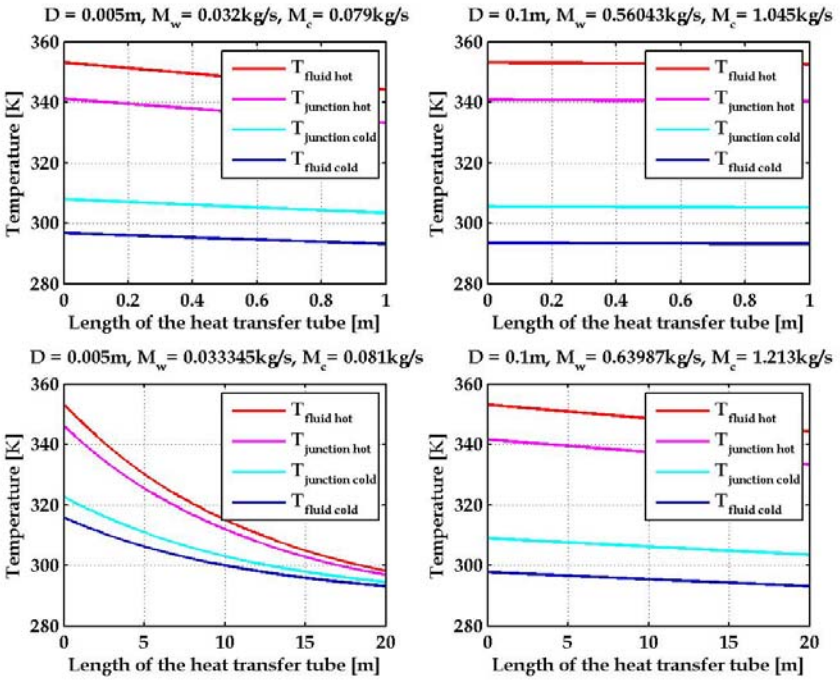

Figure B.3 : *Temperature profiles for various depth and length of the heat transfer tubes*

T_{Hin} = 80°C, T_{Cin} = 20°C, $h = h_w = h_c$ = 2000 W/m²K

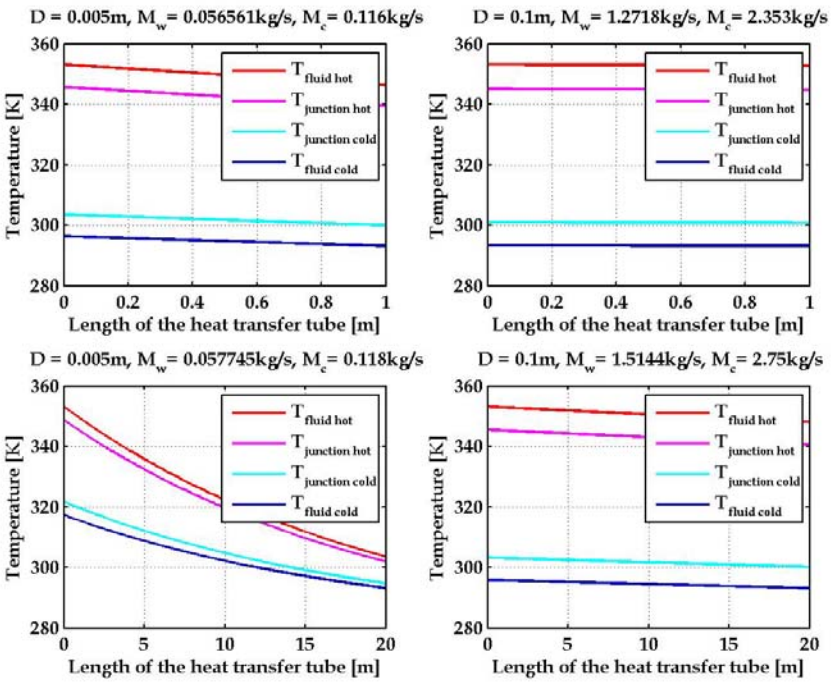

Figure B.4: *Temperature profiles for various depth and length of the heat transfer tubes*

T_{Hin} = 120°C, T_{Cin} = 20°C, $h = h_w = h_c$ = 1000 W/m²K

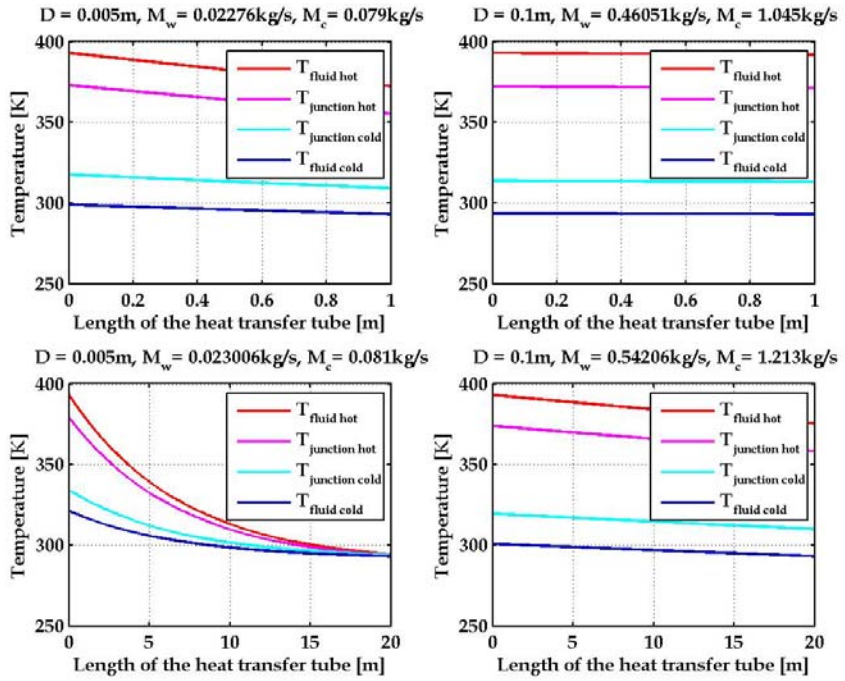

Figure B.5 : *Temperature profiles for various depth and length of the heat transfer tubes*

T_{Hin} = 40°C, T_{Cin} = 20°C, $h = h_w = h_c$ = 1000 W/m²K

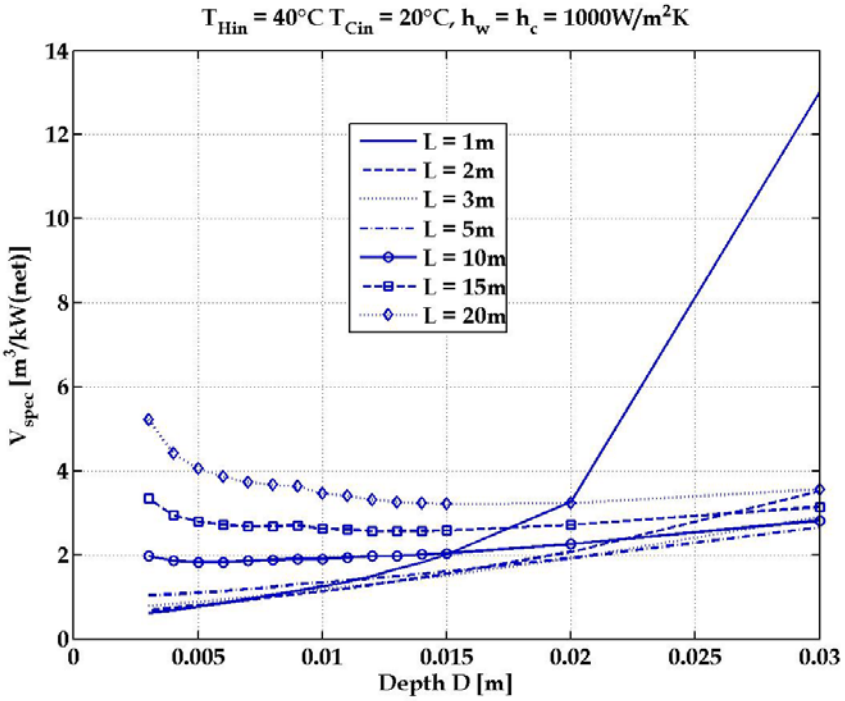

Figure B.6 : *Specific system volume as function of D and L of the heat transfer tubes*

T_{Hin} = 80°C, T_{Cin} = 20°C, $h = h_w = h_c$ = 500 W/m²K

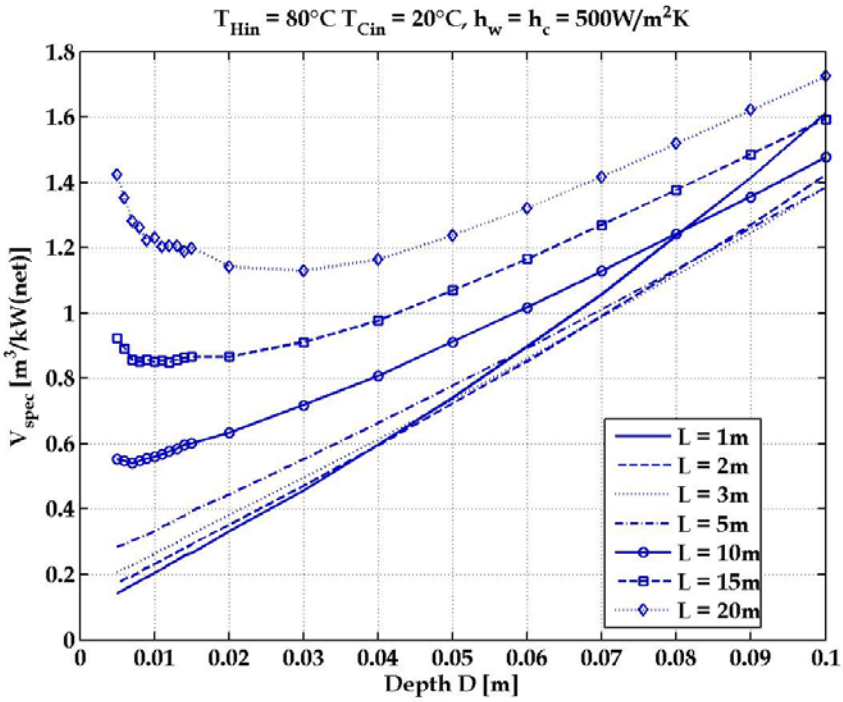

Figure B.7 : *Specific system volume as function of D and L of the heat transfer tubes*

T_{Hin} = 80°C, T_{Cin} = 20°C, $h = h_w = h_c$ = 1000 W/m²K

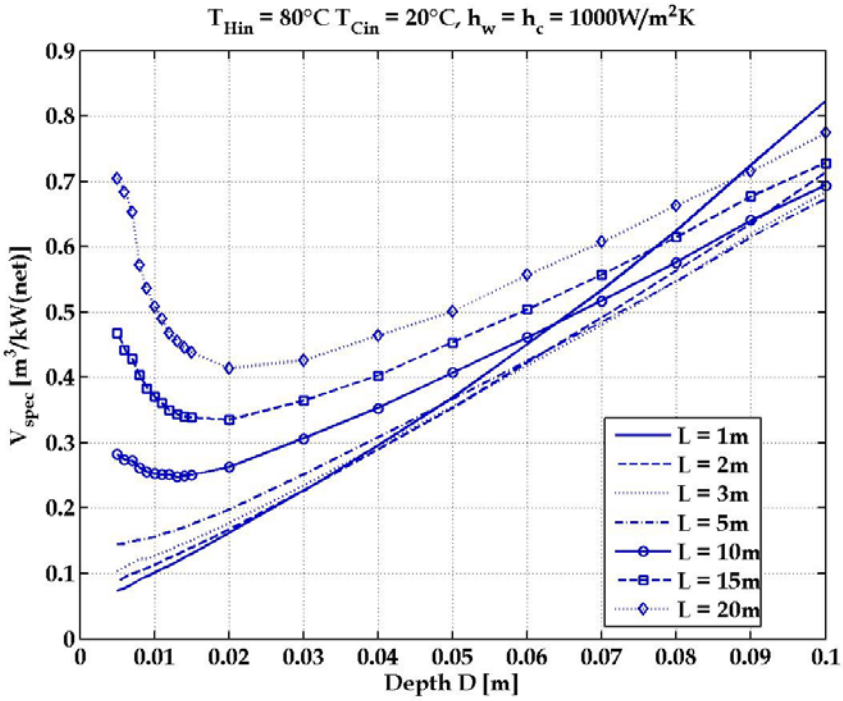

Figure B.8 : *Specific system volume as function of D and L of the heat transfer tubes*

T_{Hin} = 80°C, T_{Cin} = 20°C, $h = h_w = h_c$ = 2000 W/m²K

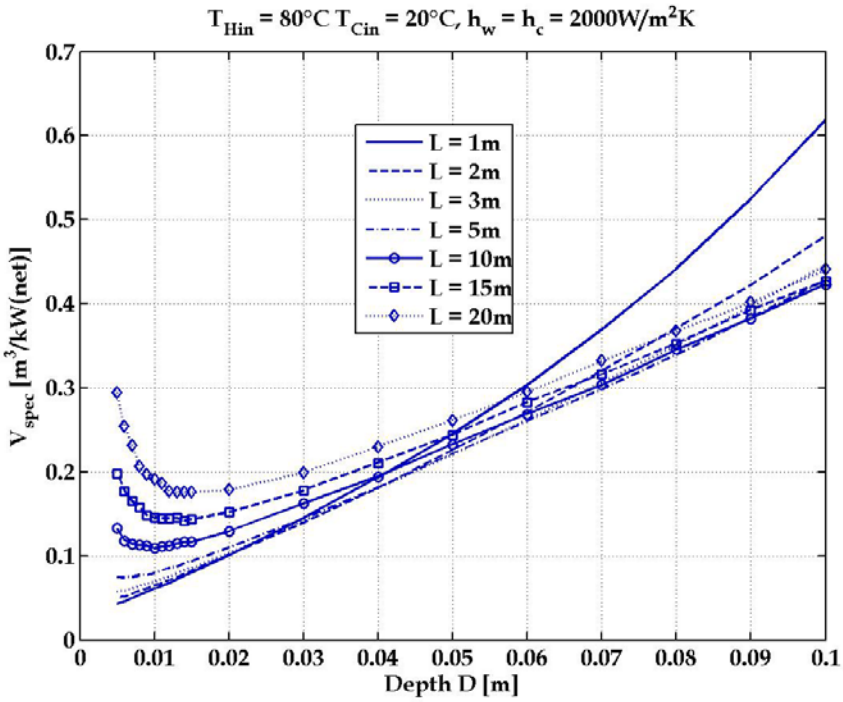

Figure B.9 : *Specific system volume as function of D and L of the heat transfer tubes*

T_{Hin} = 120°C, T_{Cin} = 20°C, $h = h_w = h_c$ = 1000 W/m²K

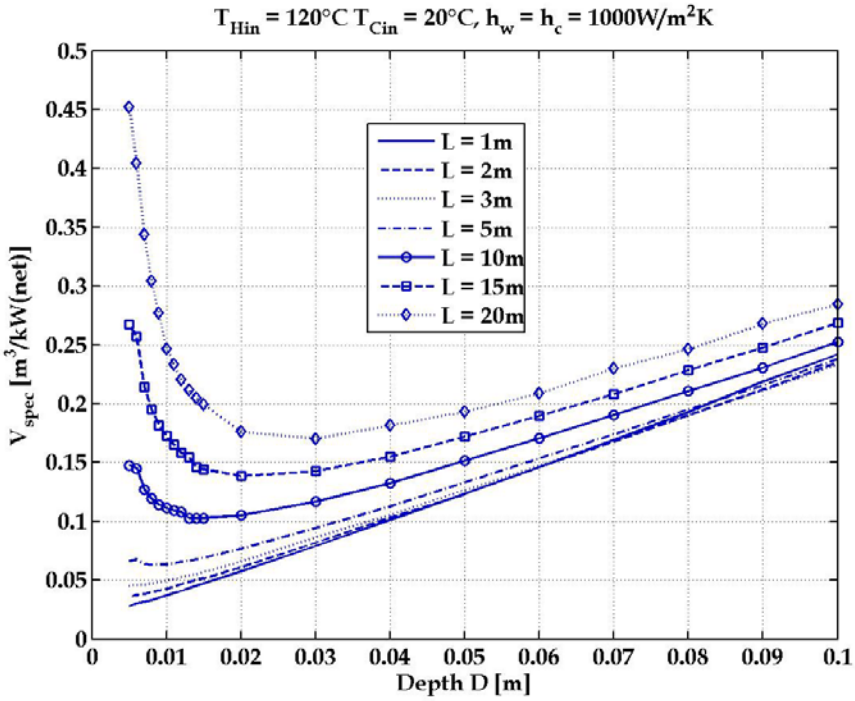

Figure B.10 : *Specific system volume as function of D and L of the heat transfer tubes*

T_{Hin} = 40°C, T_{Cin} = 20°C, $h = h_w = h_c$ = 1000 W/m²K

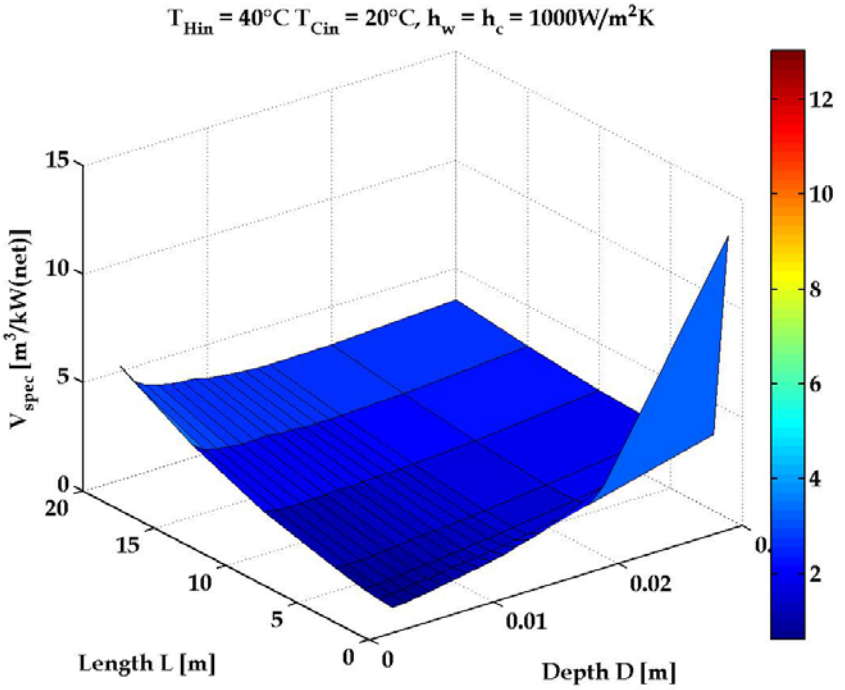

Figure B.11 : *Specific system volume as function of D and L of the heat transfer tubes*

T_{Hin} = 80°C, T_{Cin} = 20°C, $h = h_w = h_c$ = 500 W/m²K

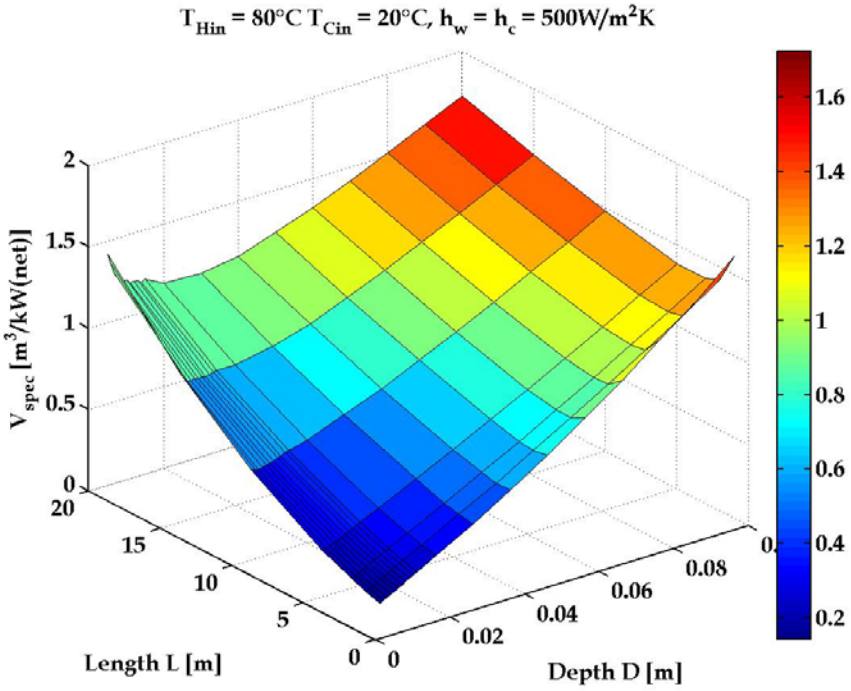

Figure B.12 : *Specific system volume as function of D and L of the heat transfer tubes*

T_{Hin} = 80°C, T_{Cin} = 20°C, $h = h_w = h_c$ = 1000 W/m²K

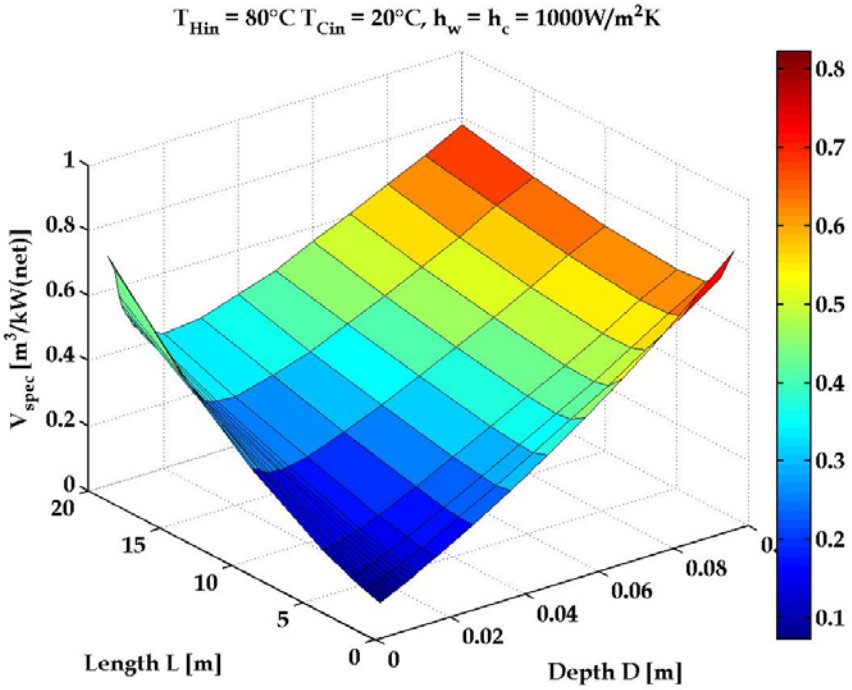

Figure B.13 : *Specific system volume as function of D and L of the heat transfer tubes*

T_{Hin} = 80°C, T_{Cin} = 20°C, $h = h_w = h_c$ = 2000 W/m²K

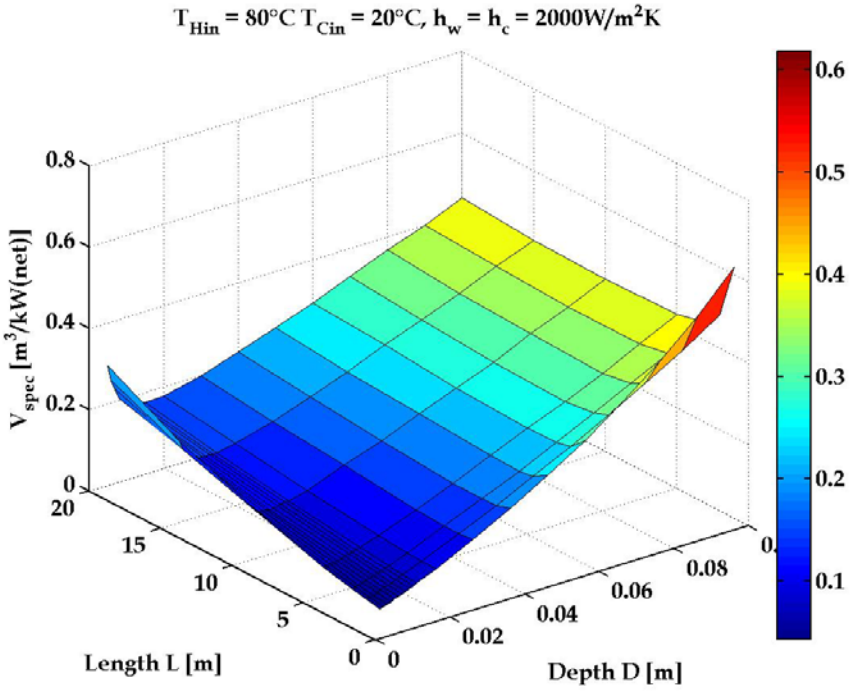

Figure B.14 : *Specific system volume as function of D and L of the heat transfer tubes*

T_{Hin} = 120°C, T_{Cin} = 20°C, $h = h_w = h_c$ = 1000 W/m²K

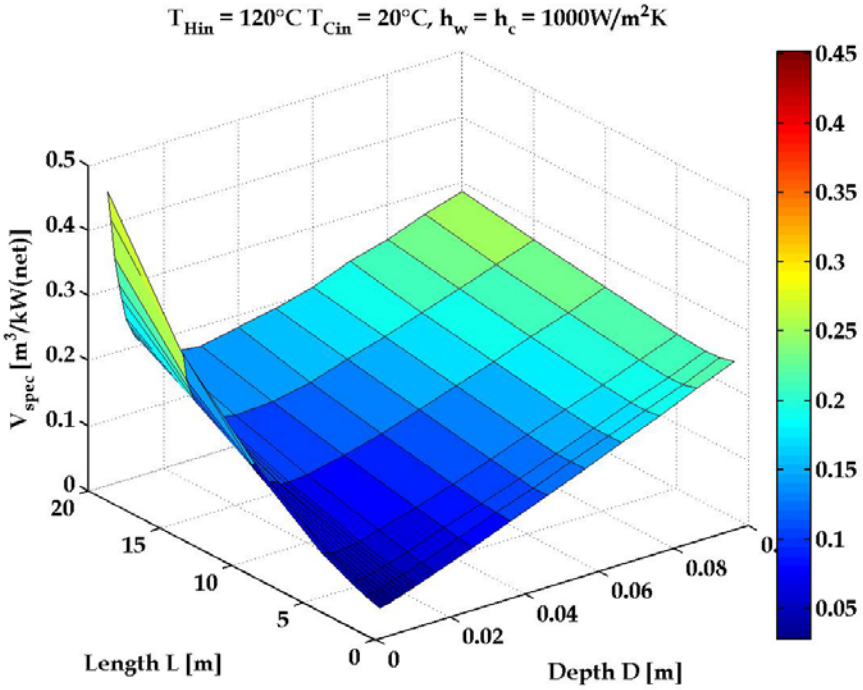

Figure B.15 : *Specific system volume as function of D and L of the heat transfer tubes*

T_{Hin} = 40°C, T_{Cin} = 20°C, $h = h_w = h_c$ = 1000 W/m²K

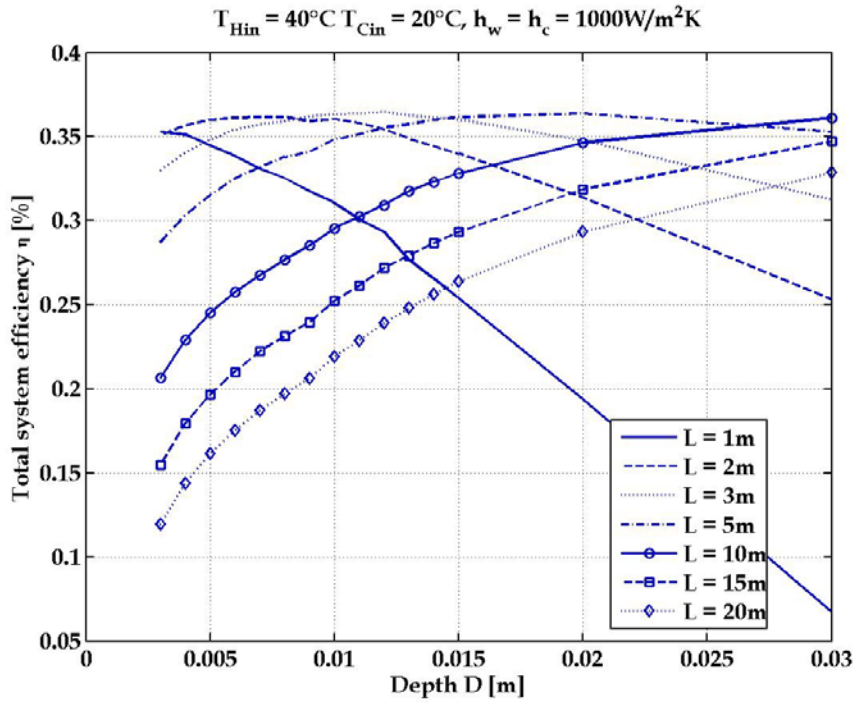

Figure B.16 : *Total system efficiency as function of D and L of the heat transfer tubes*

T_{Hin} = 80°C, T_{Cin} = 20°C, $h = h_w = h_c$ = 500 W/m²K

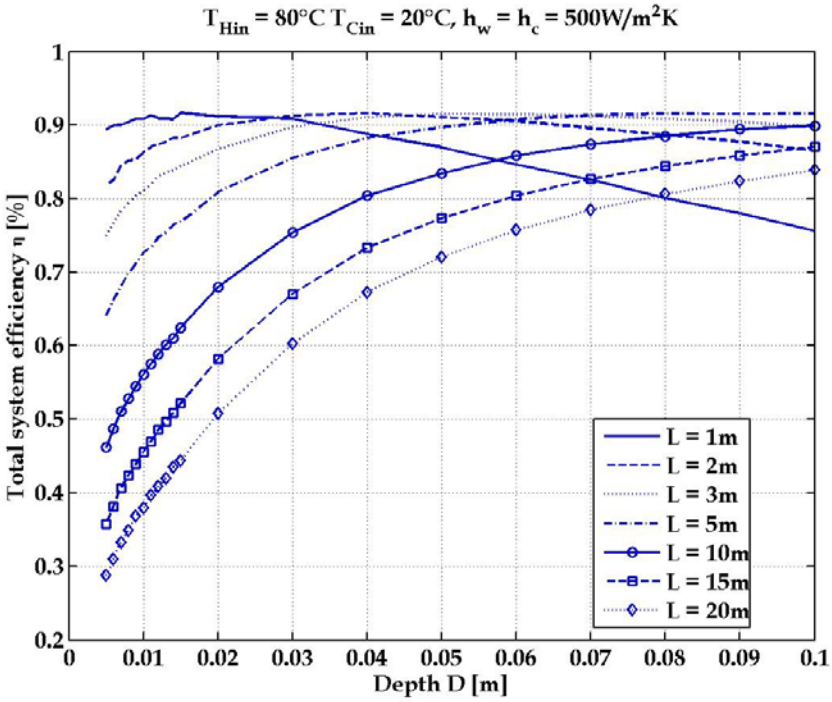

Figure B.17 : *Total system efficiency as function of D and L of the heat transfer tubes*

T_{Hin} = 80°C, T_{Cin} = 20°C, $h = h_w = h_c$ = 1000 W/m²K

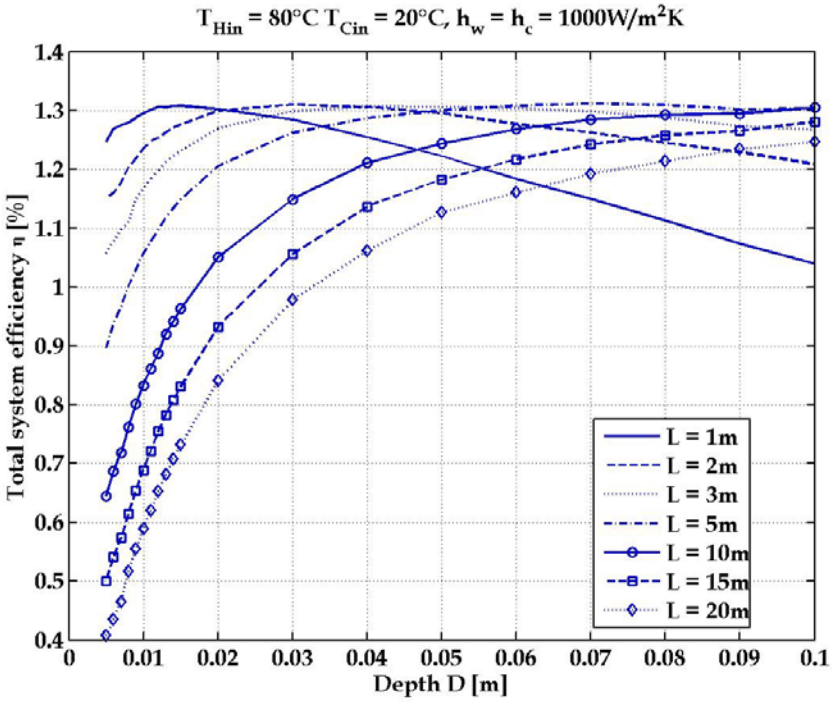

Figure B.18 : *Total system efficiency as function of D and L of the heat transfer tubes*

T_{Hin} = 80°C, T_{Cin} = 20°C, $h = h_w = h_c$ = 2000 W/m²K

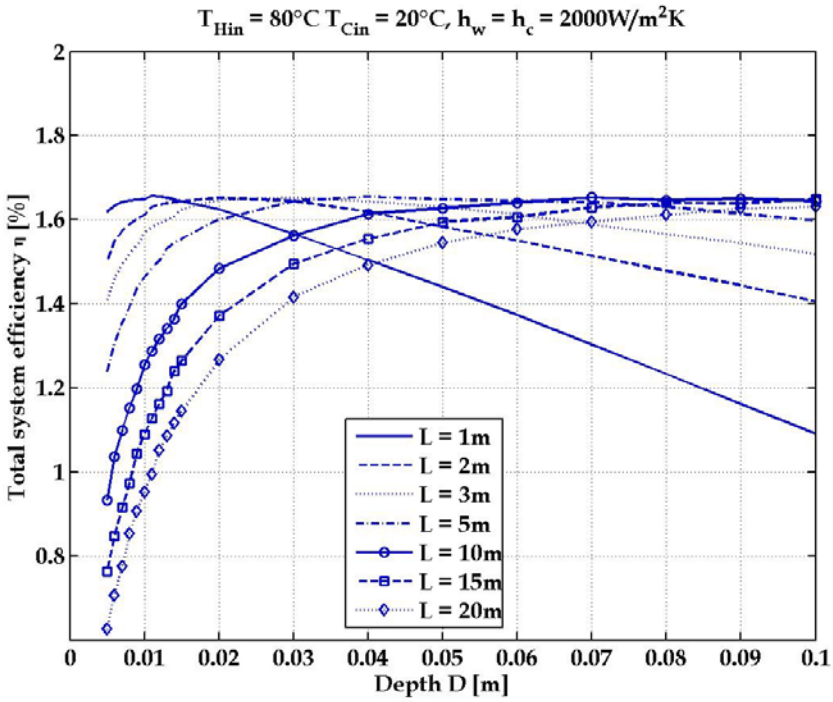

Figure B.19 : *Total system efficiency as function of D and L of the heat transfer tubes*

T_{Hin} = 120°C, T_{Cin} = 20°C, $h = h_w = h_c$ = 1000 W/m²K

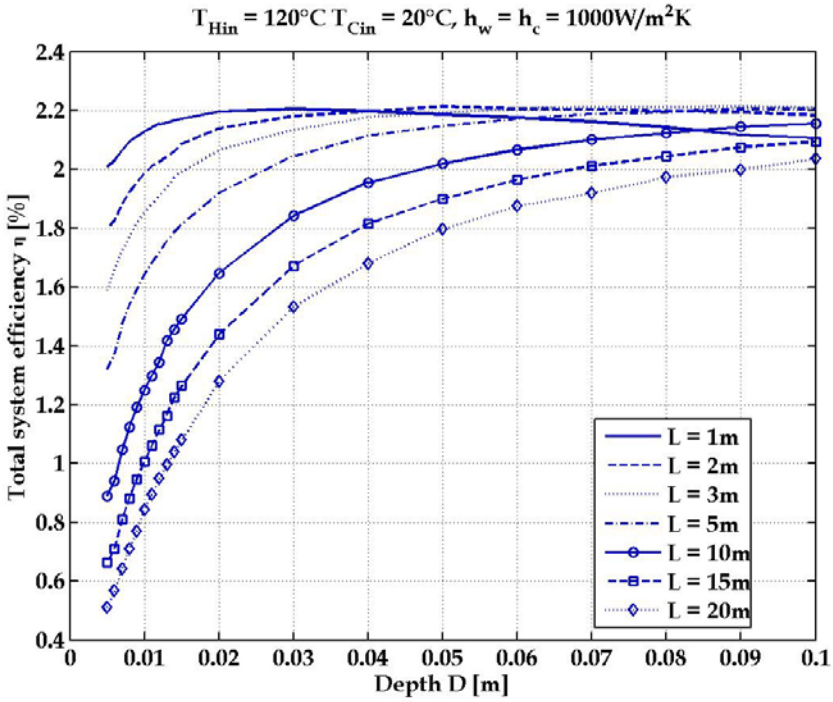

Figure B.20 : *Total system efficiency as function of D and L of the heat transfer tubes*

T_{Hin} = 40°C, T_{Cin} = 20°C, $h = h_w = h_c$ = 1000 W/m²K

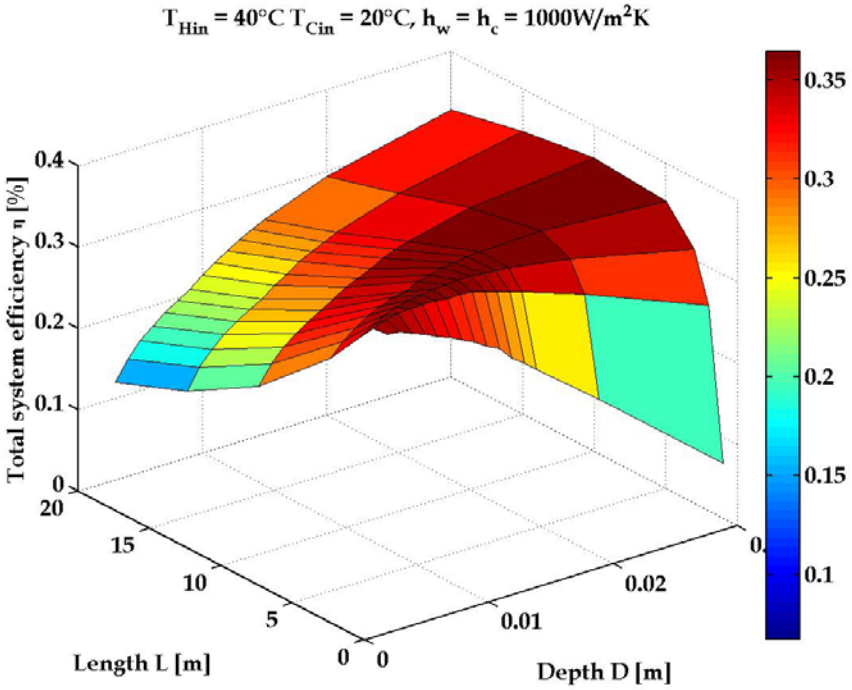

Figure B.21: *Total system efficiency as function of D and L of the heat transfer tubes*

T_{Hin} = 80°C, T_{Cin} = 20°C, $h = h_w = h_c$ = 500 W/m²K

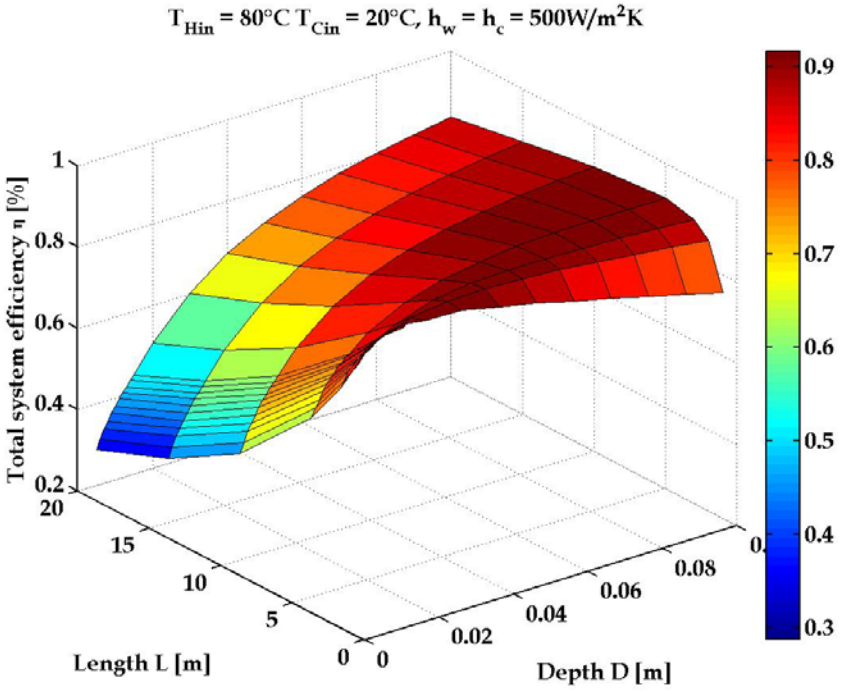

Figure B.22: *Total system efficiency as function of D and L of the heat transfer tubes*

T_{Hin} = 80°C, T_{Cin} = 20°C, $h = h_w = h_c$ = 1000 W/m²K

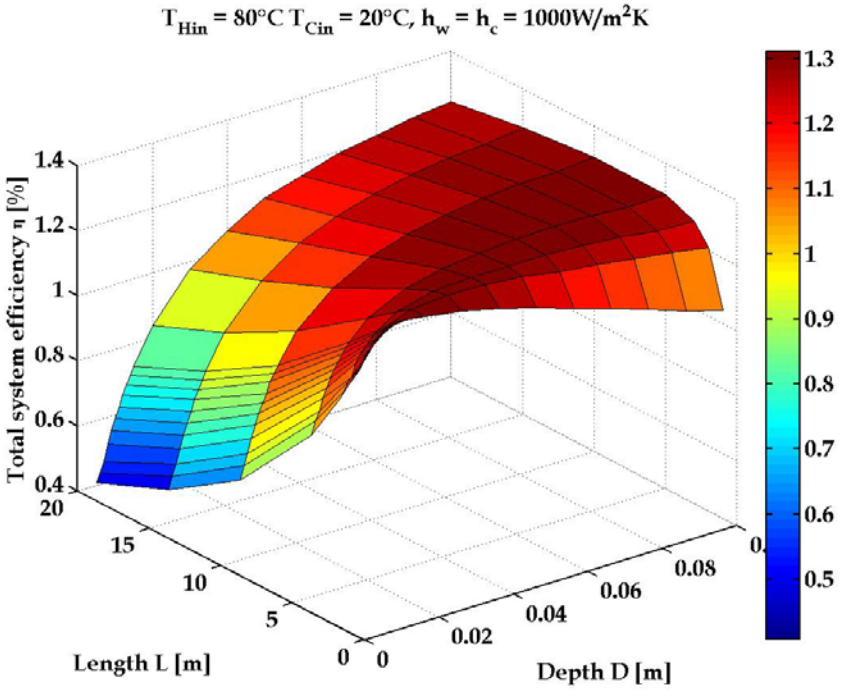

Figure B.23: *Total system efficiency as function of D and L of the heat transfer tubes*

T_{Hin} = 80°C, T_{Cin} = 20°C, $h = h_w = h_c$ = 2000 W/m²K

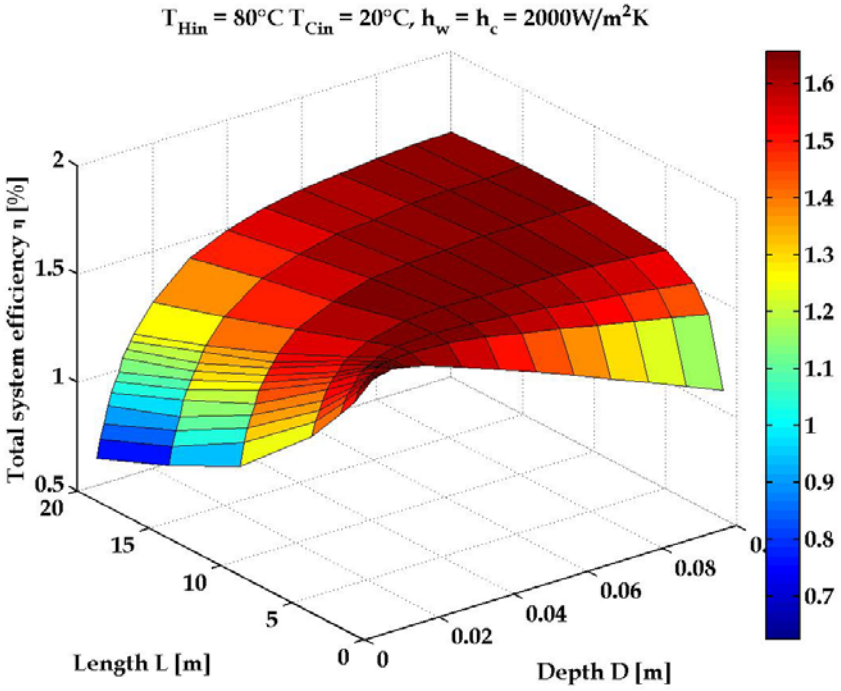

Figure B.24: *Total system efficiency as function of D and L of the heat transfer tubes*

T_{Hin} = 120°C, T_{Cin} = 20°C, $h = h_w = h_c$ = 1000 W/m²K

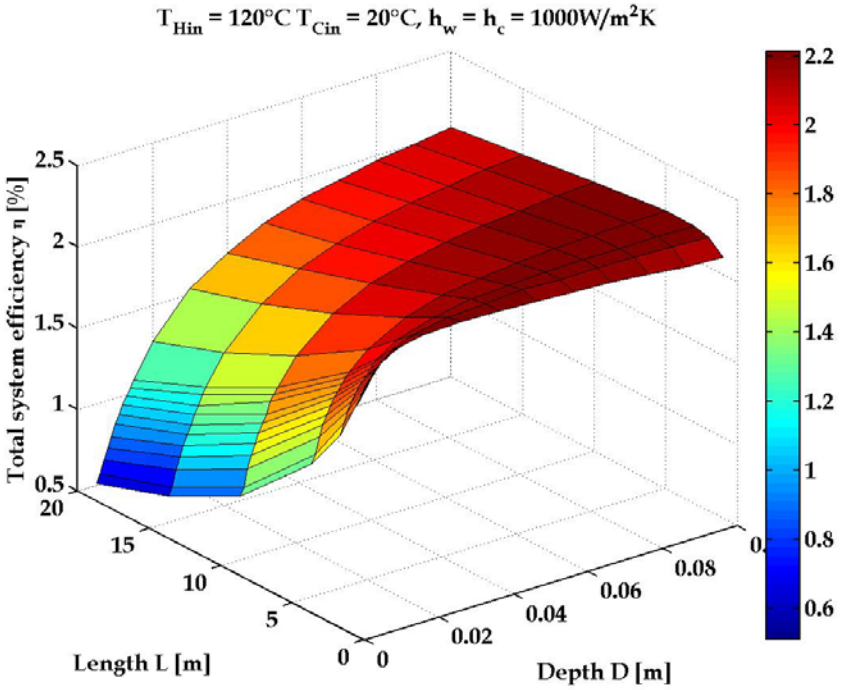

Figure B.25: *Total system efficiency as function of D and L of the heat transfer tubes*

T_{Hin} = 40°C, T_{Cin} = 20°C, $h = h_w = h_c$ = 1000 W/m²K

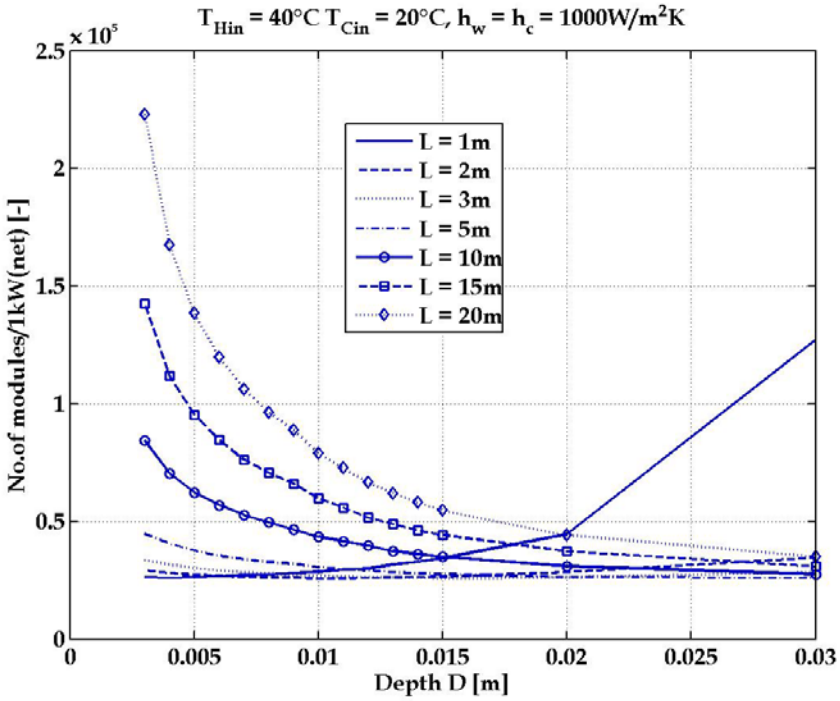

Figure B.26: *No. of modules/1kW as function of D and L of the heat transfer tubes*

T_{Hin} = 80°C, T_{Cin} = 20°C, $h = h_w = h_c$ = 500 W/m²K

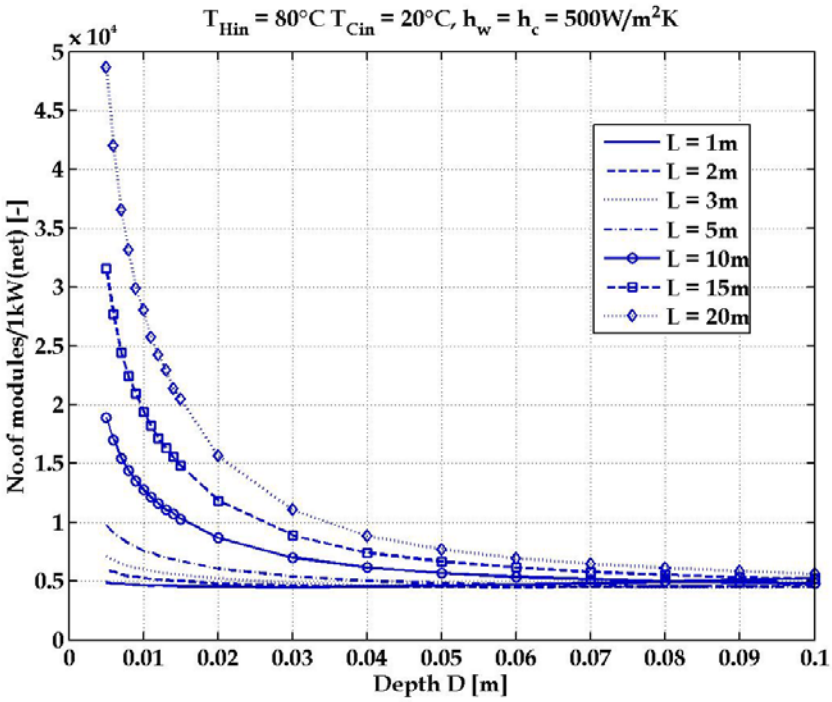

Figure B.27: *No. of modules/1kW as function of D and L of the heat transfer tubes*

T_{Hin} = 80°C, T_{Cin} = 20°C, $h = h_w = h_c$ = 1000 W/m²K

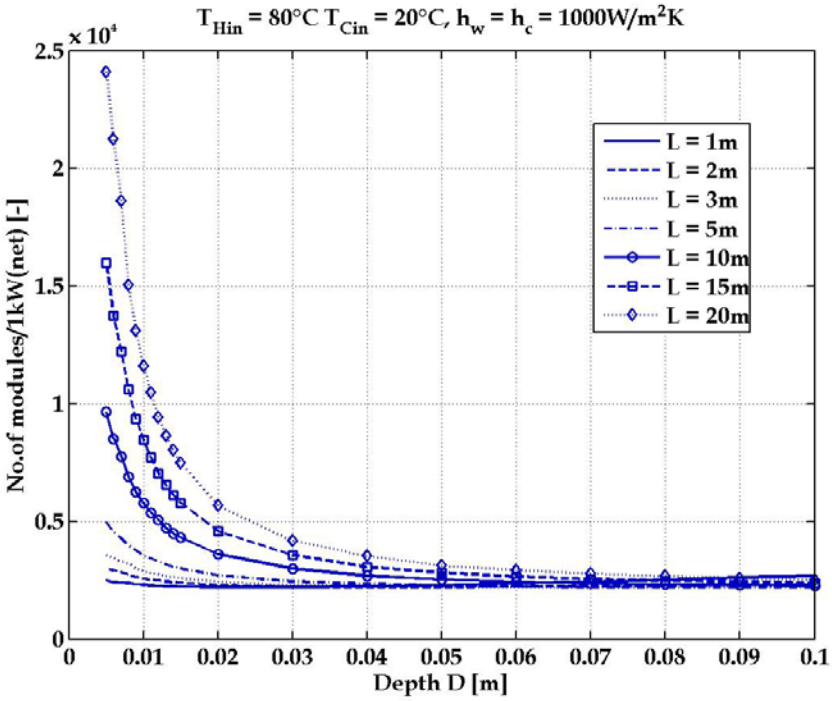

Figure B.28: *No. of modules/1kW as function of D and L of the heat transfer tubes*

T_{Hin} = 80°C, T_{Cin} = 20°C, $h = h_w = h_c$ = 2000 W/m²K

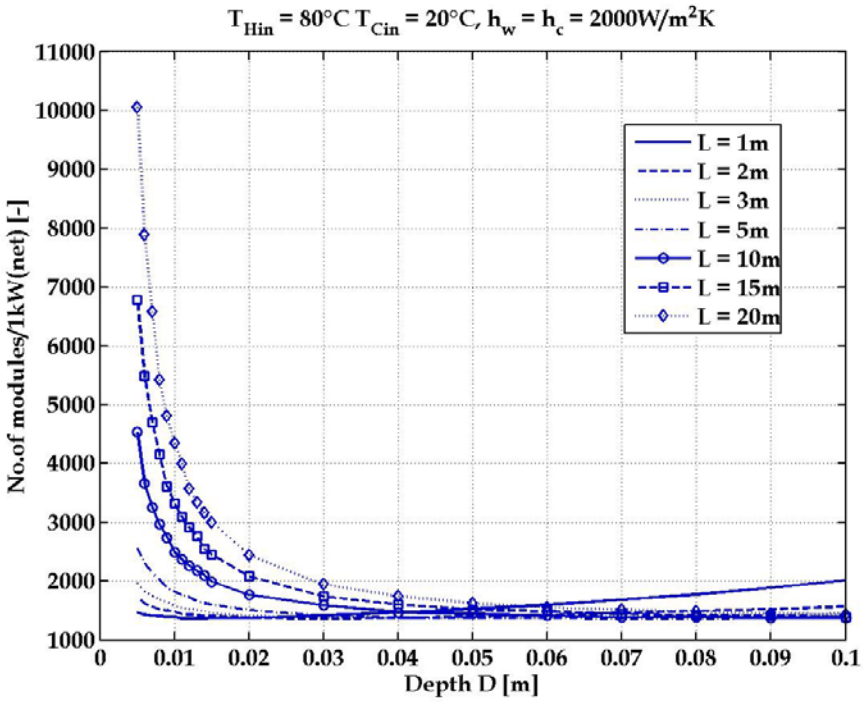

Figure B.29: *No. of modules/1kW as function of the D and L of the heat transfer tubes*

T_{Hin} = 120°C, T_{Cin} = 20°C, $h = h_w = h_c$ = 1000 W/m²K

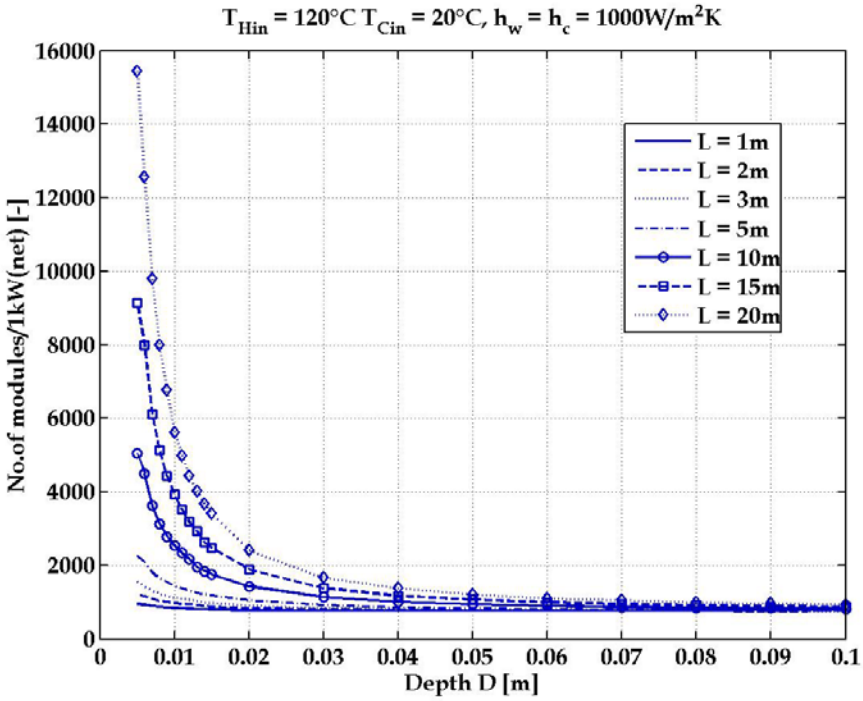

Figure B.30: *No. of modules/1kW as function of D and L of the heat transfer tubes*

T_{Hin} = 40°C, T_{Cin} = 20°C, $h = h_w = h_c$ = 1000 W/m²K

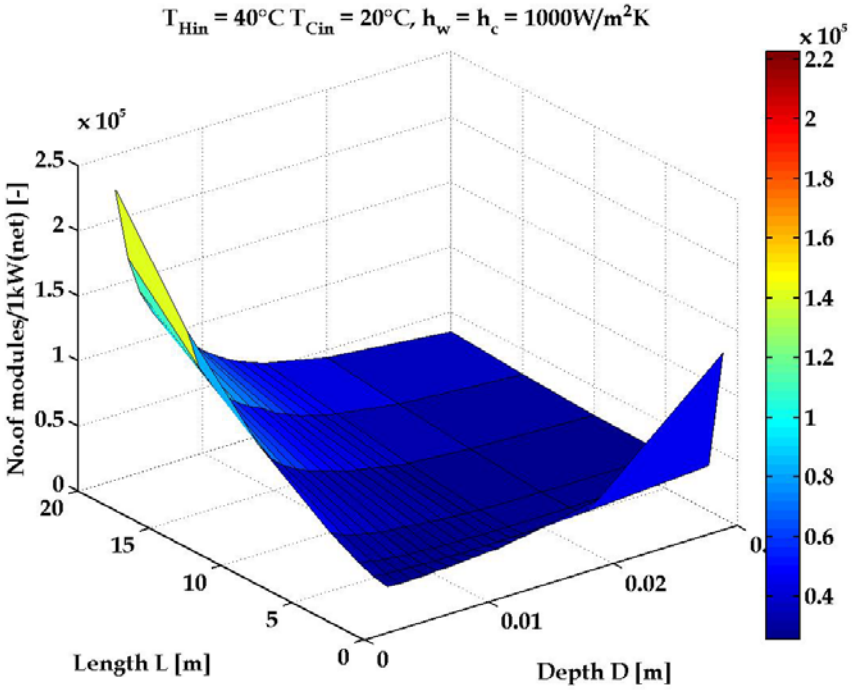

Figure B.31: *No. of modules/1kW as function of D and L of the heat transfer tubes*

T_{Hin} = 80°C, T_{Cin} = 20°C, $h = h_w = h_c$ = 500 W/m²K

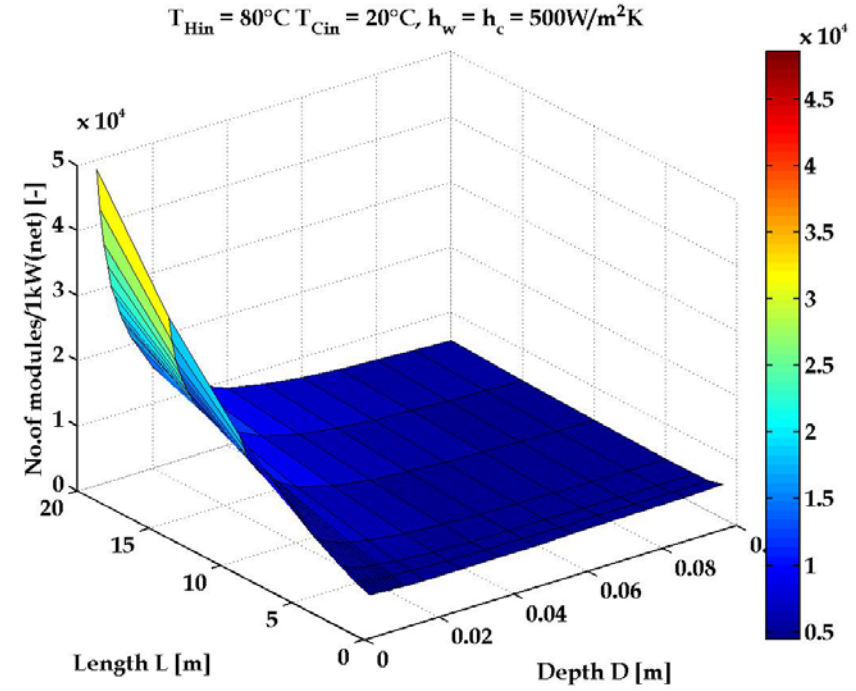

Figure B.32: *No. of modules/1kW as function of D and L of the heat transfer tubes*

T_{Hin} = 80°C, T_{Cin} = 20°C, $h = h_w = h_c$ = 1000 W/m²K

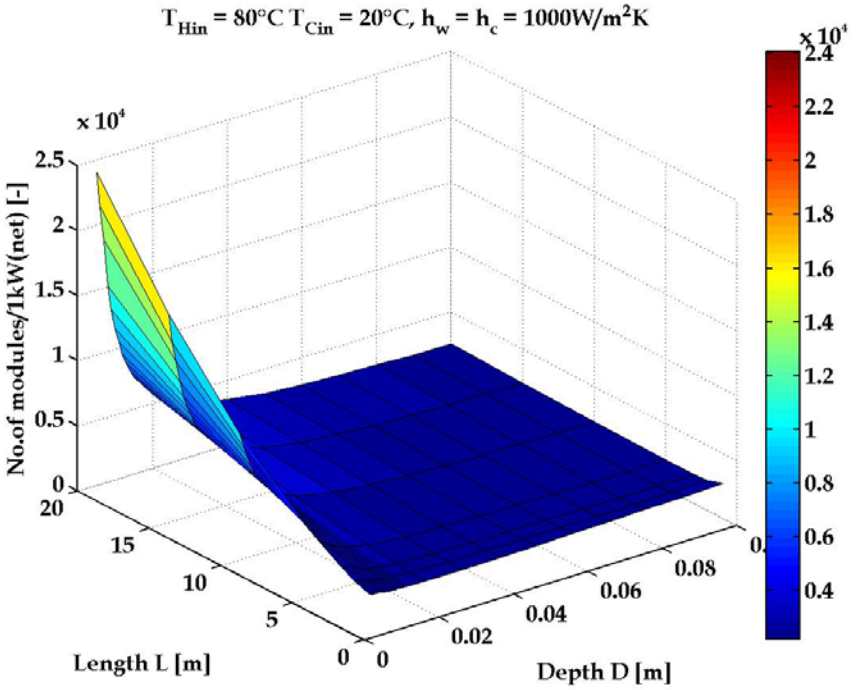

Figure B.33: *No. of modules/1kW as function of D and L of the heat transfer tubes*

T_{Hin} = 80°C, T_{Cin} = 20°C, $h = h_w = h_c$ = 2000 W/m²K

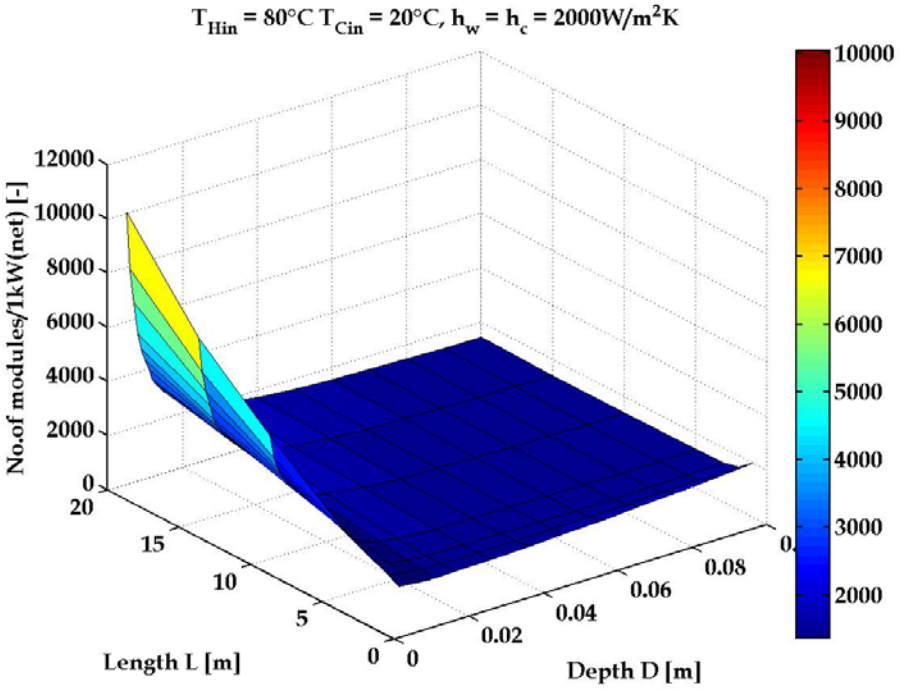

Figure B.34: *No. of modules/1kW as function of D and L of the heat transfer tubes*

T_{Hin} = 120°C, T_{Cin} = 20°C, $h = h_w = h_c$ = 1000 W/m²K

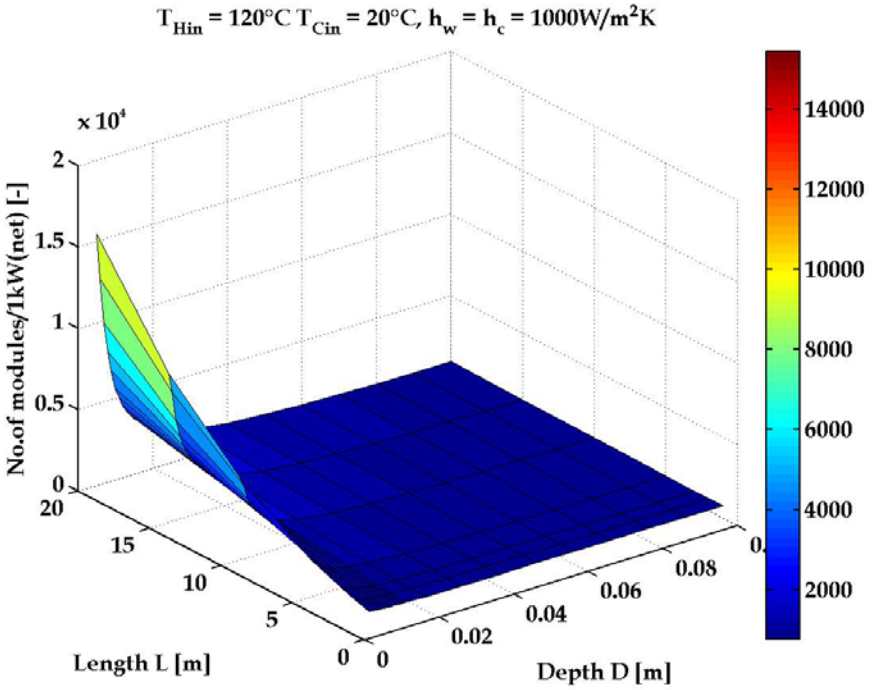

Figure B.35: *No. of modules/1kW as function of D and L of the heat transfer tubes*

Bibliographies

[1] A. Bejan, "Advanced Engineering Thermodynamics", chapter 11 Thermodynamic Optimization, pages 582–649. John Wiley & Sons, Inc., 2 edition, 1997.

[2] A. Bethancourt, R. Echigo, and H. Yoshida, "Thermoelectric conversion analysis in a counterflow heat exchanger", Proceedings of the 12th International Conference on Thermoelectrics, Tokyo, Japan, volume 12, pages 299–304. American Institute of Physics, 1994.

[3] J. Chen, B. Lin, H. Wang, and G. Lin, "Optimal design of a multi-couple thermoelectric generator", Semiconductor Science Technology, Vol. 15, pages 184–188, 2000.

[4] L. Chen, J. Gong, F. Sun, and C. Wu, "Effect of heat transfer on the performance of thermoelectric generators", International Journal of Thermal Sciences, Vol.41, pages 95–99, 2002.

[5] M. Chen and B. Liao, "Comment on 'optimal design of a multi-couple thermoelectric generator'", Semiconductor Science Technology, Vol. 19, pages 659–660, 2004.

[6] M.H. Cobble, "Analysis of a thermoelectric device having contact resistance", Proceedings of the 11th International Conference on Thermoelectrics, Arlington, TX, pages 218–222. IEEE, 1992.

[7] M.H. Cobble, "Handbook of Thermoelectrics", chapter 39 Calculations of Generator Performance, pages 489–501. CRC Press, Inc., 1995.

[8] D.T. Crane and G.S. Jackson, "Optimization of cross flow heat exchangers for thermoelectric waste heat recovery", Energy Conversion & Management, Vol. 45, pages 1565–1582, 2004.

[9] R. Decher, "Direct Energy Conversion – Fundamentals of electric power production" Oxford University press, Inc., 198 Madison Avenue, New York, 1997 ISBN 0-19-509572-3

[10] J. Esarte, G. Min, and D. M. Rowe, "Modelling heat exchangers for thermoelectric generators", Journal of Power Sources, Vol. 93, pages 72–76, 2001.

[11] T. P. Hogan, T. Shih, "Thermoelectrics Handbook, Macro to Nano", chapter 12 – Modeling and characterization of Power Generation Modules Based on Bulk Materials, pages 12.1–12.23. CRC Press, 2006.

[12] Y. Kucherov, P. Hagelstein, and V. Sevastyanenko, "Energy conversion using diode-like structures", Proceedings of the 21st International Conference on Thermoelectronics, Long Beach, CA, pages 431–434. IEEE, 2002.

[13] B. Mathiprakasam and T. Sutikno, "Analytical model for predicting the performance of cross-flow thermoelectric liquid coolers", Proceedings of the fifth international conference on thermoelectric energy conversion, Arlington, TX, pages 75–79, 1984.

[14] B. Mathiprakasam, T. Sutikno, and J. Beeson, "Analytical model for predicting the performance of thermoelectric generators", Proceedings of the fourth international conference on thermoelectric energy conversion, Arlington, TX, pages 61–66, 1982.

[15] K. Matsuura, "Large scale thermoelectric generation of low-grade heat, the future", Proceedings of the 10th International Conference on Thermoelectrics, Cardiff, UK, 1993.

[16] K. Matsuura and H. Kinoshita, "An improved method in generating thermoelectric power from low-grade heat", Proceedings of the fifth international conference on thermoelectric energy conversion, Arlington, TX , pages 10–17, 1984.

[17] K. Matsuura and D. M. Rowe, "Handbook of Thermoelectrics", chapter 44 - Low-Temperature Heat Conversion, pages 573–593. CRC Press, Inc., 1995.

[18] K. Matsuura, D. M. Rowe, K. Koumoto, G. Min, and A. Tsuyoshi, "Design optimisation for a large scale, low temperature thermoelectric generator", Proceedings of the 11th International Conference on Thermoelectrics, Arlington, TX , pages 10–16. IEEE, 1992.

[19] G. Min, "Thermoelectrics Handbook, Macro to Nano", chapter 11 - Thermoelectric Module Design Theories, pages 11.1–11.15. CRC Press, 2006.

[20] G. Min and D. M. Rowe, "Optimisation of thermoelectric module geometry for waste heat electric power generation", Journal of Power Sources, Vol. 38, pages 253–259, 1992.

[21] G. Min and D. M. Rowe, "Handbook of Thermoelectrics", chapter 38 - Peltier Devices as Generators, pages 479–487. CRC Press, Inc., 1995.

[22] G. S. Nolas, J. Sharp, H.J. Goldsmid, "Thermoelectrics – Basic Principles and New Material Developments", Springer Verlag Berlin Heidelberg, New York, 2001, ISBN 3-540-41245.

[23] A. K. Pramanick, P. K. Das, Constructual design of a thermoelectric device, Int. Journal of Heat and Mass Transfer, Vol. 49, pages 1420-1429, 2006

[24] D.M. Rowe and G. Min, ”Design theory of thermoelectric modules for electrical power generation”, IEE Proc.-Sci. Meas. Technol., volume 143, pages 351–356. IEE, November 1996.

[25] D.M. Rowe and G. Min, ”Evaluation of thermoelectric modules for power generation”, Journal of Power Sources, Vol. 73, pages 193–198, 1998.

[26] D.M. Rowe, G. Min, S.G.K. Williams, A. Aoune, K. Matsuura, V.L. Kuznetsov, and L.W. Fu, “Thermoelectric recovery of waste heat - case studies”, Proceedings of the Energy Conversion Engineering Conference, 1997.

[27] D.M. Rowe, Gao Min, and S.G.K. Williams, “Improving the power output and conversion efficiency of peltier modules when used as generators”, Proceedings of the 13th International Conference on Thermoelectrics, Kansas City, Missouri, pages 291–294, 1995.

[28] D.M. Rowe, S.G.K. Williams, and G. Min, “Evaluation of commercially available peltier modules for use in hot-water driven thermoelectric generator”, Proceedings of the 13th International Conference on Thermoelectrics, Kansas City, Missouri, 1995.

[29] E.F. Schmidt, “Unkonventionelle Energiewandler“, chapter 4 - Thermoelektrische Energiewandler, pages 95–125, Elitera-Verlag, Berlin, 1975.

[30] J.W Stevens, “Optimal design of small ΔT thermoelectric generation systems”, Energy conversion and Management, Vol. 42, pages 709-720, 2001.

[31] G.J. Snyder and T.S. Ursell, “Thermoelectric efficiency and compatibility”, Physical Review Letters, Vol. 91, pages 148301(1 - 4), 2003.

[32] R.O. Suzuki, “Mathematic simulation on power generation by roll cake type of thermoelectric double cylinders”, Journal of Power Sources, Vol. 133, pages 277–285, 2004.

[33] R.O. Suzuki and D. Tanaka, ”Mathematic simulation on thermoelectric power generation with cylindrical multi-tubes”, Journal of Power Sources, Vol. 124, pages 293–298, 2003.

[34] R.O. Suzuki and D. Tanaka, ”Mathematical simulation of thermoelectric power generation with the multi-panels”, Journal of Power Sources, Vol. 122, 201–209, February 2003.

[35] R.O. Suzuki and D. Tanaka, “Mathematic simulation on power generation by roll cake type of thermoelectric tubes”, Journal of Power Sources, Vol. 132, pages 266–274, 2004.

[36] VDI-Wärmeatlas, „Berechnungsblätter für den Wärmeübergang“, Verein Deutscher Ingenieure, VDI-Gesellschaft Verfahrenstechnik und Chemieingenieurwesen, VDI-Verlag Düsseldorf, 1984, ISBN 3-18-400415-5

[37] C. Wu, "Analysis of waste-heat thermoelectric power generators", Applied Thermal Engineering, Vol. 16, pages 63–69, 1996.

[38] C. Wu and R.L. Kiang, "Finite-time thermodynamic analysis of a carnot engine with internal irreversibility", Energy, Vol. 17, pages 1173–1178, 1992.

[39] J. Yu and H. Zhao, "A numerical model for thermoelectric generator with the parallel plate heat exchanger", Journal of Power Sources, Vol. 172, 428–434, July 2007.

[40] Zahoransky, R. Energietechnik Systeme zur Energieumwandlung; Kompaktwissen für Studium und Beruf, Edition: 3, Vieweg+Teubner Verlag, 2007, ISBN 3-8348-0215-8, 9783834802156